COMPARISON OF MAGNESIUM AMOUNT IN BLACK, GREEN, FRUIT, AND HERBAL TEAS

Michaela Zeiner[a]*, Iva Juranovic Cindric[b], Michaela Kröppl[c], Gerhard Stingeder[a]

Paper was presented at the 4th International Symposium on Trace Elements in the Food Chain, Friends or Foes, 15-17 November, 2012, Visegrád, Hungary

The diet is the main source of minerals and trace elements, thus exposure to dietary essential elements has a direct impact on human health. Magnesium is a major component of the bones, but furthermore it influences the nervous system and muscle activity. Therefore its needs must be met via nutrition. There is a non-negligible discrepancy between intake and requirements. So magnesium is often uptaken in form of nutrition supplements. Thus there is an interest in the amount of magnesium in natural products, where it is supposed to vary. In this study, various commercially available tea bags of different kinds of tea (black tea, green tea, fruit tea and herbal tea) were analysed for their magnesium content. After a microwave assisted digestion with nitric acid and water at temperatures up to 220°C, the element concentration was measured with ICP-OES (inductively coupled plasma-optical emission spectroscopy) as it is a simultaneous, fast and reliable method with low detection limits. All samples were prepared in duplicate. In all samples high amounts of magnesium (approx. 1 g kg^{-1}) could be found. No statistically significant differences were registered between the different classes of teas.

* Corresponding Author
    Fax: +43-47654-6059
    E-Mail: michaela.zeiner@boku.ac.at
[a]   Division of Analytical Chemistry, Department of Chemistry, BOKU - University of Natural Resources and Life Sciences, Muthgasse 18, 1190 Vienna, Austria
[b]   Laboratory of Analytical Chemistry, Faculty of Science, University of Zagreb, Horvatovac 102a, 10000 Zagreb, Croatia
[c]   Upper Austrian University of Applied Sciences, Campus Wels; Stelzhamerstraße 23, 4600 Wels, Austria

Introduction

Tea is one of the most popular beverages in the world since more than 2000 years.[1] Usually a tea drink or infusion is prepared by seeping dried parts of certain plants in boiling or at least hot water. Whereas infusions prepared in this way contain only little proteins, vitamins, fibres or carbohydrates, they represent a source of some essential dietary metals as well as of metal binding polyphenols.[2] The most common kinds of tea are the true tea types (black, Oolong, green and white tea) derived from the tea plants. In last decades however, the popularity of the so-called herbal or fruit tea (infusions of fruits or herbs) is increasing to the elevated ecological awareness and the trend to a healthier life style.

The determination of minerals from major down to trace elements in tea, dried fruits and their infusions is important because of the metabolic role of some essential or toxic metals. There is not only the need of knowledge of the food's nutritional value which refers to major or minor-elements,[3] but there is also a concern to verify that food does not contain minerals in toxic quantities. These elements might be harmful to the human organism, regardless whether their presence is naturally occurring or is due to contamination. Furthermore the uptake and utilisation of certain elements, such as iron and copper is reduced by the consumption of real tea infusions caused by the tannins.

This effect was not found for other minerals including magnesium.[4]

Magnesium is a physiologically essential constituent playing an important role in different vital processes occurring in the human body. It is not only a major component of the bones, but furthermore it influences the nervous system and muscle activity. Being a cofactor in almost all phosphorylation reactions involving ATP Magnesium is considered as an indirect antioxidant.[5]

As reported by Pugh and colleagues[6] vegetation represents a useful indicator of (heavy) metal contamination in the environment via root uptake of metals, and can be used for monitoring pollution across both spatial and temporal scales. The soil properties,[7] such as mother rock composition, also influence the total metal content in tea leaves and thus in infusions. Therefore leaves and blossoms used for tea preparation can be used as indicator of environmental contamination, and also for their geographical origin.

Thus it is expected that the total magnesium content in tea or tea leaves varies between different real tea types (e.g. black or green) and within these classes in certain ranges between different brands. Even higher differences are supposed to be found in fruit and herbal teas since they derive from other plants.

Due to importance of magnesium for human health tea powder and tea infusions have already been analysed, but mostly with low number of samples.

Pohl and Prusisz determined various major and trace elements in one green tea sample and in one granulated black tea sample commercially available on the Polish market. The contents found were 2.37 g kg^{-1} and 1.04 g kg^{-1}, respectively.[8]

A study of ten tea powders purchased in the USA including herbal and green tea revealed higher magnesium contents in herbal teas than in the real teas. Decaffeinated green tea even contained more Mg than caffeinated green tea, namely 4.6 g kg^{-1} and 3.3-3.7 g kg^{-1}, respectively.[9]

Regarding real tea types the investigation of McKenzie et al. has to be mentioned. They determined the magnesium content in black, green, Oolong, Pu-erh and white tea. The results are in the range from 2.0 up to 2.8 g kg^{-1} for all kinds studied.[10]

Basgel and Erdemoglu determined besides other elements the amounts of total magnesium in seven medicinal herbs cultivated in Turkey, which are commonly used for the preparation of healing infusions. The contents found ranged from 1.6 up to 3.8 g kg^{-1}.[11]

Peppermint and nettle leaves from commercially available tea bags as well as infusions derived from them were analysed for their elemental composition by Lozak and colleagues. In the former 5.8 g kg^{-1} magnesium were found.[12]

Magnesium data are also documented in literature for the medicinal plants sage and mountain germander, the contents of the whole herbs being 4.0 g kg^{-1} and 1.4 g kg^{-1}, respectively.[13]

Experimental

Tea samples

Four different tea types, real tea (black and green) as well as fruit and herbal tea have been analysed. All samples (powders) were tea bags commercially available in Austria and Croatia. An overview is given in Table 1. Prior to sample preparation the tea bags of one sample were opened and the powders were homogenised.

Table 1 Analysed Tea samples

Herbal tea	Fruit tea
H1 (chamomile, echinacea, mint)	F1 Pomegranate-Redcurrant
H2 (rooibos, ginger, chicory, liquorice, cinnamon)	F2 Strawberry
	F3 Strawberry Raspberry
H3 (lemongrass, balm, rooibos, honeybush, vervain, lemon myrtle, ginger, fennel, anise, camomile, crisped mint, peppermint)	F4 Redcurrant-Cherry
	F5 Winter tea
n=3	*n=5*
Green tea	**Black tea**
G1	B1 (English Breakfast)
G2 with lemon	B2 (Irish cream)
G3	B3 (Earl grey)
G4	
G5	
G6	
G7	
G8 with lemon	
G9 w. lemongrass ingwer	
n=9	*n=3*

Digestion of the tea samples

In order to determine the total magnesium content of the samples these were mineralised after homogenisation by acidic microwave assisted digestion. About 100 to 120 mg of each pooled tea powder sample were accurately weighed into the Teflon microwave digestion flasks. After addition of 5 mL HNO$_3$ (65 ww%, p.a, Merck) and 4 mL distilled water the flasks were left opened till gas emissions from nitric acid stopped. The flasks were then closed and put into the microwave oven (StarT" from MLS). The temperature programme applied was (time [min]/power [W]: 3/700; 9/500; 23/1000 with a maximum allowed temperature of 220°C. After cool-down to room temperature the completely digested samples were filled up to 10.0 mL with distilled water. All samples were digested in duplicate. Samples without tea powders were also prepared as blank samples.

Determination of the magnesium concentration by ICP-OES

The instrument used was a Prodigy High Dispersive ICP-OES spectrometer (Teledyne Leeman, Hudson, NH, USA) working in a simultaneous mode. The optimal instrumental conditions are listed in Table 2.

Table 2 ICP-OES operating conditions

Instrument	Prodigy High Dispersive ICP
Spectrometer	High resolution Echelle polychromator Large format programmable array detector (L-PAD)
RF-Generator	40 MHz "free-running"
Output power	1.1 kW
Argon flow	Coolant:18 L min^{-1} , Auxiliary: 0.8 L min^{-1}Nebulizer: 1 L min^{-1}
Peristaltic pump	1.0 mL min^{-1}
Nebulizer	Pneumatic (glass concentric)
Spray chamber	Glass cyclonic
Plasma viewing	Axial
Sample uptake delay	30 s
Wave lengths	280.271 nm; 285.213 nm

All measurements were performed in triplicate. All standards were prepared by dilution of the multi element stock solution Multistandard CertiPUR IV from Merck using nitric acid ($c = 1$ mol L^{-1}). Nitric acid ($c = 1$ mol L^{-1}) was also used as calibration blank and rinsing agent between the samples. The calibration range was up to 10 mg L^{-1}.

Validation parameters

In order to estimate the accuracy of the method, spiking experiments were carried out at three concentration levels (1.0, 3.0 and 5.0 mg L^{-1}) by addition of a certain volume of aqueous multielement standard stock solution to selected digested samples prepared as described above. All spiked samples were prepared in triplicate and measured by ICP-OES.

The precision was evaluated by repeatability measurements (within-day precision and day-to-day precision).

Limit of detection and limit of quantification were determined by measuring a reagent blank solution and a spiked microwave assisted digested sample ten times, whereby the calculation is based on $3\,\sigma$ for LOD and $9\,\sigma$ for LOQ.

Calculation

The elemental contents were calculated from the measured concentrations in the digested solutions taking into consideration blanks, dilutions, and mass of dried sample used for digestion to obtain results of mass concentrations per dry weight. All standard deviations are based on measurements in triplicate. The obtained data were statistically analysed by a *t*-test (p 0.05) for revealing statistically significant differences.

Results and discussion

Analytical figures of merit

The recoveries found were 94.7% at 280.271 nm and 86.3% at 285.213 nm. The precision was comparable for both wavelengths, ranging from 0.5 up to 3%. The LOD determined was 0.1 ng g^{-1} dry tea powder without significant difference between the two wavelengths. The correlation coefficients for the calibration curves at both wavelengths were beyond 0.9995. Due to the better findings for the measurements at 280.271 nm, the data registered this wavelength were used for further evaluation.

Table 3 Total magnesium concentrations in the different tea powder samples

| Type of tea	Sample	Content [g kg^{-1}]	(Mean content ± standard deviation) [g kg^{-1}]
green tea	G1	1.07 ± 0.02	
	G2	1.10 ± 0.08	
	G3	1.09 ± 0.06	
	G4	1.11 ± 0.11	
	G5	0.907 ± 0.03	1.01 ± 0.09
	G6	1.01 ± 0.01	
	G7	0.899 ± 0.002	
	G8	0.901 ± 0.03	
	G9	1.00 ± < 0.01	
black tea	B1	1.02 ± 0.01	
	B2	0.826 ± 0.081	0.971 ± 0.13
	B3	1.06 ± 0.09	
herbal tea	H1	1.31 ± 0.03	
	H2	0.889 ± 0.001	1.14 ± 0.22
	H3	1.20 ± 0.02	
fruit tea	F1	1.02 ± 0.19	
	F2	1.21 ± 0.12	
	F3	1.39 ± 0.15	1.15 ± 0.16
	F4	1.15 ± 0.09	
	F5	0.999 ± 0.003	

Magnesium content in the tea powders

The results for the total magnesium contents in the tea powders tested are shown as mean values in Table 3 along with the respective standard deviations. The content was

calculated for each sample (triplicate measurement of duplicate digestion) as well as for each tea type as mean.

These data underwent a *t*-test (p 0.05) in order to see if there are any statistically significant differences between the various types of tea powder. Due to low number of samples and the high variability within one kind of tea powder, the differences in the magnesium contents found were all not statistically significant. This finding can be easily seen from the following diagram with the error bars (Figure 1).

The results found in the present study fit to those reported in the Polish study on black tea.[12] The data obtained for the other tea types are in the same order of magnitude as given in literature, but a little bit lower. The biggest difference is evident for herbal tea based on the diverse composition of herbs in the mixtures analysed. Differences might be caused by different cultivars, soil compositions and agricultural practices.
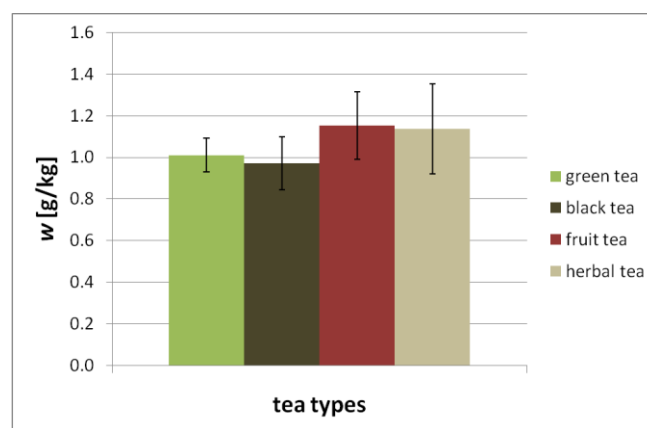
Figure 1. Magnesium contents in the different teas types

Especially regarding fruit and herbal tea it can be assumed that the tendency of accumulation of a certain element strongly depends on the plant species.

Conclusions

The present investigation of various tea types did not reveal statistically significant differences between them. Real tea types (black and green) as well as herbal and fruit tea powders contain about 1 g kg^{-1} magnesium. These results are in the same of order of magnitude as data in tea leaves and medicinal herbals reported in literature.

Further studies will enlarge the data basis of metal concentrations in tea powders and tea infusions. Furthermore a correlation study between magnesium and other elements as well as with organic compounds present in the different tea types is planned.

References

[1]Karak, T., Bhagat, R.M., *Food Res. Int.*, **2010**, *43*, 2234–2252.

[2]Powell, J. J., Burden, T. J., Thompson, R. P. H., *Analyst*, **1998**, *123*, 1721-1724.

[3]Xie, M., Bohlen, A., Klockenkämper, R., Jian, X., Günther, K., *Z. Lebensm. Unters. For.,* **1998**, *A207*, 31–38.

[4]Prystai, E.A., Kies, C.V., Driskell, J.A., *Nutr. Res.*, **1999**, *19*, 167-177.

[5]Lukaski, H.C., *Nutrition*, **2004***, 20,* 632-644..

[6]Pugh, R.E., Dick, D.G., Fredeen, A.L., *Ecotox. Environ. Safety*, **2002**, *52*, 273-279.

[7]Street, R., Drabek, O., Szakova,, J., Mladkova, L., *Food Chem..*, **2007**, *104*, 1662–1669.

[8]Pohl, P., Prusisz, B., *Talanta*, **2006**, *69*, 1227-1233.

[9]Gallaher, R.N., Gallaher, K., Marshall, A.J., Marshall, A.C., *J. Food Comp. Anal.*, **2006**, *19,* S53–S57.

[10]McKenzie, J.S., Jurado, J.M., de Pab, F., *Food Chem.*, **2010**, *123*, 859-864

[11]Basgel, S., Erdemoglu, S.B., *Sci. Tot. Environ.*, **2006**, *359,* 82-89.

[12]Łozak, A., Sołtyk, K., Ostapczuk,P., Fijałek, S., *Sci. Tot. Environ.*, **2002**, *289,* 33-40.

[13]Juranovic Cindric, I. Zeiner, M., Glamuzina, E., Stingeder, G., *Microchem. J.*, **2012**, doi:10.1016/j.microc.2012.06.013

AN OVERVIEW ON SYNTHETIC METHODS OF ISOPROPYL CHLOROACETATE

Liu Shu[a]*and You Hongjun[b]

Keywords: overview; synthetic study; isopropyl chloroacetate; catalysts

Nowadays a lot of synthetic methods of isopropyl chloroacetate using different catalysts such as sulfonic acids (p-toluene-sulfonic acid and amino-sulfonic acid), inorganic metal salts of organic sulfonates ($Ce(CH_3SO_3)_3 \cdot H_2O$, $Ca(CH_3SO_3)_2 \cdot 2H_2O$, $Al(CH_3SO_3)_3 \cdot 4H_2O$, $Zn(CH_3SO_3)_2 \cdot 4H_2O$, $La(CH_3SO_3)_3 \cdot 4H_2O$, $Cu(CH_3SO_3)_2 \cdot 4H_2O$, $Zn(p-CH_3C_6H_4SO_3)_2 \cdot 5H_2O$, $Zn(C_6H_5SO_3)_2 \cdot 6H_2O$, $CH_3(CH_2)_{11}SO_3Na$ and $(CH_3(CH_2)_{11}SO_3)_3Fe$), ionic liquids ($[(CH_2)_4SO_3HPy]HSO_4$ and $[C_1imCH_2COOH]HSO_4$), inorganic salts ($Ce(SO_4)_3 \cdot 4H_2O$, $NaHSO_4$, $KHSO_4$, $[Fe_2(OH)_n(SO_4)_{3-n/2}]_m$, $CPVC-FeCl_3$, $NH_4Fe(SO_4) \cdot 12H_2O$, $PVC-FeCl_3$, $FeCl_3 \cdot 6H_2O$ and $SnCl_4$), PCl_3, heteropolyacids ($H_3PO_{40}W_{12} \cdot xH_2O$ and $TiSiW_{12}O_{40}/TiO_2$), solid superacids ($SO_4^{2-}- Fe_2O_3$, SO_4^{2-}/TiO_2-La^{3+}, SO_4^{2-}/TiO_2, SO_4^{2-}/TiO_2-Sm^{3+}, $SO_4^{2-}—NiO$, SO_4^{2-}/TiO_2-Nd^{3+}, $SO_4^{2-}- Al_2O_3$, SO_4^{2-}/TiO_2-Gd^{3+} and SO_4^{2-}/TiO_2-Ce^{3+}) and inorganic salts of organic acids ($Nd(CF_3COO)_3$) have been reviewed in the present paper. The yields of isopropyl chloroacetate are improved by the addition of above catalysts. These methods are having the advantages of simple process and low investment costs.

* Corresponding Author
    Fax: 86-24-56860869
    E-Mail: youhongjun@hotmail.com
[a]   Liaoning Shihua University, Fushun, Liaoning, P.R. China.
[b]   SAIT Polytechnic, Calgary AB, Canada.

Introduction

Isopropyl chloroacetate is one of the important organic chemical materials, intermediates and a colourless liquids. It is used as an organic solvent or as a synthetic medicine. Its molecular formula, boiling point, relative density (25 °C), refractive index n_D^{20} and flash point are $C_5H_9O_2Cl$, 149.5 °C, 1.0812, 1.0423 and 56 °C,[1] respectively. The demands for isopropyl chloroacetate have gradually increased in the country like *China*. It is used mainly in pharmaceutical industries to synthesize non-steroid anti-inflammatory drug such as naproxen and ketoprofen, etc. It is beneficial for industrial processes to use isopropyl chloroacetate instead of ethyl chloroacetate.[2] Concentrated sulphuric acid is one of the main catalysts, but apart from several advantages, such as more secondary reaction taking place, low yield and purity of isopropyl chloroacetate, it has a lot of disadvantages also. Lot of waste water is discharged during the process causing severe environmental pollution problem and at the same time equipments are corroded. [3]

In the present paper, different catalysts such such as sulfonic acids (p-toluene-sulfonic acid and   amino-sulfonic acid), inorganic metal salts of organic sulfonates ($Ce(CH_3SO_3)_3 \cdot H_2O$, $Ca(CH_3SO_3)_2 \cdot 2H_2O$, $Al(CH_3SO_3)_3 \cdot 4H_2O$, $Zn(CH_3SO_3)_2 \cdot 4H_2O$, $La(CH_3SO_3)_3 \cdot 4H_2O$, $Cu(CH_3SO_3)_2 \cdot 4H_2O$, $Zn(p-CH_3C_6H_4SO_3)_2 \cdot 5H_2O$, $Zn(C_6H_5SO_3)_2 \cdot 6H_2O$, $CH_3(CH_2)_{11}SO_3Na$ and $(CH_3(CH_2)_{11}SO_3)_3Fe$), ionic liquids ($[(CH_2)_4SO_3HPy]HSO_4$ and $[C_1imCH_2COOH]HSO_4$), inorganic salts ($Ce(SO_4)_2 \cdot 4H_2O$, $NaHSO_4$, $KHSO_4$, $[Fe_2(OH)_n(SO_4)_{3-n/2}]_m$, $CPVC-FeCl_3$, $NH_4Fe(SO_4) \cdot 12H_2O$, $PVC-FeCl_3$, $FeCl_3 \cdot 6H_2O$, $SnCl_4$), PCl_3, heteropolyacids ($H_3PO_{40}W_{12} \cdot xH_2O$ and $TiSiW_{12}O_{40}/TiO_2$), solid superacids ($SO_4^{2-}- Fe_2O_3$, SO_4^{2-}/TiO_2-La^{3+}, SO_4^{2-}/TiO_2, SO_4^{2-}/TiO_2-Sm^{3+}, $SO_4^{2-}—NiO$, SO_4^{2-}/TiO_2-Nd^{3+}, $SO_4^{2-}- Al_2O_3$, SO_4^{2-}/TiO_2-Gd^{3+} and SO_4^{2-}/TiO_2-Ce^{3+}) and inorganic salts of organic acids ($Nd(CF_3COO)_3$) have been discussed.

DISCUSSION

Sulfonic acids as catalysts to produce isopropyl chloroacetate

Shi Lei[4] introduced the preparation of isopropyl chloroacetate and the effect of the reaction conditions on its yield. In microwave conditions, using p-toluene-sulfonic acid as a catalyst and chloroacetic acid and isopropanol as feedstocks, isopropyl chloroacetate was produced. The optimum conditions were the reaction time (0.75 hours) and the weight ratio of p-toluene-sulfonic acid to chloroacetic acid (11.11%). The maximum yield and purity of isopropyl chloroacetate were 78.3% and 99.8%, respectively. The experimental results indicated that out of a few catalysts tested the performance of p-toluene-sulfonic acid was good enough. The secondary reaction almost did not take place at all. It was also observed that equipment corrosion and environmental pollution by p-toluene-sulfonic acid was less than that of concentrated sulphuric acid. Therefore, p-toluene-sulfonic acid was one of the good catalysts and replaced the concentrated sulphuric acid.

Jing Boyi [5] described the synthetic method of isopropyl chloroacetate and studied that the different conditions had also an effect on its yield. Using amino-sulfonic acid as a catalyst and chloroacetic acid and isopropanol as feedstocks synthesised isopropyl chloroacetate. The experimental results indicated that the best conditions were that the reaction time, the molar ratio of chloroacetic acid to isopropanol and the amount of amino-sulfonic acid were 2.5 hours, 1.0:1.3 and 2.65% of chloroacetic acid weight, respectively. The maximum yield of isopropyl chloroacetate was 85.0%. Amino-sulfonic acid showed a good catalytic performance in the process, further it has an advantage to be controlled easily in the reaction process and proved to be a good, stable and solid catalyst.

Inorganic metal salts of organic sulfonates as catalysts to generate isopropyl chloroacetate

Table 1 showed that different inorganic metal salts of organic sulfonates, such as $Ce(CH_3SO_3)_3 \cdot H_2O$, $Ca(CH_3SO_3)_2 \cdot 2H_2O$, $Al(CH_3SO_3)_3 \cdot 4H_2O$, $Zn(CH_3SO_3)_2 \cdot 4H_2O$, $La(CH_3SO_3)_3 \cdot 4H_2O$,

$Cu(CH_3SO_3)_2 \cdot 4H_2O$, $Zn(p-CH_3C_6H_4SO_3)_2 \cdot 5H_2O$, $Zn(C_6H_5SO_3)_2 \cdot 6H_2O$, $CH_3(CH_2)_{11}SO_3Na$ and $(CH_3(CH_2)_{11}SO_3)_3Fe$, had an effect on the yield of isopropyl chloroacetate. Methanesulfonate included $Ce(CH_3SO_3)_3 \cdot H_2O$, $Ca(CH_3SO_3)_2 \cdot 2H_2O$, $Al(CH_3SO_3)_3 \cdot 4H_2O$, $Zn(CH_3SO_3)_2 \cdot 4H_2O$, $La(CH_3SO_3)_3 \cdot 4H_2O$, $Cu(CH_3SO_3)_2 \cdot 4H_2O$. They almost had the same construction, but only had the different metal element. The experimental results showed that the yield of isopropyl chloroacetate had big difference. This maybe related with their metal performance such as metal activity. The higher the metal activity is in the reactivity series, the higher the yield of

isopropyl chloroacetate became. Organic sulfonic acid zinc consisted of $Zn(p-CH_3C_6H_4SO_3)_2 \cdot 5H_2O$, and $Zn(C_6H_5SO_3)_2 \cdot 6H_2O$. Their catalytic performance was very poor because the yield of isopropyl chloroacetate was very low. Sodium dodecyl sulfate and iron dodecyl sulphate had the same results like methanesulfonate. Sodium activity was more than that of iron so the yield of isopropyl chloroacetate with additional use of sodium dodecyl sulphate was more than that of iron dodecyl sulphate. $Ce(CH_3SO_3)_3 \cdot H_2O$ was one of the best catalysts in inorganic metal salts of organic sulfonates based on the above review.

Table 1. The effect of different inorganic metal salts of organic sulfonates on the yields of isopropyl chloroacetate

Catalyst	Chloroacetic acid/ isopropanol ratio	Weight ratio of catalyst to chloro- acetic acid (%)	Reaction time (hours)	Yield of isopropyl chloro- acetate	Reference
$Ce(CH_3SO_3)_3 \cdot H_2O$	1:1.1	1.0	2.5	98.6	6
$Ca(CH_3SO_3)_2 \cdot 2H_2O$	1:1.2	1.0	2.5	98.1	7
$Al(CH_3SO_3)_3 \cdot 4H_2O$	1:1.2	1.0	2.5	96.8	8
$Zn(CH_3SO_3)_2 \cdot 4H_2O$	1:1.2	1.0	2.5	92.7	9
$La(CH_3SO_3)_3 \cdot 4H_2O$	1:1.2	1.0	2.5	88.7	10
$Cu(CH_3SO_3)_2 \cdot 4H_2O$	1:1.2	1.0	2.5	75.3	10
$Zn(p-H_3C_6H_4SO_3)_2 \cdot 5H_2O$	1:1.2	1.0	2.5	74.9	9
$Zn(C_6H_5SO_3)_2 \cdot 6H_2O$	1:1.2	1.0	2.5	73.2	9
$CH_3(CH_2)_{11}SO_3Na$	1:1.2	1.0	2.5	97.2	11
$(CH_3(CH_2)_{11}SO_3)_3Fe$	1:1.3	2.0	1.0	86.7	12

Table 2. The effect of different inorganic salts on the yield of isopropyl chloroacetate

Catalyst	chloroacetic acid/ isopropanol ratio	Weight ratio of catalyst to chloroacetic acid (%)	Reaction time (Hours)	Yield of isopropyl chloroacetate	Reference
$Ce(SO_4)_3 \cdot 4H_2O$	1.0:1.3	3.5	3.0	97.5	15
$NaHSO_4$	1.0:1.2	1.0	3.0	97.1	16
$KHSO_4$	1.0:1.3	17.6	2.5	87.4	17
$[Fe_2(OH)_n(SO_4)_{3-n/2}]_m$	1.0:2.0	3.8	6.0	84.9	18
$CPVC-FeCl_3$	1.0:2.0	21.2	2.5	81.8	19
$NH_4Fe(SO_4).12H_2O$	1.0:1.3	10.6	4.0	81.4	20
$PVC-FeCl_3$	1.0:2.0	10.5	2.5	80.3	21
$FeCl_3 \cdot 6H_2O$	1.0:2.0	5.3	2.5	80.0	22
$SnCl_4$	1.0:1.6	4.6	4.0	77.0	23

Ionic liquids as catalysts to produce isopropyl chloroacetate

Zhu Xaingqin [13] described the synthetic method of isopropyl chloroacetate by using $[(CH_2)_4SO_3HPy]HSO_4$ as a catalyst. The effect of the reaction conditions such as the reaction time, temperature, molar ratio of ionic liquid to chloroacetic acid and isopropanol, the amount of ionic liquid and the number of reusable catalyst had been discussed. The best conditions were that the reaction time, the reaction temperature, the molar ratio of ionic liquid to chloroacetic acid to isopropanol and the number of reusable catalyst were 4 hours, 60 °C, 1.0:5.0:5.0 and 5 times respectively. The maximum yield of isopropyl chloroacetate was 91.0%. After recovery and reuse of $[(CH_2)_4SO_3HPy]HSO_4$ as a catalyst, it was noticed that its catalytic performance was very good. For example, when $[(CH_2)_4SO_3HPy]HSO_4$ was reused 5 times, the yield of isopropyl chloroacetate still reached 89.0%.

Wang Chan [14] explained why $[C_1imCH_2COOH]HSO_4$ as a catalyst replaced concentrated sulfuric acid to synthesise isopropyl chloroacetate. The effect of the reaction conditions such as the reaction time, the reaction temperature, the molar ratio of ionic liquid to chloroacetic acid to isopropanol and the number of reusable catalyst had been discussed. The experimental results indicated that the best conditions were that the reaction time, the reaction temperature, the molar ratio of ionic liquid to chloroacetic acid to isopropanol and the number of reusable catalyst were 3 hours, 60 °C, 1.0:5.0:5.0 and 5 times, respectively.

The maximum yield of isopropyl chloroacetate was 90.6%. When $[C_1imCH_2COOH]HSO_4$ as a catalyst was recovered and reused, their catalytic performance was found to be very good. For example, when $[C_1imCH_2COOH]HSO_4$ was reused 5 times, the yield of isopropyl chloroacetate still reached 89.1%.

Inorganic salts as catalysts to generate isopropyl chloroacetate

Table 2 presented the effect of different inorganic salts on the yield of isopropyl chloroacetate such as $Ce(SO_4)_3 \cdot 4H_2O$, $NaHSO_4$, $KHSO_4$, $[Fe_2(OH)_n(SO_4)_{3-n/2}]_m$, $CPVC\text{-}FeCl_3$, $NH_4Fe(SO_4) \cdot 12H_2O$, $PVC\text{-}FeCl_3$, $FeCl_3 \cdot 6H_2O$ and $SnCl_4$. Different inorganic salt had different catalytic performance. This did not follow any rules. $Ce(SO_4)_3 \cdot 4H_2O$ and $NaHSO_4$ were two of the best catalysts in inorganic salt used so far. Furthermore, their yields reached more than 97.0%. On the other hand, $SnCl_4$ was found to be one of the worst catalysts in inorganic salts. Its yield only arrived at 77.0%. PCl_3 as a catalyst to produce isopropyl chloroacetate

Liang Chungen [24] described the synthetic method of isopropyl chloroacetate by using PCl_3 as a catalyst. The effect of the reaction conditions such as the amount of n-butanol, the molar ratio of chloroacetic acid to isopropanol and the amount of catalyst had been discussed. The best conditions were that the amount of isopropanol, the molar ratio of chloroacetic acid to isopropanol and the amount of PCl_3 were 0.35 mol, 1.0:1.4 and 6.65% of chloroacetic acid weight, respectively. The maximum yield of isopropyl chloroacetate was 89.5%.

Heteropolyacids as catalysts to generate isopropyl chloroacetate

Liu Xinhe [25] studied the preparation of heteropolyacids $(H_3PO_{40}W_{12}.xH_2O)$ and the effect of the reaction conditions such as the molar ratio of chloroacetic acid to isopropanol and the amount of catalyst on the yield of isopropyl chloroacetate. The best conditions were that the molar ratio of chloroacetic acid to isopropanol and the amount of $H_3PO_{40}W_{12}.xH_2O$ were 1 hour, 1.0:1.4 and 2.12% of chloroacetic acid weight,

respectively. The maximum yield of isopropyl chloroacetate was 87.2%.

Yang Shuijin [26] used $TiSiW_{12}O_{40}/TiO_2$ as a catalyst to produce isopropyl chloroacetate. The effect of the reaction conditions such as the reaction time, the molar ratio of chloroacetic acid to isopropanol and the amount of catalyst had been discussed. The best conditions were the reaction time, the molar ratio of chloroacetic acid to isopropanol and the amount of $TiSiW_{12}O_{40}/TiO_2$ were 2.0 hours, 1.0:1.3 and 1.5% of total reactant weight, respectively. The maximum yield of isopropyl chloroacetate was 73.3%.

Solid superacids as catalysts to produce isopropyl chloroacetate

Table 3 showed that different solid superacids had an effect on the yield of isopropyl chloroacetate such as $SO_4^{2-}\text{-}Fe_2O_3$, $SO_4^{2-}/TiO_2\text{-}La^{3+}$, SO_4^{2-}/TiO_2, $SO_4^{2-}/TiO_2\text{-}Sm^{3+}$, $SO_4^{2-}\text{—}NiO$, $SO_4^{2-}/TiO_2\text{-}Nd^{3+}$, $SO_4^{2-}\text{-}Al_2O_3$, $SO_4^{2-}/TiO_2\text{-}Gd^{3+}$ and $SO_4^{2-}/TiO_2\text{-}Ce^{3+}$. The catalysts had the same acid active centre, but it had the different load such as $SO_4^{2-}\text{-}Fe_2O_3$, $SO_4^{2-}\text{—}NiO$ and $SO_4^{2-}\text{-}Al_2O_3$.

The experimental results showed that Fe_2O_3 was one of the best loads because acid was evenly distributed on its surface, so the yield of isopropyl chloroacetate was very high. On the other hand, the catalyst had the same acid active centre, however it had the different metals such as $SO_4^{2-}/TiO_2\text{-}La^{3+}$, SO_4^{2-}/TiO_2, $SO_4^{2-}/TiO_2\text{-}Sm^{3+}$, $SO_4^{2-}/TiO_2\text{-}Nd^{3+}$, $SO_4^{2-}/TiO_2\text{-}Gd^{3+}$ and $SO_4^{2-}/TiO_2\text{-}Ce^{3+}$. This phenomenon maybe related with their metal acidity. Higher the metal acidity, higher the yield of isopropyl chloroacetate observed.

Table 3. effect of different t solid super acid on the yield of isopropyl chloroacetate

Catalyst	Chloroacetic acid/ isopropanol ratio	Weight ratio of catalyst to chloroacetic acid (%)	Reaction time (hours)	Yield of isopropyl chloroacetate	Reference
$SO_4^{2-}\text{-}Fe_2O_3$	1.0:3.0	4.0	4.0	91.6	27
$SO_4^{2-}\text{-}NiO$	1.0:3.0	3.8	5.0	84.8	28
$SO_4^{2-}\text{-}Al_2O_3$	1.0:3.0	3.4	4.0	81.8	29
$SO_4^{2-}/TiO_2\text{-}La^{3+}$	1.0:3.0	4.5	4.0	90.7	30
$SO_4^{2-}/TiO_2\text{-}Sm^{3+}$	1.0:3.0	4.5	4.0	86.6	30
$SO_4^{2-}/TiO_2\text{-}Nd^{3+}$	1.0:3.0	4.5	4.0	84.5	30
$SO_4^{2-}/TiO_2\text{-}Gd^{3+}$	1.0:3.0	4.5	4.0	81.3	30
$SO_4^{2-}/TiO_2\text{-}Ce^{3+}$	1.0:3.0	4.5	4.0	74.3	30

Organic salts as catalysts to generate isopropyl chloroacetate

Lai Junling [2] used $Nd(CF_3COO)_3$ as a catalyst to generate isopropyl chloroacetate. The effect of the reaction conditions such as the reaction time, the molar ratio of chloroacetic acid to isopropanol and the amount of $Nd(CF_3COO)_3$ had been discussed. The best conditions were that the reaction time, the molar ratio of chloroacetic acid to isopropanol and the amount of $Nd(CF_3COO)_3$ were 0.75 hours, 1.0:1.2 and 3.17% of chloroacetic acid weight, respectively. The maximum yield of isopropyl chloroacetate was 91.2%.

CONCLUSION

Based on the above discussion and review, $Ce(CH_3SO_3)_3 \cdot H_2O$ is found to be one of the best catalysts. It is used to produce the highest isopropyl chloroacetate yields (98.6%). However, due to costly chemical, $Ce(CH_3SO_3)_3 \cdot H_2O$ as a catalyst, it was not included as a good choice. Due to the economic viability $NaHSO_4$ is used as a good catalyst, though its yield of isopropyl chloroacetate (97.1%) is less than that of $Ce(CH_3SO_3)_3 \cdot H_2O$. $NaHsO_4$ is still popular because it is very cheap, stable and insoluble in organic acids and organic alcohol. After the reaction is over, $NaHSO_4$ becomes insoluble material and is

easily separated from the reaction system. It has high catalytic and selectivity performance. On the other hand, $TiSiW_{12}O_{40}/TiO_2$ is found to be one of the worst catalysts and its maximum yield of isopropyl chloroacetate only reaches 73.3%.

REFERENCES

[1] You, H. J. *J Liaoning Univ. Petrol. Chem. Technol.*, **2004**, *24*(3), 35.

[2] Lai, J. L., Cheng, Y. L., Liu, C. S. and Luo, G. X. *Chem. Agents*, **2009**, *31(3)*, 197.

[3] Gao, X. H., Gao, J., Zhang, H. F. and Lin, L. *Chem. Ind. Eng.*, **2011**, *28(6)*, 6.

[4] Shi, L., Wu, D. H., Su, G. J. and Wu, D. H. *Fine Chemical Intermediates*, **2003**, 33(3), 37.

[5] Jing, B. Y. *Journal of Hetao University*, **2007**, 4(2), 33.

[6] Wang, M., Jiang, H., Gong, H. and Su, T. T. *Fine Chemical Intermediates*, **2004**, 34(4), 36.

[7] Wang, M., Jiang, H., Gong, H., Su, T. T. and Liu, L. J. *Chemical Agents*, **2004**, 26(4), 201.

[8] Wang, M., Jiang, H., Gong, H., Wang, R. and Liu, L. J. *Science & Technology in Chemical Industry*, **2003**, 11(5), 40.

[9] Ma, J. Wang, X. K., Jiang, H., Gong, H. and Wang, R. *Science & Technology in Chemical Industry*, **2005**, 13(1), 49.

[10] Wang, M., Tian, J. J., Liu, L., J. Jiang, H., Gong, H. and Su, T. T. *Chinese Journal of Inorganic Chemistry*, **2003**, 19(7), 731.

[11] Xu, J. S., Wang, M. Jiang, H., Gong, H. and Wang, R. *Journal of Fudan University*, **2003**, 42(3), 329.

[12] Li, X. O., Liu, C. S. Huang, Z. K. and Luo, G. X. *Journal of Liaoning Shihua University*, **2004**, 24(1), 26.

[13] Zhu, X. Q., Gui, J. Z., Liu, D., Zhang, X. T., Song, L. J. and Sun, Z. L. *Industrial Catalysts*, 2006, 14(11), 33.

[14] Wang, C. and Yan, Y. L. *Science & Technology in Chemical Industry*, **2010**, 18(2), 38.

[15] Yang, L. Z., Chu, L. F., Li, F. and Zhang, D. H. *Speciality Petrochemicals*, **2000**, 3, 27.

[16] Zhang, J. Xu, J. S. and Qian, J. H. *Science Technology and Engineering*, **2011**, 11(11), 2519.

[17] Liu, G. H., Zhu, X. R., Chu, K. H. and Qian, Y. *Chemical World*, **2002**, 3, 153.

[18] Du, Q. Y., Shen, Y. Y. and Guo, X. M. *Speciality Petrochemicals*, **2000**, 2, 17.

[19] Wang, C. R., Yu, S. X. and Zeng, Y. *Journal of Gansu Education College*, **2000**, 14(1), 34.

[20] Li, Y. Q. *Chemical World*, **1998**, 9, 482.

[21] Ping, W. J. and Yu, S. X. *Journal of Hunan Light Industry College*, **1999**, 1(2), 7.

[22] Yu, S. X., Zhao, Z. B. and Peng, X. Z. *Journal of Hunan Normal University*, **1995**, 18(4), 31.

[23] Wu, D. H., Luo, J. and Yang, X. J. *Synthetic Chemistry*, **2001**, 9(4), 347.

[24] Liang, C. G., Lin, Y. B. and Shen, D. S. *Natural Science Journal of Xiantan Univeristy*, **1997**, 19(2), 49.

[25] Liu, X. H. *Journal of Shenyang Institute of Chemical Technology*, **2000**, 14(4), 313.

[26] Yang, S. J., Yu, X. Q. and Liang, Y. G. *Advances in Fine Petrochemicals*, **2000**, 12(1), 1.

[27] Jiang, S. B., Liao, G. Y., Qu, X. L. and She, W. N. *Chemical Engineering*, **2001**, 5, 6.

[28] Jiang, S. B., Liao, G. Y., She, W. N and Qu, X. L. *Petrochemical Technology & Application*, **2001**, 19(4), 238.

[29] Jiang, S. B., Liao, G. Y., Qu, X. L. and She, W. N. *Chemical World*, **2001**, 42(1), 368.

[30] Li, D. J. and Fu, H. Q. *Science & Technology in Chemical Industry*, **2005**, 13(3), 20.

CALORIMETRIC DETERMINATION OF PHOSPHOLIPID-MELITTIN INTERACTIONS

Linus N. Okoro

The effect of melittin incorporated into the phospholipid bilayer of 1,2-dipalmitoyl-*sn*-glycero-3-phosphocholine (DPPC) at mole fractions up to 3.75 mol% have been investigated. The study reveals a considerable influence of melittin on the phase transition profile and volumetric properties of the DPPC bilayer. The temperature dependence of the coefficient of expansion, α, and the volume fluctuations of DPPC – melittin bilayer membranes in their different transition phases were determined by using pressure perturbation calorimetry (PPC), a relatively new and efficient technique, and differential scanning calorimetry (DSC). The experiments were carried out in the temperature range from 10 to 85 °C. Incorporating melittin up to 1.25 mol% into the lipid bilayer abolishes the pretransition. Remarkably, there is no shift in the transition temperature up to 2.5 mol% melittin, while more than one shoulder is observed at the low-temperature side of the DSC peak for 3.75 mol%, and a slight shift in melting temperature, T_m to 32°C. This could be linked to the lytic property of melittin at these high peptide concentrations.

* Corresponding Authors
　　E-Mail: linus.okoro@aun.edu.ng
[a]　American University of Nigeria, Lamido Zubairu Way, Yola, Adamawa State, Nigeria

Introduction

Melittin

Melittin constitutes 50% of the dry weight of the honeybee venom. The active peptide melittin is released from its precursor, promelittin, during its biosynthesis in honey bee and later gets formylated.[1] It is a peptide composed of 26 amino acids (NH2-G-I-G-A-V-L-K-V-L-T-T-G-L-P-A-L-I-S-W-I-K-R-K-R-Q-Q-CONH2) with no disulphide bridge, the N-terminal region (residues 1–20) is predominantly hydrophobic and the C-terminal region (residues 21–26) is hydrophilic due to the presence of a stretch of positively charged amino acids. Melittin is water soluble due to its amphiphilic property and yet it spontaneously associates with both natural and artificial membranes.[2] The crystal structures of melittin have been resolved by X-ray crystallography.[3] It has been observed that in an aqueous solution of high peptide concentration, high pH value, or high ionic strength, tetrameric melittin of high symmetry is formed readily.[2]

Lipid – Melittin Interaction

Melittin causes bilayer micellization and membrane fusion and has also been observed to form voltage-dependent ion channels across planar lipid bilayers.[4,5] The characteristic action of melittin is its hemolytic activity.[6,7] It is commonly believed and accepted that multimeric pore formation is the mode of action of many naturally produced peptides such as antimicrobial peptides and toxins.[8,9] The structure and function of such pores and their results show that melittin forms pores that have a rather wide distribution of sizes. For example, the sizes of the melittin pores that are characterized by the inner pore diameter have been reported to be in the range of 10–60 A°, 13–24 A° and 25–30 A° from vesicle leakage experiments.[8] The diameter of these pores is expected to increase when the peptide concentration is increased.

Under certain conditions, melittin molecules insert into the lipid bilayer and form multiple aggregated forms that are controlled by temperature, pH, ionic strength, lipid composition and the lipid-to-peptide ratio. It has been observed that lipid composition and phase separation appears to play a critical role in melittin-induced pore formation. The action of melittin on membrane proteins has been studied and apart from its ability to disrupt lipid bilayers, melittin affects the dynamics of membrane proteins. For instance, it has been reported that lytic concentrations of melittin dramatically reduce the rotational mobility of band 3 protein in human erythrocyte membranes.[10,11]

Further DSC study has revealed membrane fusion between liposomes composed of acidic phospholipids and neutral phospholipids induced by melittin, in which the roles of hydrophobic and electrostatic interactions were investigated in membrane fusion induced by melittin.[12]

In this study, we investigated the influence of melittin incorporation on the thermodynamic and equilibrium volumetric properties of the 1,2-Dipalmitoyl-*sn*-glycero-3-phosphocholine (DPPC) bilayer membrane. To accomplish this, pressure perturbation calorimetry (PPC) has been used to determine the temperature dependence of the coefficient of expansion coefficient, α, as well as volume changes accompanying lipid phase transitions. DSC thermogram was also recorded to show the temperature-dependent phase changes.

Materials and methods

Sample Preparation

Multilamellar vesicles preparation for calorimetric studies

1,2-Dipalmitoyl-*sn*-glycero-3-phosphocholine (DPPC) was obtained from Avanti Polar Lipids (Alabaster, AL). Melittin

(≥97% purity) as a lyophilized solid was obtained from Calbiochem (Germany). Both samples were used without further purification. Multilamellar vesicles (MLV) of DPPC and melittin with designated mole ratios were mixed in a chloroform-methanol mixture (3:1 v/v) and dried as a thin film under a stream of nitrogen and then freeze-dried in a freeze-dryer (Christ, Osterode, Germany) under high vacuum overnight. The lipid films were hydrated in a Tris buffer (10 mM Tris-HCl, 100 mM NaCl, pH 7.4), followed by vortexing at ~62°C (above the main phase transition temperature, T_m, of DPPC (~41.5°C [Cevc 1987]), and five freeze-thaw cycles, resulting in homogeneous multilamellar vesicles (MLVs). The final DPPC concentration used in the calorimetric measurements was 5 mg/ml.

Calorimetric measurements

Differential scanning calorimetry

Pressure perturbation calorimetry and differential calorimetry measurements were performed with a MicroCal (Northampton, USA) VP-DSC micro-calorimeter, equipped with a pressurizing system from the same manufacturer.

The reference cell was filled with the Tris buffer solution. Both buffer and sample solutions were degassed before being injected into the respective cells. Included in the standard VP-DSC instrument is a pressuring cap that allows application of 1.8 bars to the cells in order to avoid air bubbles at elevated temperatures. The instrument was operated in the high gain mode at a scanning rate of 40 °C h^{-1}. Baseline subtraction (pure buffer) and normalization with respect to scan rate and concentration were performed by the instrument software, yielding the temperature-dependent apparent (excess) molar heat capacity of the vesicles, C_p, with respect to the buffer solution.

Pressure perturbation calorimetry (PPC)

Pressure perturbation calorimetry (PPC) measurements were carried out on the VP-DSC calorimeter equipped with MicroCal's (Northampton, MA, USA) PPC accessory. A description of the technique and its potential applications is placed elsewhere [37-43].This method enables the measurement of heat effects induced by small periodic changes of gas pressure ($\Delta p = \pm 5$ bar) above the solution.[13-16] The physical principle is the same as in a heat-induced thermal expansion, although the measurable is ΔQ - the heat released upon a pressure change of Δp at temperature T. Three control and calibration measurements were performed, namely water (sample cell) versus water (reference cell), buffer versus water and buffer versus buffer. The results of these control experiments were fit by second-order polynomials and were used for the evaluation of the coefficient of thermal expansion α (T) of the measured system (fig. 1). From the relative volume changes $\Delta V/V$, the absolute volume changes ΔV can be determined when the specific volume and the molar mass of the sample are known.[17]

Knowing the thermal expansion coefficient of the solvent, α_0, mass, m, and partial specific volume of the solute, V_s, through a series of reference measurements, one can calculate the apparent thermal expansion coefficient of the dissolved particles.
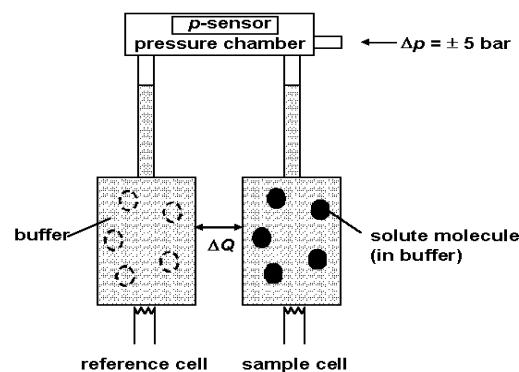
Figure 1. Schematic diagram of PPC describing the measurement curves and the derived thermodynamic parameters (*Microcal user note, 2000*).

Theory

The basic theory of pressure perturbation calorimetry is outlined below:

The heat of a reversible process, dQ_{rev}, is related to the entropy change, dS, at the temperature T.

$$dQ_{rev} = TdS \qquad (1)$$

Differentiation with respect to pressure, p, yields

$$\left(\frac{\partial Q_{rev}}{\partial p}\right)_T = T\left(\frac{\partial S}{\partial p}\right)_T \qquad (2)$$

From $dG = Vdp - SdT$, it follows that

$$\left(\frac{\partial S}{\partial p}\right)_T = -\left(\frac{\partial V}{\partial T}\right)_p \qquad (3)$$

Eqn. (2) can thus be rewritten as

$$\left(\frac{\partial Q_{rev}}{\partial p}\right)_T = -T\left(\frac{\partial V}{\partial T}\right)_p \qquad (4)$$

The thermal expansion coefficient of volume V is defined as

$$\alpha_v = \frac{1}{V}\left(\frac{\partial V}{\partial T}\right)_p \qquad (5)$$

and can thus be determined from an isothermal measurement of the heat consumed or released upon a small pressure change:

$$\alpha_v = -\frac{\Delta Q_{rev}}{TV\Delta p} \qquad (6)$$

Moreover, the relative volume change $\Delta V/V$ at a phase or structural transition, taking place in the temperature range from T_o to T_e can be obtained by

$$\frac{\Delta V}{V} = \int_{T_O}^{T_e} \alpha(T)\,dT \qquad (7)$$

For two-component systems, such as biopolymer solutions, one has to extend these equations [Lin 2002, Kujawa 2001]. If the sufficiently dilute solution is composed of m_s grams of a solute dissolved in m_0 grams of solvent, the total solution volume V may be expressed as

$$V = m_0 V_0 + m_s \overline{V_s} \qquad (8)$$

where V_0 is the specific volume of the pure solvent, and V_s is the partial specific volume of the solute in the solution. The partial volume of the solute includes not just its intrinsic volume, but also any volume changes induced as a result of interactions with the solvent. Differentiating Eqn. (8) with respect to temperature at constant pressure yields

$$\left(\frac{\partial V_{total}}{\partial T}\right)_p = m_0 \left(\frac{\partial V_0}{\partial T}\right)_p + m_s \left(\frac{\partial \overline{V_s}}{\partial T}\right)_p \qquad (9)$$

and after substituting the right hand side of Eq. (9) into Eq. (4) and (5), we obtain (10)

$$\left(\frac{\partial Q_{rev}}{\partial p}\right)_T = -T\left[m_0\left(\frac{\partial V_0}{\partial T}\right)_p + m_s\left(\frac{\partial \overline{V_s}}{\partial T}\right)_p\right] =$$

$$-T\left[m_0 V_0 \alpha_0 + m_s \overline{V_s}\,\overline{\alpha}_s\right] \qquad (10)$$

where

$$\alpha_0 = (1/V)(\partial V_0 / \partial T)_p$$

is the α of the solvent volume and

$$\overline{\alpha}_s = (1/\overline{V}_s)(\partial \overline{V}_s\,\partial T)_p$$

is the α of the solute partial volume. The heat arising from pressure perturbation of the solution can thus be viewed as the sum of that arising from the perturbation of the solvent and from the perturbation of the solute in solution. Integration of Eqn. (10) over a small pressure range Δp

$$\Delta Q_{rev} = -T\left[m_0 V_0 \alpha_0 + m_s \overline{V_s}\,\overline{\alpha}_s\right]\Delta p \qquad (11)$$

leads to

In a differential PPC experiment, with sample solution in the sample cell and buffer in the reference cell, both cells are subjected to the same Δp so that the net heat change ΔQ_{rev} will be equal to the difference between Eqn. (11) for the sample cell and that for the reference cell. If the cells have an identical volume, then ΔQ_{rev} arises because the volume occupied by the solute in the sample cell, is replaced by solvent in the reference cell, *i.e.*,

$$\Delta Q_{rev} = -T(m_s \overline{V_s}\,\overline{\alpha}_s - m_s \overline{V_s}\,\alpha_0)\Delta p \qquad (12)$$

which then rearranges to

$$\overline{\alpha}_s = \alpha_0 - \frac{\Delta Q_{rev}}{T m_s V_s \Delta p} \qquad (13)$$

where the total mass of solute, m_s, is obtained by multiplying its concentration, c_s [g/mL] with the cell volume, V_{cell} [mL].

Results and discussion

The excess heat capacity (C_p-profiles) of multilamellar vesicle (MLV) suspensions of DPPC with different concentrations of melittin added is displayed in figure 2. The heat capacity trace of pure DPPC displays a maximum at 41 °C, referred to as the main phase transition temperature, T_m. It is also observed that pure DPPC displays a small endothermic peak due to the $L_{\beta'}$-$P_{\beta'}$ pretransition which appears around 35 °C. Overall, the heat capacity increase in the transition regime is mainly due to cooperative fluctuations of a large number of lipid molecules.

When the DPPC liposomes are prepared in the presence of melittin concentrations of 1 to 2.5 %, there is no change in the temperatures of the main transition.

Addition of 1 mol% melittin leads to a reduction of the lipid pre-transition peak. The peak is not completely abolished; however the temperature of the pre-transition shifts slightly to a lower temperature (32°C). The pre-transition is completely abolished at a melittin concentration of 1.25 mol% and at this particular concentration there appears a noticeable base peak broadening, a small asymmetry at the low-temperature wing and a reduction in transition profile which continues to increase with increasing melittin concentration. There is a concomitant reduction in the cooperativity of the chain melting transition, as a result of melittin incorporation, which is evidenced by the broadening of the transition profile. A shoulder (a small peak) appears at the low-temperature side (at 39 °C) of the main transition peak for 2.5 % melittin, with a further reduction of the transition profile and cooperativity.

Additionally, we observe no shift in the main transition temperature up to 2.5 mol% melittin. More than one shoulder is observed at the low-temperature side of the peak for 3.75 mol%, and a slight shift in T_m to 32°C. Oliynyk et al. observed a similar low-temperature shoulder in the C_p-

profile at higher melittin concentrations, in good agreement with our data.[18]
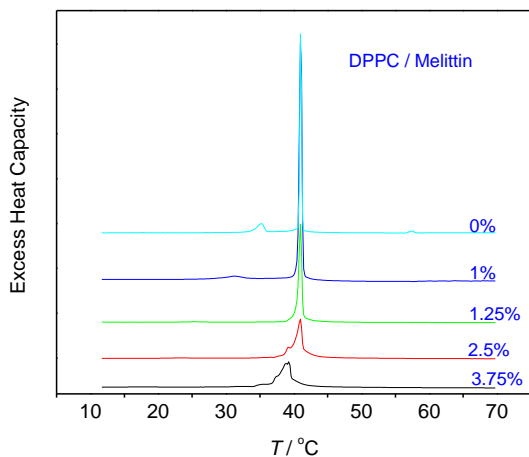
Figure 2. DSC thermograms of melittin in DPPC multilamellar vessicles

The PPC stacked plot of the coefficient of thermal expansivity versus temperature curves of the DPPC melittin mixtures is revealed in figure 3.
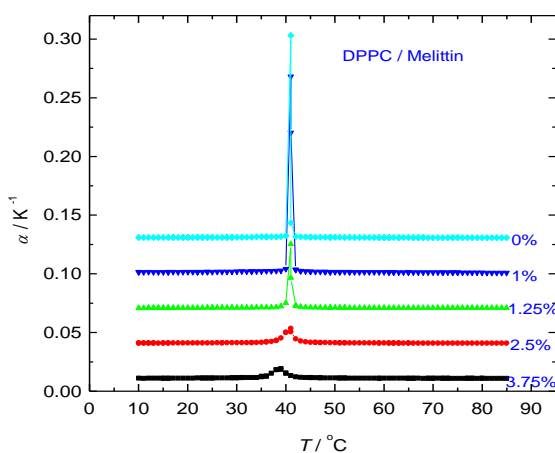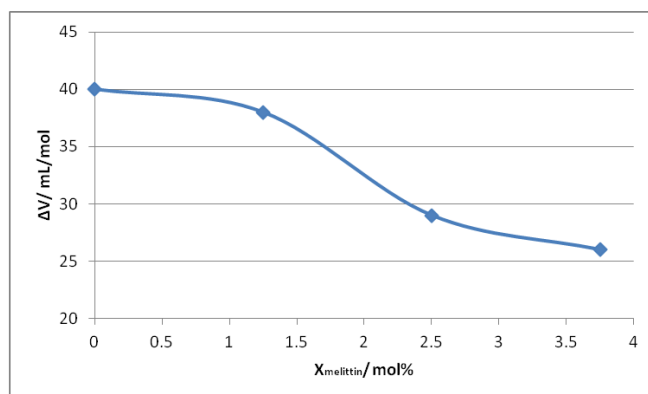

Figure 3. α, of DPPC/Melittin mixture

The PPC scans were carried out with solutions of DPPC/melittin in Tris buffer yielding the changes with temperature of the thermal expansion coefficient, α. The plots can be divided into three temperature regimes. We observe a slight increase in α below the pretransition with increase in melittin concentration, but not in any particular order.

For instance, as reported in our previous publication[14], below the main phase transition temperature of pure DPPC, α increases slightly with increasing temperature. At the main phase transition temperature, α undergoes a rather sharp increase, reaches a maximum of about 0.15 K^{-1} at T_m (41ºC), which then rapidly decreases with increasing temperature, to

reach a value close to that obtained below the transition temperature (α is ~0.9·10^{-3} K^{-1} below the pretransition (20 ºC) and ~1.0·10^{-3} K^{-1} above the main transition (65 ºC)). Similar α values for melittin concentrations 0% and 1% was observed. $\alpha = 1.01 \times 10^{-3}$ K^{-1} for 2.5 mol%, and $\alpha = 1.12 \times 10^{-3}$ K^{-1} for 3.75 mol% at 20ºC. Above T_m (65 ºC), Just below the pretransition, a very slight increase in α, with increase in melittin concentration (as an example, $\alpha = 0.92 \times 10^{-3}$ K^{-1} and $\alpha = 1.02 \times 10^{-3}$ K^{-1} at 65 ºC for 1.25 % and 2.5 % melittin respectively), whereas the main peak height of α in the transition region decreases and broadens markedly with increase in melittin concentration.

Figure 4. Concentration dependence of the absolute volume change, ΔV, of the DPPC/melittin mixtures

From the integration of α over the temperature range where the main transitions occur, we obtain the volume volume changes, ΔV, as shown in figure 4, for the pure DPPC and for each of the DPPC / melittin concentrations. $\Delta V/V = 0.04 \pm 0.007$ (4 %), which corresponds to an absolute volume change of 29 mL/mol, for pure DPPC, $\Delta V/V$ is 0.038 ± 0.001 for 1.25 mol%, 0.029 ± 0.002 for 2.5 mol%, and 0.026 ± 0.002 for 3.75 mol% melittin. The corresponding width of the overall transition, $\Delta T_{1/2}$, increases from about 1 ºC for the main transition of pure DPPC to about 3 ºC for the DPPC / 3.75 mol% melittin mixture.

Conclusion

The study has provided further insights into the disruptive effects of melittin on membrane bilayers having explored the use of calorimetry (pressure perturbation calorimetry and differential scanning calorimetry) to determine the absolute and relative volume change of DPPC – melittin bilayer membranes in their different phases.

We have shown that as the concentration of membrane-bound melittin increases, the relative volume change at the main transition of the lipid bilayer decreases. From the calorimetric measurements, upon incorporation of melittin into the lipid bilayer up to 1.25 %, it is observed that the pretransition is completely abolished. At this particular concentration, we observe a noticeable base peak broadening and a reduction in transition profile which continues with increase in melittin concentration. The appearance of a small endothermic peak at 39 ºC for 2.5 % melittin could possibly reflect morphological changes of free lipid vesicles in solution, the onset of the disruptive effect of melittin in DPPC bilayers. Remarkably, there is no

shift in the transition temperature up to 2.5 %, while more than one shoulder was observed at the low-temperature side of the peak for 3.75 %, and a slight shift in T_m to 32 °C. This implies a disordering effect, which could be attributed to melittin pore formation (disruptive effect), at this higher melittin concentration. At the main transition region, the peak height of α decreases and broadens markedly with increase in melittin concentration.

Peptides in both model and biological membranes have been observed to strongly affect the local state of the system, and the effect of peptide may equally depend on the overall state of the membrane.[18] At the main transition region, the peak height of α decreases and broadens markedly with increase in melittin concentration.

Acknowledgement

REFERENCES

[1]Habermann, E., *Science,* **1972,** *177,* 314-322.

[2]Dempsey, C. E., *Biochim. Biophys. Acta.* **1990**, *1031*, 143-161.

[3]Terwilliger, T.; Weissman L., and Eisenberg, D., *Biophys. J.* **1982**, *37*, 353-361.

[4]Bechinger, B. *J. Membr. Biol.* **1997**, *156*, 197-211.

[5]Monette, M. and Lafleur, M., *Biophys. J.*, **1995**, *68*, 187-195.

[6]Raghuraman H. andChattopadhyay, A., *Chem. Phys. Lipids,* **2005**, *134*, 183-189.

[7]Rudenko S. V. and Patelaros, S. V.. *Biochim. Biophys. Acta,* 1995., 1235, 1-9.

[8]Rex S., *Biophys. Chem.* **1996**, *58*, 75-85.

[9]Allende D., Simon, S. A. and McIntosh, T. J., *Biophys. J..* **2005**, *88*, 1828-1837.

[10]Clague M. J. and Cherry, R. J., *Biochem. J.,* **1988,** *252*, 791-794.

[11]Hui S. W., Stewart, C. M., and Cherry, R. J., *Biochim. Biophys. Acta,* **1990**, *1023*, 335-340.

[12]Bourinbaiar, A. S.; Coleman, C., *Arch Virol.,* **1997,** *142*, 2225-2235.

[13]Heerklotz, H. and seelig, J., *Biophys. J.*, **2002**, *82*, 1445-1452.

[14]Okoro, L. N. and Winter, R., *Z. Naturforsch.,* **2008,** *63b*, 769-778.

[15]Okoro, L. N., . *Int. J. Chem.,* **2011**, *3(1)*, 166-175

[16]Okoro, L. N., *Can. J. Pure Appl. Sci.,* **2010**, *4(3),* 1323 – 1332.

[17]Seemann, H. and Winter, R., *Z. Phys. Chem.* **2003**, *217*, 831-846.

[18]Oliynyk, V., kaatze, U. and Heimburg, T., *Biochim. Biophys. Acta* **2007,** *1768,* 236-245.

HIGH SPECIFICITY OF MOLECULARLY IMPRINTED POLYMER PARTICLES TOWARD TARGET COMPOUND IN COMPETITIVE ENVIRONMENTAL BINDING

Samar Alsudir and Edward P.C. Lai[*]

Molecularly imprinted polymer (MIP) particles tailored for bisphenol A (BPA) were prepared using a 1:8:7 molar ratio of BPA the template, methacrylic acid (MAA) the functional monomer, and ethylene glycol dimethacrylate (EGDMA) the cross-linker. These colloidal particles were tested for rapid competitive binding by capillary electrophoresis with ultraviolet detection (CE-UV). Good interface binding efficiencies were obtained for BPA even in the presence of 2-hydroxy-4-methoxy benzophenone (HMB) as a structurally related compound at high concentrations. The specifically bound BPA could be desorbed rapidly out of the interface cavities by 5% triethylamine in methanol. However reusability was demonstrated by repeated injections of BPA that bound to MIP particles without regeneration of the cavities.

* Corresponding Authors
    Tel: (613) 520-2600 ext. 3835
    Fax: (613) 520-3749
    E-Mail: edward_lai@carleton.ca
[a]   Ottawa-Carleton Chemistry Institute, Department of Chemistry, Carleton University, Ottawa, ON K1S 5B6, Canada

Introduction

Bisphenol A (BPA) (2,2-bis(4-hydroxyphenyl)propane) has recently drawn the attention of scientific community and the general public due to its potent estrogenic activity,[1-4] having a hazard quotient of 2.24 in surface water.[5] Consequently, it is of great importance to develop a treatment technology that can efficiently remove BPA and other contaminants from water to boost human health. About 28 million chemicals are known up to date, which provokes the need for highly selective sorbents.[6] Water treatment demands for inexpensive, highly selective, and reusable sorbents with no significant loss in adsorption capacity make this research field of critical importance.

Molecular imprinting has gained considerable interest as a feasible route to fabricate tailored recognition materials featuring receptor sites in the form of molecularly imprinted polymers (MIPs).[7] The prime approach of imprinting involves the synthesis of reticulated polymers in the presence of a template ranging from small molecules to biological macromolecules as well as microorganisms. Functional monomers and cross-linkers interact with the template to hold it in place during polymerisation.[8] Removal of the template by an appropriate solvent produces a polymer with accessible binding sites that are complementary in shape and functionality to the template.[9] As a promising alternative to traditional SPE sorbents including silica gel, polyamide, ion-exchange resins and reverse-phase packing materials, MIPs have been extensively utilized to overcome the dissatisfactory cross-reactivity of such sorbents.[10] MIPs have been used in a wide range of applications including chemical sensing,[11] extraction of pollutants,[12] chromatography separation,[13] catalysis,[14] drug delivery,[15] and enzyme inhibition.[16] MIPs possess inherent advantages including a high affinity for the template molecule, great chemical and thermal stability, reusability, multiplicity in the choice of functional monomers and cross-linkers, as well as simplicity in preparation at low cost.[17]

A rapid CE-UV method was recently developed in our lab for rapidly testing the binding of MIPs tailored for BPA with various environmentally hazardous compounds.[18] The CE technique allows for a high loading capacity of particles in aqueous suspension for clog-free analysis. After sequential injection of particles and compounds, migration through the capillary provided an opportunity for binding during the momentary overlap. A high binding efficiency of 99±1% was obtained for BPA over a short interaction time of several seconds. MIP selectivity for its target compound in the presence of neutral, cationic and anionic interferences was successfully demonstrated in competitive binding tests.

Reusability of colloidal MIP particles is an important feature that warrants further research to demonstrate the key factor of cost savings, so as to open the opportunity for large-scale applications including water treatments.[19] In this work, a CE-UV reusability test was performed by injecting MIP particles first followed by multiple injections of BPA. The main objective was to demonstrate the repeated use of MIP particles without desorption of the already bound analytes. The reusability test was repeated in the presence of a structurally related compound, 2-hydroxy-4-methoxy benzophenone (HMB), to reveal the excellent specificity of MIP in recognizing its target compound rapidly.

Material and methods

Materials

2,2′-azobis(2-isobutyronitrile) (AIBN) was bought from Pfaltz & Bauer (Waterbury, CT, USA). Bisphenol A (BPA), ethylene glycol dimethacrylate (EGDMA), 2-hydroxy-4-methoxy benzophenone (HMB), and methacrylic acid (MAA) were all obtained from Sigma-Aldrich (Oakville,

ON, Canada). Hydrochloric acid was obtained from Anachemia (Montreal, QC, Canada). Sodium phosphate dibasic was obtained from Fisher Scientific (Fair Lawn, NJ, USA). Triethylamine (TEA) was purchased from Fluka (Buchs, Switzerland). Trifluoroacetic Acid (TFA) was bought from Aldrich (Milwaukee WI, USA). HPLC grade methanol and acetonitrile, spectro grade acetone, and sodium hydroxide were all purchased from Caledon Laboratories (Georgetown, ON, Canada).

Apparatus and Analytical Method

CE-UV analyses were performed on a modular system built in our laboratory, which includes a Spellman CZE1000R high-voltage power supply (Hauppauge, New York, USA). Fused-silica capillary (51 mm i.d., 356 mm o.d.) was obtained from Polymicro Technologies (Phoenix, AZ, USA). The capillary total and effective lengths were 53.5 cm and 46.1 cm, respectively. The background electrolyte (BGE) was composed of 10 mM Na_2HPO_4 in deionized distilled water (DDW) to attain pH 7.5±0.2. Prior to initial use, the capillary was typically conditioned with 1 M NaOH, 0.1 M NaOH and the BGE. Daily conditioning was done by flushing the capillary with pure methanol, 1.0 M HCl, 1.0 M NaOH, DDW, and the BGE.

All subsequent CE running at an applied voltage of 17 kV had the capillary inlet 2 mm away and below the electrode tip to improve both precision and baseline stability. A Bischoff Lambda 1010 (Leonberg, Germany) UV detector was set up at a wavelength of 200 nm to monitor the analytes (BPA, HMB) and particles. A PeakSimple chromatography data system (SRI model 203, Torrance, CA, USA) was used to acquire the detector output signal. The capillary was re-equilibrated by running the BGE at 17 kV for 1 min in between sample analyses to eliminate any carrryover contamination from the previous electrophoretic run.

Preparation of MIP and NIP Particles

The preparation procedure for BPA-MIP and non-imprinted polymer (NIP) particles was detailed elsewhere.[18] Briefly, at a molar ratio of 1:8:7, BPA the template, MAA the functional monomer, and EGDMA the cross-linker were dissolved in acetone/acetonitrile (1:3 v/v) the porogen. At 2% by weight of the total monomer and crosslinker, AIBN the initiator was added. The pre-polymerization mixture was sonicated, deoxygenated, and placed in a 60°C water bath for 24 h to yield BPA-MIP submicron particles. To generate binding cavities in MIP particles, 5 mL of 5% TEA in methanol was used to wash out the template and any residual monomer or crosslinker. After sonication for 10 min, the suspension of MIP particles was centrifuged for 10 min and then the supernatant was discarded. This washing step was repeated several times to ensure complete removal of the template. Subsequently, the particles were rinsed three times with ACN to remove any TEA remaining in the pores and imprinted cavities. The MIP particles were finally dried overnight to be ready for experimental use. NIP particles were prepared in a similar procedure without BPA.

CE-UV Desorption Test

A suspension was prepared to contain 10 mg mL^{-1} BPA-MIP (MIP with BPA in the binding cavities) in the BGE (10 mM Na_2HPO_4, pH 7.5±0.2). Both 5% TEA in methanol and 5% TFA in methanol were evaluated as eluents to elute BPA out of MIP cavities. Capillary desorption tests were performed by sequential injection of BPA-MIP particles first and 5% TEA in methanol next for 3 s at 17 kV of applied voltage. Mesityl oxide (MO) was run individually for ionic charge determination of BPA, TEA, TFA and particles.

External Desorption Test

In-capillary desorption test was confirmed by performing an external desorption test. It was done by mixing 10 mg mL^{-1} of BPA-MIP particles with 5% TEA in methanol or 5% TFA in methanol in the sample vial. After sonication for 5 min, the mixture was analyzed by CE-UV with electrokinetic injection for 3 s at 17 kV.

Reusability of MIP Particles

MIP and NIP suspensions (10 mg mL^{-1}) were prepared in the BGE, as well as a stock solution of BPA (100 ppm) when needed. A stock solution of HMB (5000 ppm) was prepared in methanol due to its insolubility in water. A working solution of 200 ppm HMB was daily prepared by dilution with the BGE. MIP reusability was investigated by injecting MIP particles for 21s followed by up to five injections of BPA, each for 3s. Peak overlapping between NIP particles and BPA restricted the multiple injections of BPA up to 3, following the NIP injection.

Chemical Interference

To study the effect of an interfering compound on BPA % binding, a CE-UV experiment was conducted using first injection of MIP particles for 21s, second injection of HMB for 3s, third injection of BPA for 3s, and finally fourth injection of BPA for 3s. To further investigate the effect of HMB on BPA % binding, gradual increase of HMB injection time was carried out using 6, 9, 12, and 15s of injection time. The experiment was repeated for NIP particles.

Results and Discussion

CE-UV Desorption Test

In the presence or absence of BPA, polymerization of MAA and EGDMA in acetone/ acetonitrile (1:3 v/v) at 60°C for 24 h yielded BPA-MIP or NIP submicron particles. The average diameters (or sizes) of these BPA-MIP and NIP particles were first determined by scanning electron microscopy (SEM) and then confirmed by dynamic light scattering. The SEM images illustrated the morphology, size and distribution of the prepared BPA-MIP and NIP particles. Their average diameters were 164±15 nm and 187±7 nm, respectively, as reported with more details elsewhere.[18]

CE-UV analysis was carried out by electrokinetic injection of a BPA-MIP suspension prepared in the BGE. The electrophoretic mobility, which signifies the amount of positive or negative charges carried by the particles, was obtained by subtracting the electroosmotic mobility of the neutral marker (MO) from the apparent mobility of analytes or particles.[20] MIP and NIP particles both migrated after the neutral marker, yielding negative electrophoretic mobility values as presented in Table 1. Both BPA and TEA were determined to be neutral compounds since they migrated at velocities nearly identical to that for MO. TEA is neutral in the BGE because of the presence of methanol that works as an alcohol modifier preventing the protonation of TEA.[21]

Table 1. Electrophoretic mobility values of particles, analytes and eluents signifying the amount of positive or negative charges they carried at pH 7.5±0.2.

	t_{nmt}, min *	MW, g mol^{-1}	φ_{eph}, m^2 V^{-1} s^{-1}
MIP particles	8.1	------	-2.30x10^{-6}
NIP particles	7.1	------	-1.88x10^{-6}
Bisphenol A	3.75	228.29	-1.03x10^{-7}
Mesityl oxide	3.7	98.14	0.00
Triethylamine	3.7	101.19	0.00
CF$_3$COOH	11.6	114.02	-2.67x10^{-6}

t_{nmt} = Net Migration Time after injection; MW=molecular weight, $\varphi_{eph = e}$lectrophoretic mobility

An in-capillary desorption test was conducted by injecting BPA-MIP particles first and TEA next, each for 3s. The BPA-MIP peak shape changed (after TEA injection) as shown in Fig .1(a) and 1(b). A small peak, appearing around 5.4 min in front of the MIP peak, was suspected to be the eluted BPA. To investigate the identity of this peak, the BPA-MIP suspension was spiked with 100 ppm BPA. An increase in peak area (and height) was observed at 5.4±0.2 min, thus proving the peak to be BPA.
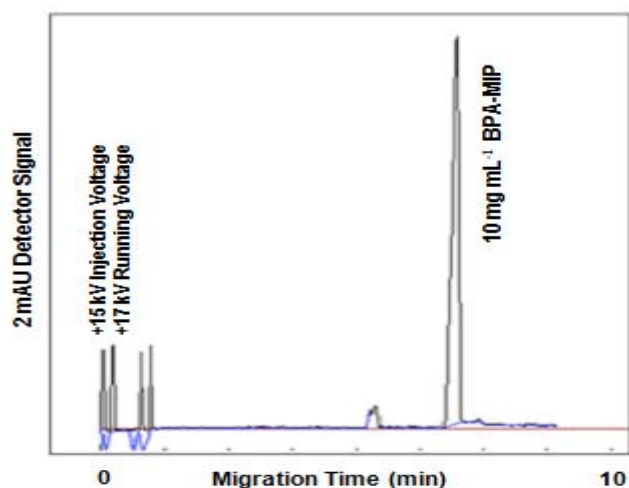
Figure 1(a). CE-UV characterization of BPA-MIP particles. Electrokinetic injection at 15 kV: first injection of BPA-MIP particles for 3s; second injection of BGE for 3 s. CE analysis at 17 kV; UV detection at 200 nm.

Full y-scale represents 2 milli-absorbance units (mAU). This seems to contradict the migration time of 3.75 min for BPA in Table 1. However, it can be explained by the transfer of two protons (H$^+$) from BPA to 5% TEA, which

changed the analyte into a negatively charged ion with an increase in migration time. In future work, TEA can be added to the BGE for in-capillary desorption of BPA from MIP particles
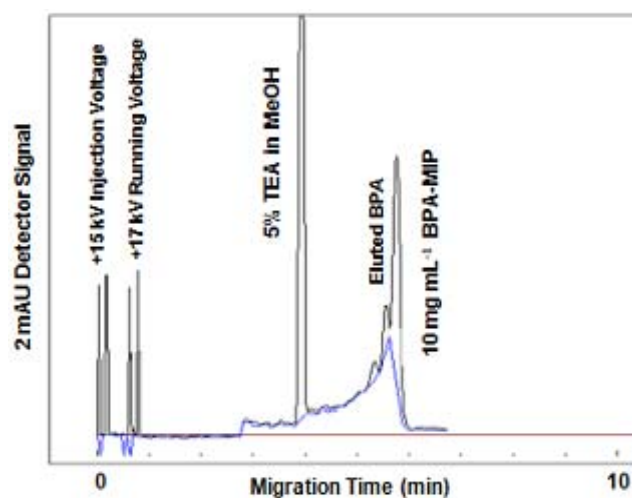
Figure 1(b). CE-UV desorption test. Electrokinetic injection at 15 kV: first injection of BPA-MIP particles for 3 s; second injection of 5 % TEA in methanol for 3 s. CE analysis at 17 kV; UV detection at 200 nm.

External Desorption Test

An external desorption test was next carried out to confirm the eluent ability of TEA. A mixture of BPA-MIP and TEA was sonicated for 5 min before injection for CE-UV analysis. As shown in Fig. 2, other than the TEA and BPA-MIP peaks, a new peak was observed at 4.9±0.1 min. This peak was confirmed to be BPA by spiking the mixture with 100 ppm BPA and observing an increase in peak area (and height). One plausible explanation of this shorter migration time (than 5.4 min above) is the transfer of only one proton from BPA to 2.5% TEA. When 5% TEA was next used, the migration time of BPA increased to 5.4±0.1 min.
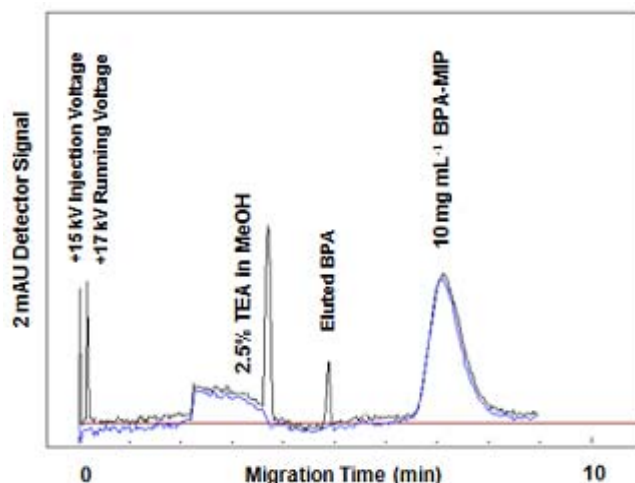
Figure 2. External desorption test. Electrokinetic injection at 15 kV of a mixture of BPA-MIP particles and 2.5% TEA in methanol for 3 s. CE analysis at 17 kV; UV detection at 200 nm.

The selection of an appropriate eluent is crucial for achieving the highest desorption efficiency. Therefore it was necessary to add an acidic/basic modifier with the ability to disrupt the hydrogen bonds formed between BPA and MAA, the functional monomer that provides carboxyl functional groups inside the MIP cavities. [22] Having two phenolic hydroxyl groups, BPA can act as a weak acid (pK$_a$=9.6). [23] TEA is an organic base that can interfere with the binding equilibrium between BPA and MAA, releasing BPA out of the cavity. Martin *et al.* explored the ability of basic and acidic modifiers to overcome the electrostatic interactions between basic analytes and acidic MIPs. They reached a conclusion that only TEA achieved this with superior performance when compared with TFA. [24] In addition, methanol contains an -OH group that can form a hydrogen bond with MAA and force BPA out of the cavity. However, methanol cannot quantitatively desorb BPA on its own. [25]

After injecting TEA first and BPA next for 3s, proton exchange occurred. As shown in Fig. 3, the BPA peak showed up at a slightly longer migration time due to an increase in its negative charge after the transfer of a proton to TEA. . BPA works as a hydrogen bond donor while TEA is a hydrogen bond acceptor (since it contains a lone pair of electrons on the nitrogen atom). All in all, 5% TEA in methanol is a proper eluent (or elution reagent) that can quantitatively desorb BPA out of the MIP cavities. In spite of the finite time interval required for the elution reagent to desorb all of the bound BPA out of the cavities, in-capillary desorption was demonstrated to be a rapid test for evaluating the desorption ability of an eluent.
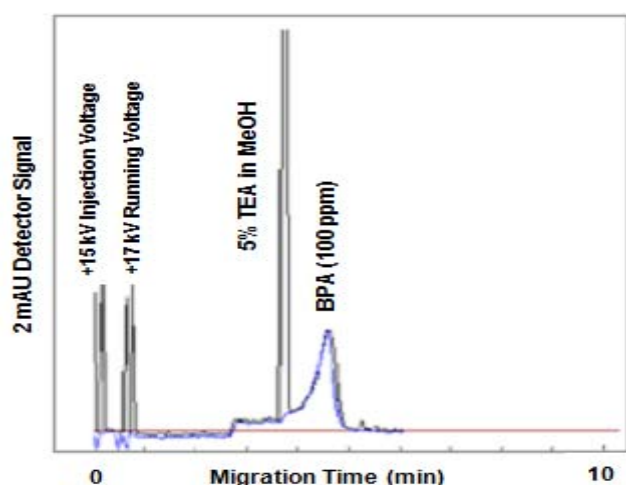
Figure 3. CE-UV binding test. Electrokinetic injection at 15 kV: first injection of 5% TEA in methanol for 3 s; second injection of BPA (100 ppm) for 3s. CE analysis at 17 kV; UV detection at 200 nm.

The elution ability of TFA was next investigated. TFA is negatively charged in the BGE, based on its electrophoretic mobility value presented in Table 1. A mixture of 5% TFA in methanol and 100 ppm BPA in BGE was injected for 3s to examine the interaction of TFA with BPA. 5% TFA in methanol was sufficient to interact quantitatively with BPA and still fell within the dynamic range of CE-UV detection. As shown in Fig. 4, a single peak was observed at 10.9±0.1 min, which is believed to be the TFA-BPA complex. When injected individually, BPA appeared at a migration time of

3.7±0.1 min while TFA appeared at 11.6±0.1 min. Based on the new migration time for the complex peak, the electrostatic interactions between BPA and TFA formed an overall negatively charged complex. Varying concentrations of BPA (10, 50, 100 and 200 ppm) were used to further investigate whether the obtained peak is the TFA-BPA complex. Figure 5 shows an increasing peak area of the TFA-BPA complex as the BPA concentration was increased. This is a convincing proof of the complex formation.
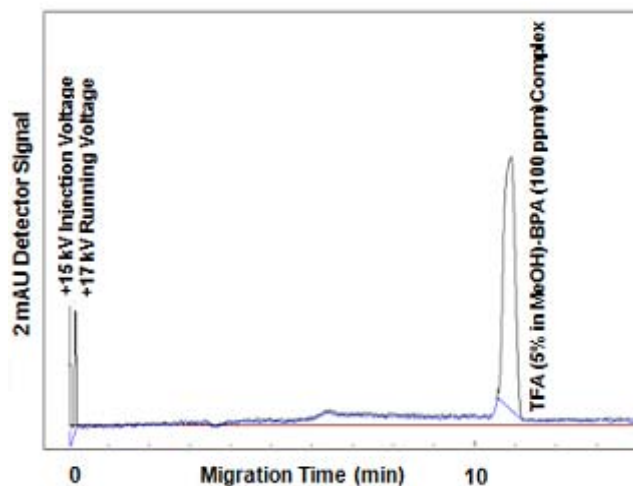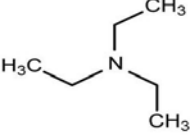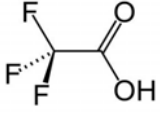
Figure 4. CE-UV binding test. Electrokinetic injection at 15 kV of a mixture of 5% TFA in methanol and 100 ppm BPA in BGE for3 s. CE analysis at 17 kV; UV detection at 200 nm.
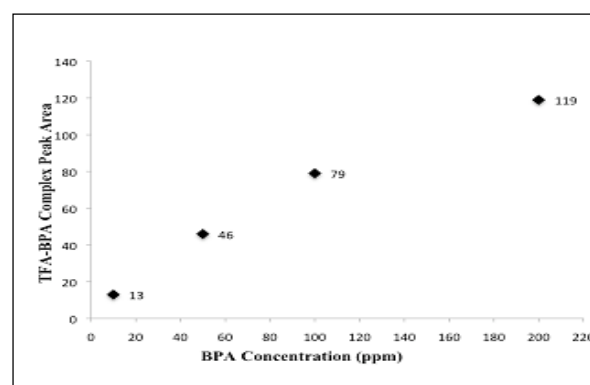
Figure 5. Effect of BPA concentration on area of TFA-BPA complex peak.

10% acetic acid had previously been used to elute BPA out of MIP cavities. TFA had also been utilized as an organic modifier in the mobile phase to elute BPA out of HPLC columns. [26] Although TFA could form a complex with BPA, it was apparently not able to break up the binding interactions between BPA and MAA inside the MIP binding cavities. Both in-capillary and external desorption tests showed no impact of TFA on BPA desorption. It is believed that Coulomb/electrostatic repulsion between TFA and MIP particles would not allow TFA to approach the MIP cavities. It is also possible that TFA just attaches itself to BPA without breaking up with MAA. Consequently, TFA cannot be used as an eluent for BPA bound inside methacrylate-based MIP particles. Table 2 compares TEA and TFA for use as elution reagents.

Table 2. Comparison between TEA and TFA in their capability to elute BPA out of MIP particles.

	5% TEA in MeOH	5% TFA in MeOH
Chemical Structure		
pK$_a$	10.8 (basic) [27]	0.6 (strongly acidic) [28]
Charge in 10 mM Na$_2$HPO$_4$	Neutral	Negatively charged
Interaction with BPA	BPA exchanged protons with TEA, resulting in a change in its migration time from 3.7 min to 5.4 min.	TFA and BPA formed a complex (via electrostatic interactions) peak in between the migration times of BPA and TFA.
Ability to break up MAA and BPA	TEA was able to disrupt the binding between MAA and BPA and eventually elute BPA out of MIP cavities.	TFA was not able to break up the binding interactions between MAA and BPA to elute BPA out of MIP cavities.

Reusability of MIP Particles

Reusability was demonstrated over several adsorption tests without regeneration of the MIP particles (by desorbing the already bound analytes). Figure 6(a) shows a typical CE-UV analysis for five consecutive injections of 100 ppm BPA (each for 3s), following one injection of MIP particles. As 48 s of MIP injection was needed to bind 99±1% of the BPA, 21s of MIP injection would not be quantitatively enough even for the first BPA injection. However, all subsequent BPA injections were observed to bind onto the MIP particles, with a gradual decrease in % binding as shown in Fig. 6(b). Similarly, a gradual decrease is observed in Fig. 6(c) even though peak overlapping between NIP particles and BPA allowed only three injections of BPA (following the injection of NIP particles). The % binding results of all adsorption tests are summarized in Table 3 for easy comparison; they also show the significantly higher % binding results obtained from MIP than NIP particles. The progressive decreases in BPA % binding to MIP and NIP particles imply that binding as a physicochemical interaction was dictated by an equilibrium constant (K$_{eq}$):

$$BPA + MIP = BPA\text{-}MIP \qquad (1)$$

The first injection of BPA did not bind completely probably because the effective equilibrium constant does not have a very high value: [29]

$$K_{eq} = \frac{\left[\dfrac{C_i - C_e}{C_e}\right]}{\left[\dfrac{V}{m}\right]} = \frac{\left[\dfrac{\% \, binding}{1 - \% \, binding}\right]}{\left[\dfrac{V}{m}\right]} \qquad (2)$$

where C_i is the initial concentration of analyte, C_e is the concentration of analyte at binding equilibrium, V is the volume of solution (mL) and m is the mass of particles (g). An effective equilibrium constant can be calculated for the first injection of BPA binding with MIP particles to be $K_{eq}' = 212$ g mL^{-1}; for NIP particles, $K_{eq}' = 35$ g mL^{-1}. As less and less binding sites were available, all subsequent injections of BPA obtained lower % binding results than the first injection.

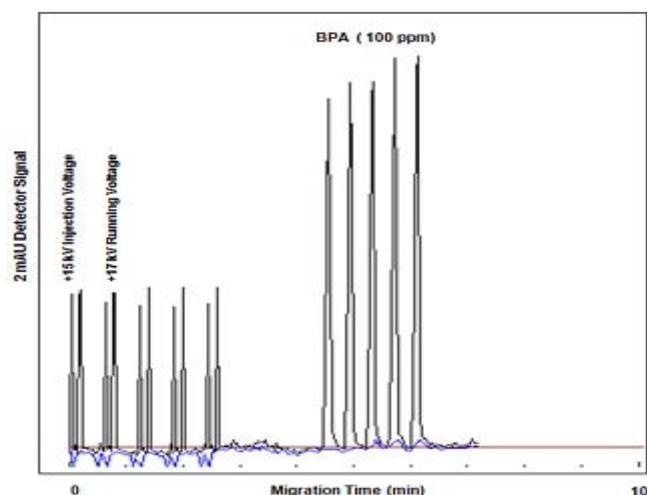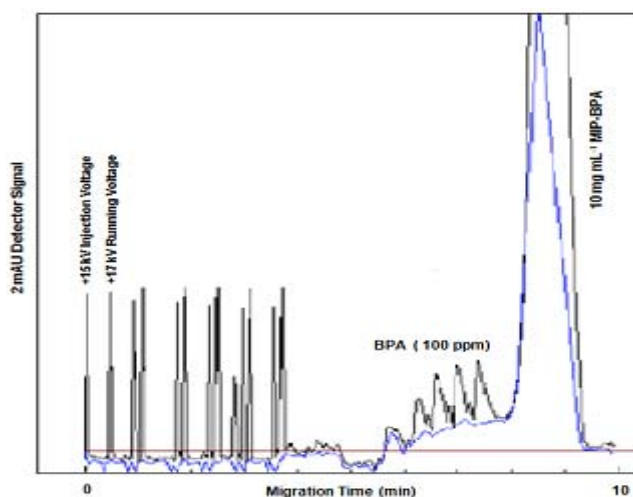**Figure 6(a).** CE-UV characterization of multiple BPA (100 ppm) injections (for 3s each). Electrokinetic injection at 15 kV. CE analysis at 17 kV; UV detection at 200 nm.

Figure 6(b). CE-UV binding test. Electrokinetic injection at 15 kV: first injection of MIP particles for 21s, followed by five injections of BPA (100 ppm) for 3s each. CE analysis at 17 kV; UV detection at 200 nm.

Table 3. % binding results for multiple injections of BPA (injection time = 3s each) with MIP and NIP particles (injection time = 21s) at pH 7.5.

% Binding	Injection of BPA				
	1st	2nd	3rd	4th	5th
MIP	68±2	62±1	60±1	58±1	51±2
NIP	26±1	23±1	22±1	--------	---------
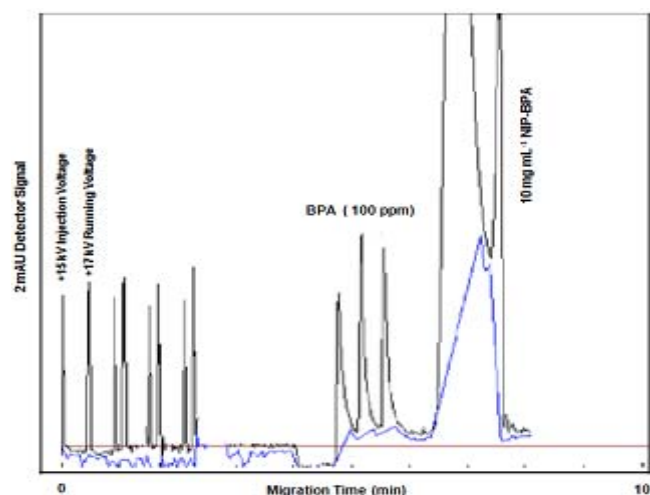
Figure 6(c). CE-UV binding test. Electrokinetic injection at 15 kV: first injection of NIP particles for 21 s, followed by three injections of BPA (100 ppm) for 3 s each. CE analysis at 17 kV; UV detection at 200 nm.

Chemical Interference

The presence of other organic compounds in real-world samples can interfere with the % binding of BPA with MIP. A structurally related compound, HMB, was next employed for the investigation of chemical interference. HMB, also known as oxybenzone, is an organic compound used in sunscreen and other cosmetics because it absorbs UVB and short-wave UVA rays. It was nice to observe that 3s of 200 ppm HMB injection had no significant effect on BPA % binding onto either MIP or NIP particles, in spite of the high % bindings of HMB with both MIP and NIP particles as shown in Fig. 7. As discussed elsewhere, [18] HMB has high affinity to non-speci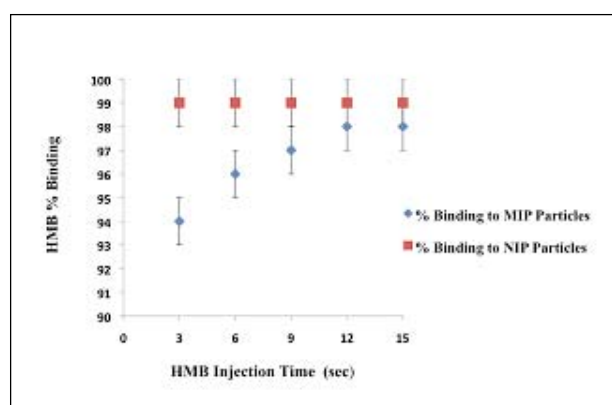fic binding sites as it demonstrated a complete binding to NIP particles. Next, the HMB injection time was increased to 6, 9, 12 and 15s.
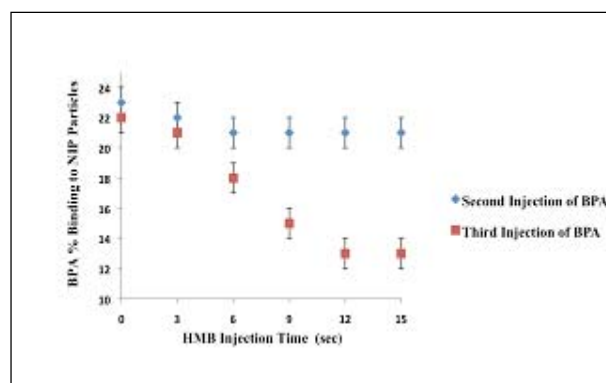

Figure 7. CE-UV investigation of HMB (200 ppm) binding efficiencies with MIP and NIP particles (21s of injection).

In spite of the large quantity of HMB bound to the (non-specific binding sites inside) MIP particles, BPA % binding to MIP particles was not significantly decreased in the two next injections. Figure 8(a) presents the results of BPA % binding to MIP particles after the first injection of HMB over various time durations. Apparently, HMB had only slight impact (due to occupation of non-specific binding

sites) on decreasing the BPA % binding to MIP particles in the second injection. The notable decreases in BPA % binding to MIP particles (from the second injection to the third injection) could be explained by a lower number of specific binding sites available. Figure 8(b) presents the results of BPA % binding to NIP particles at different injection time durations of HMB.
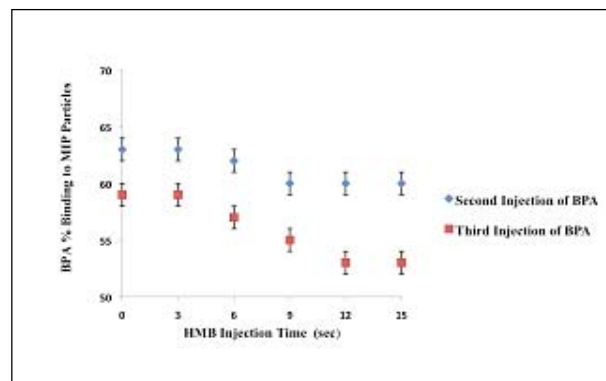
Figure 8(a). CE-UV investigation of BPA (100 ppm) binding efficiencies with MIP particles (21s of injection) after injection of HMB (200 ppm) for various time durations.

Figure 8(b). CE-UV investigation of BPA (100 ppm) binding efficiencies with NIP particles (21 s of injection) after injection of HMB (200 ppm) for various time durations.

In summary, HMB exhibited almost insignificant impact on decreasing BPA % binding to MIP particles in the second and third injections, demonstrating that MIP particles are not affected by the non-specific binding of HMB despite its large quantities (injection of 200 ppm over 3–15s). MIP particles can still remove a reasonably high percentage of BPA in the next two injections (2nd and 3rd). This is an excellent demonstration of MIP capability to recognize and specifically bind BPA in the presence of interfering compounds. These results are in agreement with the results obtained by Watabe *et al*. They concluded that the removal of interferences from water by the surface modified MIP particles through non-specific binding did not hinder BPA binding to MIP cavities. [30]

Conclusions

A rapid CE-UV desorption test was demonstrated using 5% TEA in methanol to elute BPA out of the interface cavities of colloidal MIP particles. The ability of TEA was

confirmed by an external desorption test. On the contrary, 5% TFA in methanol did not work well as an eluent due to electrostatic repulsion between the negatively charged TFA and MIP particles. Reasonably high % bindings of BPA were attained after one injection of MIP particles for 21s followed by multiple injections of BPA for 3s each. This ascertained the reusability of MIP particles over several adsorption cycles (without regeneration of the interface cavities by desorbing the already bound analyte) until all specific binding sites were occupied. It was further demonstrated that the MIP particles had excellent capability to recognize BPA even in the presence of large quantities of HMB (3–15s of injection of 200 ppm). Such high specificity of colloidal MIP particles toward the target compound in a rapid competitive binding test represents a major advantage of MIP over non-specific SPE sorbents in targeting water contaminants individually. The colloidal state would allow MIP particles to stay suspended in water over an extended period of time for removing any new introduction of contaminants.

Abbreviations

AIBN	2,2′-azobis(2-isobutyronitrile)
BGE	background electrolyte
BPA	bisphenol A
CE	capillary electrophoresis
DDW	deionized distilled water
EGDMA	ethylene glycol dimethacrylate
HMB	2-hydroxy-4-methoxybenzophenone
MAA	methacrylic acid
MIP	molecularly imprinted polymer
MO	mesityl oxide
NIP	non-imprinted polymer
TEA	triethylamine
TFA	trifluoroacetic acid
UV	ultraviolet

Acknowledgements

References

[1] Ren, Y., Maa, W., Ma, J., Wena, Q., Wang, J., Zhao, F., *J. Colloid Interface Sci.,* **2012**, *367*, 355.

[2] Li, Y., Burns, K. A., Arao, Y., Luh, C. J., Korach, K. S., *Environ Health Perspect.,* **2012**, *120,* 1029.

[3] De Schepper, W., Vanparys, C., Dries, J., Geuens, L., Blust, R., *Ozone: Science & Engineering,* **2010**, *34,* 32.

[4] Zhang, W., Li, Y., Wu, Q., Hu, H., *Environ Eng Sci***, 2012**, *29,* 195.

[5] Chen, T. C., Shue, M. F., Yeh, Y. L., Hsieh, C. Y., Kuo, Y. T., Kuo, C. T., *J. Environ. Sci. Heal A,* **2009**,*44,* 1244.

[6] Denderz, N., Lehotay, J., Cizmarik, J., *Ceska Slov Farm,* **2012**, *61*, 79.

[7] Puoci, F., Iemma, F., Cirillo, G., Curcio, M. Parisi, O. I., Spizzirri, U. G., Picci, N., *Eur. Polym. J.,* **2009**, *45*, 1634.

[8] Sellergren, B., Hall, A. J., *Molecularly Imprinted Polymers. Supramolecular Chemistry: From Molecules to Nanomaterials, INFU, Technical University of Dortmund, Dortmund, Germany,* **2012**.

[9] Turner, N. W., Wright, B. E., Hlady, V., Britt, D. W., *J. Colloid Interface Sci.,* **2007**, *308*, 71.

[10] Pardo, A., Mespouille, L., Dubois, P., Duez, P., Blankert, B., *Cent. Eur. J. Chem.,* **2010**, *10*, 751.

[11] Puoci, F., Iemma, F., Cirillo, G., Curcio, M., Parisi, O. I., Spizzirri, U. G., Picci, N., *Eur. Polym. J.,* **2009**, *45*, 1634.

[12] Hoshina, K., Horiyama, S., Matsunaga, H., Haginaka**,** J., *J. Pharmaceut. Biomed.,* **2011**, *55*, 916.

[13] Ichi, K. K., Isao, Y., Takako, H., Hiroko, K., Sadao, A., *J. Chromatogr. A,* **2010**, *1217*, 7249.

[14] Ma, C., Sun, N., Liu, X. F., Wu, B., Chen, H. X., *Chem. Ind. Eng.,* **2012**, *29, 66.*

[15] Sellergren, B., Allender, C. J., *Advanced Drug Delivery Reviews,* **2005**, *57*, 1733.

[16] Cutivet, A., Schembri, C., Kovensky, J., Haupt, K., *J. Am. Chem. Soc.,* **2009**, *131*, 14699.

[17] Xu, X., Chen, S., Wua, Q., *J. Colloid Interface Sci.,* **2012**, *385*, 193.

[18] Alsudir, S., Iqbal, Z., Lai, E. P. C., *Electrophoresis,* **2012**, *33*, 1255.

[19] Khayyat, M. H., Lai, E. P. C., Kollu, K., Ormeci, B., *J. Water Res. Protect.,* **2011**, *3*, 643.

[20] Lai, E. P. C., DeMaleki, Z., Wu, S., *J. Appl. Polym. Sci.,* **2010**, *116*, 1499.

[21] Thomasa, D. P., Foleya, J. P., *J. Chromatogr. A,* **2008**, *1205*, 36.

[22] Wang, X., Zhou, Q., Zhai, M., *Anal. Methods,* **2012**, *4*, 394.

[23] Clara, M., Strenn, B., Saracevic, E., Kreuzinger, N., *Chemosphere,* **2004,** *56,* 843.

[24] Martin, P., Wilson, I. D., Morgan, D. E., Jones, G. R., Jones, K., *Anal. Commun.,* **1997,** *34*, 45.

[25] Zhang, J. H., Jiang, M., Zou, L., Shi, D., Mei, S. R., Zhu, Y. X., Shi, Y., Dai, K., Lu, B., *Anal Bioanal Chem.,* **2006**, *385*, 780.

[26] Nantasenamat, C. Isarankura-Na-Ayudhya, C. Bülow, L., Ye, L., Prachayasittikul, V., *EXCLI Journal,* **2006**, *5,* 103.

[27] Blitz, J. P., Shreedhara- Murthy, R. S., Leyden, D. E., *J. Colloid Interface Sci.,* **1998,** *126*, 387.

[28] Namazian, M., Zakery, M., Noorbala, M. R., Coote, M. L., *Chem. Phys. Lett.,* **2008**, *451*, 163.

[29] Yavuz, H., Karakoc̣, V., Turkmen, D., Say, R., Denizli, A., *Int. J. Biol. Macromol.,* **2007**, *41*, 8.

[30] Watabe, Y., Hosoyaa, K., Tanakaa, N., Kubob, T., Kondoc, T., Moritac, M., *J. Chromatogr. A,* **2005**, *1073*, 363.

EFFECTS OF DIFFERENT REACTION CONDITIONS ON THE SYNTHESIS OF ISOAMYL BENZOATE

Liu Shu[a]*, Zhang Yongmei [a] and You Hongjun[b]

Effects of the different reaction conditions on the synthetic method of isoamyl benzoate have been reviewed in the present article. Different catalysts that consist of p-toluenesulfonic acid (PTSA), $Zr(SO_4)_2 \cdot 4H_2O$, $NaHSO_4 \cdot H_2O$ and $Ti(SO_4)_2/TiO_2$ have also been introduced. The reaction conditions include the reaction time, the molar ratio of benzoic acid to isoamyl alcohol, the amount of the catalyst, the microwave heating method and the Ti loading amount, etc. The optimum reaction time, the molar ratio of benzoic acid to isoamyl alcohol, the amount of the catalyst, the microwave heating method and the Ti loading amount are beneficial to improve the yield of the product, isoamyl benzoate.

*Corresponding Author
    Fax: 862456860869
    E-Mail: youhongjun@hotmail.com
[a]   Liaoning Shihua University, Fushun, Liaoning, P.R. China
[b]   SAIT Polytechnic, Calgary AB, Canada.

INTRODUCTION

Isoamyl benzoate is not only a colourless liquid with fruit aroma but also one of the important chemical products.[1] Further, due to its floral fragrance, it is widely used in different daily use chemical essence as a mobilizing agent for fragrance in different types of fixative spices and fruit/food derivatives etc.[2] It is also used as a solvent for fats or resins. Benzoic acid in the presence of concentrated sulphuric acid as catalyst is reacted with isoamyl alcohol to produce isoamyl benzoate at industrial scale process. This method has a lot of disadvantages also such as poor quality of products, serious equipment corrosion, complicated operating system and pollution environmental issues, etc.[3]

In the present paper, different catalysts such as p-toluenesulfonic acid (PTSA) which refers an organic compound with the formula $CH_3C_6H_4SO_3H$, $Zr(SO_4)_2 \cdot 4H_2O$, $NaHSO_4 \cdot H_2O$ and $Ti(SO_4)_2/TiO_2$ have been discussed. Effects of different reaction conditions, such as the reaction time, the molar ratio of benzoic acid to isoamyl alcohol, the amount of the catalyst, the microwave heating method and the Ti loading amount, on the synthetic method of isoamyl benzoate have also been reviewed. Further, a few the optimum reaction conditions are also discussed.

DISCUSSION

Effects of the reaction time on the yield of isoamyl benzoate by the addition of p-toluenesulfonic acid (PTSA) as a catalyst

Li Xiuyu [4] introduced the synthetic method of isoamyl benzoate and studied that the different conditions had an effect on the yield of isoamyl benzoate. To synthesise isoamyl benzoate, PTSA was used as a catalyst whereas benzoic acid

and isoamyl alcohol were used as feedstocks respectively. The molar ratio of benzoic acid to isoamyl alcohol (1.0:2.0) and the weight ratio of PTSA to benzoic acid (3%) kept at constants. Effects of the reaction time on the yield of isoamyl benzoate had also been discussed. Table 1 showed effects of the reaction time on the yield of isoamyl benzoate. The experimental results showed that the yield of isoamyl benzoate first increased and then decreased with an increase with the reaction time. It was observed that when the reaction time was 3.0 hours, the maximum yield of isoamyl benzoate (98.75%) was obtained. Therefore, the optimum reaction time to be considered was 3.0 hours.

Table 1. The effect of the reaction time on the yield of isoamyl benzoate

Reaction time , h	1.0	2.0	3.0	4.0	5.0
Yield , %	95.24	98.35	98.75	97.42	97.00

Effects of the molar ratio of benzoic acid to isoamyl alcohol on the yield of isoamyl benzoate by the addition of $Zr(SO_4)_2 \cdot 4H_2O$ as a catalyst

Zhang Fuxing [5] used $Zr(SO_4)_2 \cdot 4H_2O$ as a catalyst and benzoic acid and isoamyl alcohol as feedstocks to synthesise isoamyl benzoate. The reaction time and the weight ratio of $Zr(SO_4)_2 \cdot 4H_2O$ to benzoic acid kept at constants were 2.5 hours and 6.56%, respectively. Effects of the molar ratio of benzoic acid to isoamyl alcohol on the yield of isoamyl benzoate had been discussed. Table 2 showed effects of the molar ratio of benzoic acid to isoamyl alcohol on the yield of isoamyl benzoate. The yield of isoamyl benzoate first increased and then decreased with an increase in the molar ratio of benzoic acid to isoamyl alcohol. When the molar ratio of benzoic acid to isoamyl alcohol was 1.0:2.5, the maximum yield of isoamyl benzoate attained was 96.3%.

Table 2. The effect of the molar ratio of benzoic acid to isoamyl alcohol on the yield of isoamyl benzoate

Molar ratio	1.0:1.0	1.0:1.5	1.0:2.0	1.0:2.5	1.0:3.0
Yield, %	75.8	86.4	92.7	96.3	94.8

Effect of the amount of NaHSO₄·H₂O on the yield of isoamyl benzoate by the addition of NaHSO₄·H₂O as a catalyst

Guang Shibin [6] replaced concentrated sulfuric acid with NaHSO₄·H₂O as a catalyst to synthesise isoamyl benzoate. The reaction time and the molar ratio of benzoic acid to isopropanol kept at constants were 2.0 hours and 1.0:1.4, respectively. The effect of the amount of NaHSO₄·H₂O on the yield of isoamyl benzoate had also been discussed. Table 3 presented effects of the amount of NaHSO₄·H₂O on the yield of isoamyl benzoate. The yield of isoamyl benzoate first increased and then decreased with an increase in the amount of NaHSO₄·H₂O. It was noticed that when the amount of NaHSO₄·H₂O was 24.59% of benzoic acid weight, the maximum yield of isoamyl benzoate attained was 83.3%.

Table 3. The effect of the amount of NaHSO₄·H₂O on the yield of isoamyl benzoate

Weight ratio of NaHSO₄·H₂O to PhCOOH, %	4.10	8.20	16.39	24.59	32.78
Yield (%)	75.0	77.1	81.3	83.3	79.2

Effect of microwave heating method on the yield of isoamyl benzoate by the addition of p-toluenesulfonic acid (PTSA) as a catalyst

Shi Lei [7] also studied the effect of the reaction conditions on the yield of isoamyl benzoate. He synthesised it by using PTSA as a catalyst and benzoic acid and isoamyl alcohol as feedstocks produced isoamyl benzoate. It was observed that the molar ratio of benzoic acid to isopropanol and the amount of PTSA kept at constants at 1.0:3.0 and 14.88% of benzoic acid weight, respectively. Table 4 showed that different heating methods had a different effect on the yield of isoamyl benzoate. The experimental results revealed that two types of methods had almost the same yield, but they applied the different reaction time. The yield of isoamyl benzoate in the microwave heating methods reached 95.0% in 0.5 hour; however the yield in the oil bath heating methods attained at 94.8% in 2 hours.

Table 4. the effect of heating method on the yield of isoamyl benzoate

Conditions	Microwave heating method	Oil bath heating method
Temperature, °C	120 - 136	136 – 148
Yield, %	95.0	94.8
Reaction time, h	0.5	2.0

Effect of Ti loading amount on the yield of isoamyl benzoate by the addition of Ti(SO₄)₂/TiO₂ as a catalyst

Zhang Fujuan [8] used Ti(SO₄)₂/TiO₂ as a catalyst to synthesise isoamyl benzoate. The effect of Ti loading amount on the yield of isoamyl benzoate had been discussed. It was observed that the reaction time, the molar ratio of benzoic acid to isopropanol and the amount of Ti(SO₄)₂/TiO₂ kept at constants were 1.5 hours, 1.0:4.0 and 40.98% of benzoic acid weight, respectively. Table 5 showed effects of different Ti loading amount on the yield of isoamyl benzoate. The yield of isoamyl benzoate firstly increased and then decreased with an

increase in the Ti loading amount. When the Ti loading amount was 10%, the maximum yield of isoamyl benzoate was found to be 92.7%.

Table 5. The effect of different Ti loading amount on the yield of isoamyl benzoate

Ti loading amount, %	6	8	10	12	14
Yield, %	70.2	78.2	92.7	89.9	89.9

CONCLUSION

Based on the above mentioned results, discussion and review, using benzoic acid and isopropanol as feedstocks and p-toluenesulfonic acid (PTSA), Zr(SO₄)₂·4H₂O, NaHSO₄·H₂O and Ti(SO₄)₂/TiO₂ as catalysts, effects of he reaction time, the molar ratio of benzoic acid to isoamyl alcohol, the amount of the catalyst, the microwave heating method and the Ti loading amount on the yield of isoamyl benzoate, the experimental observations obtained are as follows:

(1) The maximum yield of isoamyl benzoate attained 98.75% in 3 hours by the addition of PTSA.

(2) The maximum yield of isoamyl benzoate attained 96.3% under the condition of benzoic acid/isopropanol ratio (1.0:2.5) when Zr(SO₄)₂·4H₂O as the catalyst was added into this reaction system.

(3) The maximum yield of isoamyl benzoate was 83.3% when the amount of NaHSO₄·H₂O was 24.59% of benzoic acid weight.

(4) The maximum yield of isoamyl benzoate got 95.0% under the condition of the microwave heating method (0.5 hour) and the molar ratio of benzoic acid to isopropanol (1.0:3.0) and the weight ratio of PTSA to benzoic acid (14.88%).

(5) The maximum yield of isoamyl benzoate reached 92.7% under the condition of the Ti loading amount (10%), the reaction time (1.5 hours), the molar ratio of benzoic acid to isopropanol (1.0:4.0) and the weight ratio of Ti(SO₄)₂/TiO₂ to benzoic acid (40.98%) .

REFERENCES

[1] Yu, S. X. and Wen, R. M. *Journal of Jiangxi Institute of Education*, **2002**, 23(6), 35.

[2] Zhang, F. J., Zhang, H. Y., Sheng, S. L. and Zhang, X. F. *Industrial Catalysis*, **2004**, 12(11), 24.

[3] Yang, S. J., Yu, X. Q. and Liang, Y. G. *Gangdong Chemical Industry*, **2001**, 3, 29.

[4] Li, X. Y., Hua, Y. Y. and Cao, M. *Guangzhou Chemical Industry*, **2000**, 28(4), 4.

[5] Zhang, F. X. *Journal of Hengyang Teachers College*, **1996**, 14(2), 41.

[6] Guang, S. B. and Yu, S. X. *Journal of Hengyang Normal University*, **2001**, 22(3), 18.

[7] Shi, L., Zhang, H. J. and Wu, D. H. *Advances in Fine Petrochemicals*, **2003**, 4(7), 19.

[8] Zhang, F. J., Zhang, H. Y., Sheng, S. L. and Zhang, X. Y. *Industrial Catalysis*, **2004**, 12(11), 24.

ASSESSMENTS OF PLANTS FOR PHYTOREMEDIATION OF ARSENIC-CONTAMINATED WATER AND SOIL

María T. Alarcón-Herrera[a]*, Mario A. Olmos-Márquez[a], Cecilia Valles-Aragon[a], Esther Llorens[a], Ignacio R. Martin Domínguez[a]

Phytoremediation is an innovative technology that uses plants in order to remediate polluted water and soil. A 10 week study in flower pots was performed in order to determine the arsenic (As) removal potential of *Shoenoplectus americanus*, *Eleocharis macrostachya* and *Baccharis salicifolia* and also to evaluate their tolerance capacity to increasing doses of As. The experiment involved five different treatments with distinct As concentrations (1, 2, 3, 4 and 5 mg L^{-1}) and a control (tap water) to determine the acclimatization capacity of the species to the different concentrations. The number of plants and their height were determined during the experiment. The values for the factors of translocation, accumulation and enrichment were obtained at the end of the experiment; the maximum values for these factors were, respectively, 1.86, 92.13 and 1.63 for *E. macrostachya*, 1.73, 59.74 and 0.56 for *S. americanus* and 8.96, 27.94 and 6.72 for *B. salicifolia*. The maximum growth value belonged to the *S americanus*. The maximum concentration of As in water tolerated by *E. macrostachya* and *B. salicifolia* were 2 and 3 mg L^{-1} respectively. *B. Salicifolia*, has no tolerance for environments with high concentrations of arsenic. *S. americanus* showed the highest As accumulation capacity and the greatest tolerance in the tested concentrations. *E. macrostachya* proved to be translocator plants and *S. americanus* was confirmed to be a stabilizer plant with a high potential for phytostabilization and rhizofiltration techniques.

* Corresponding Author
    Maria Teresa Alarcón-Herrera
    E-Mail: teresa.alarcon@cimav.edu.mx
[a]   Miguel de Cervantes 120, Complejo Industrial Chihuahua
    31109 Chihuahua, Chih. Mexico

INTRODUCTION

As removal of water sources for human consumption is one of the great challenges in the world. Millions of people have been or are being exposed to excessive levels of As through drinking water[1,-3]. The health effects attributed to the consumption of water with high concentrations of As include: skin diseases, cardiovascular, neurological, hematological, renal and respiratory and liver cancer, kidney and prostate [4] . Therefore minimizing the metalloid concentrations in soils and water contaminated through various physical, chemical and biological, processes is one of the current challenges. Phytoremediation has been proposed as an alternative technology eco-friendly and cost-effective to remediate soils contaminated with As.[5,6] This technique has been applied to the removal of different contaminants (including metals and metalloids) of soil, surface water, ground water and municipal and industrial wastewaters.[7] In Mexico there are several areas affected by high concentrations of As in groundwater. In recent decades, studies conducted at different sources of drinking water in the state of Chihuahua, have shown the presence of arsenic in concentrations exceeding the maximum permissible limits of NOM-127-SSA1-1994,[8] for human consumption, with an average concentration of 0.152 mg L^{-1} and a maximum concentration of 0,517 mg L^{-1} . In addition, the population growth and overexploitation of the different aquifers have

caused an increase in the concentrations of this metalloid, which is found naturally in subsurface geological formations. *E. macrostachya, S. americanus and B. salicifolia* are three species of native plants from the state of Chihuahua that have been reported as As tolerant with potential application in phytoremediation techniques [9],[10]). Thus, the aim of this study was to determine the translocation, accumulation, enrichment and tolerance factors of these plants species, for potential use in the phytoremediation of arsenic in water and soil.

EXPERIMENTAL

The experiment was performed in pots, for a period of 10 weeks, with 3 suspected As tolerant species: *E. macrostachya*, *S. americanus* (Cyperaceaes family) and *B. salicifolia* (Asteraceae family). The plants were subjected to increasing doses of As prepared with sodium arsenite (1, 2, 3, 4 and 5 mg L^{-1}) using tap water as a control. The experiment was performed by duplicate in two different media: one with soil (loamy sand) composed of 91% sand and 9% of fine particles. The other was a hydroponic medium prepared with tap water and Arsenic.

Collection and acclimation of plants

E. macrostachya, S. americanus, and *Bacharis salicifolia* were collected in the state of Chihuahua, Mexico (28 ° 35 '53.55 "N, 105 ° 33' 41.93"). Plant species were removed completely (leaf, stem and root) from their native place and transplanted into plastic pots. The soil was composed of

silty sand. Plants were kept under flooded conditions with tap water, adding nutrients once a week for an acclimatization period of three months prior to the start of the experiment. Before placing the plants in pots, their size were measured, the wet weights determined, and the number of plants per pot was counted. These data were considered as the initial values of the experiment. The plants in hydroponic medium were placed in plastic bottles (2 L).

Plant monitoring

Throughout the period of experiment, the number of plants per pot were counted weekly, thereby determining the reproduction of plants subjected to various doses of As. To determine the growth, three individuals per pot were randomly selected, and their growth was measured weekly. At the end of the experiment, all plants were weighed to determine the biomass produced by each species.

Chemical analysis of plants

At the end of the experiment all the plants were extracted from their pots, washed with water, separated in different sections (roots, stems and leaf) and placed in plastic bags previously identified. The samples were dried at 60 ° C for 24h in an oven, and subsequently digested in a CEM microwave equipment Model MarsX. A certificated standard of tomato leafs was used as an analytical control.

The determination of As was carried out by atomic absorption spectrophotometry with hydride generator, GBC brand, model Avanta Σ, and an inductively coupled plasma (ICP-OES) Thermo Jarrell Ash brand, model AP-Duo Iris. To ensure the quality of analyzes, duplicate samples and controls were considered, as well as the measuring of certified standards.

Determination of translocation, accumulation and enrichment coefficient

The translocation factor (TF) was calculated according to the criteria established by Fitz and Wenzel[11], by dividing the concentration of As in shoot biomass (mg kg^{-1}) by the concentration of As in the root biomass (mg kg^{-1}). The accumulation factor (AF) was calculated by the ratio of As in the stem of the plant and the concentration of As in the stalk. Finally the enrichment coefficient (EC) was calculated by the ratio of As concentration in the treated plants, and the concentration of arsenic in soil[12]).

RESULTS AND DISCUSSION

The highest concentration of As was found in the roots of the analyzed plants. *E. macrostachya and S. americanus* had the highest accumulation of arsenic in the hydroponic medium (Table 1), while *B. salicifolia* in soil (Table 2).

E. macrostachya presents a proportional accumulation of As with the concentration increase of arsenic in the feed water. At lower As concentrations (>2 mg L^{-1}), the plant behaves as a tolerant, absorbing and holding As in the root.

Whereas at higher As concentrations (≤ 4 mg L^{-1}) the plant allows to accumulate greater amounts of As in the shoot also.

S. americanus tolerated arsenic concentrations up to 4 mg L^{-1} in hydroponic medium for a period of 10 weeks. At concentrations of 5 mg L^{-1}, the plant decreased its capacity of arsenic accumulation; this may be due to a blocking defense or to prevent damage from the element in their tissues[13]). The plant accumulated 30 times more arsenic from soil, than from the hydroponic media, behaving as a tolerant during all tests.

B. salicifolia behaves poorly under high arsenic concentrations in the media. Showing a possible saturation or activation in defense mechanisms to inhibit the toxic effects of arsenic. The plant behaves as traslocator in hydroponic media.

The biomass of *E. macrostachya as S. americanus*, had increased proportionally with the increase of As concentration in water. In contrast *B. salicifolia* produced more biomass at low As concentrations in water. At the end of the experiment it was observed that *E. macrostachya and S. americanus,* roots developed rapidly at high As concentrations, while the size of stem decreased.

S. americanus showed positive reproduction at all As concentrations in both media (soil, hydroponic). The maximum increase was of 73 new plants. *E. macrostachya* plants showed an increase in the number of plants under concentrations of As in the range of 1-3 mg L^{-1}. Under these concentrations, reproduction was the largest (76 new plants). *B. salicifolia* reproduction didn't occur in any of the As concentrations.

With regard to size, all plants showed positive values in both mediums, but the plants developed better in flooded soil. *E. macrostachya* showed the higher size with a maximum value of 40 cm in hydroponic media and 104 cm. in soil.

Plant growth is a major parameter used to assess survival and adaptation of a given species to the environment. Plants responded to the excess of As supply in water and soil mediums by developing visible symptoms of toxicity, besides decreasing stem biomass[14].

B. salicifolia accumulated Arsenic in the root (11 to 329 mg kg^{-1}) and in the stem from 29 to 141 mg kg^{-1}, in the loamy sand media (soil), irrigated with arsenic concentrations between 0.02 and 4 mg L^{-1}. Although the plant could accumulate arsenic, its reproductive capacity was inhibited, and the plant damage was evident for all arsenic concentrations tested in this study. Therefore, the plant is not suitable for phytoremediation purposes. The translocation factor was 4.79, which is about six times higher than the value reported for plants belonging to the same family as *B. sarothroides* (TF = 0.80) (Haque et al., 2008[15]). High translocation of arsenic by *B. salicifolia* may be the cause of its damage.

E. macrostachya showed a severe clorosis damage in the stem by the forth week of experimentation, for arsenic concentrations greater than 2 mg L^{-1} in the hydroponic media.

Table 1. Biosorption of arsenic by plants (mean ± standard deviation), translocation, and biomass accumulation using a hydroponic medium.

(mgAs L⁻¹)	Arsenic, mg kg⁻¹			TF	AF	Biomass (g)
	Root	Stalk	leaves			
Test Solutions	*E. macrostachya*					
Control	42.4 ± 2.2	1.8 ± 0.4	-	0.0	-	20.0
1	93.9 ± 4.1	35.6 ± 1.2	-	0.4	18.9	51.2
2	54.9 ± 3.4	73.4 ± 3.7	-	1.3	38.9	29.0
3	91.9 ± 6.0	156.1 ± 6.5	-	1.7	82.6	34.8
4	124.7 ± 6.3	162.7 ± 10.9	-	1.3	86.1	33.8
5	183.6 ± 8.3	174.1 ± 10.2	-	1.0	92.1	71.8
Test Solutions	*S. americanus*					
Control	39.2 ± 2.2	2.9 ± 0.1	-	0.1	-	60.6
1	62.8 ± 3.8	31.4 ± 1.2	-	0.5	10.5	125.5
2	239.4 ± 9.8	34.1 ± 2.2	-	0.1	11.4	108.2
3	357.7 ± 22.7	52.7 ± 3.9	-	0.1	17.6	101.3
4	616.5 ± 26.6	178.6 ± 11.4	-	0.3	59.7	149.6
5	419.5 ± 24.9	130.6 ± 6.8	-	0.3	43.7	166.6
	Hydroponic media					
Control	1.0 ± 0.1	2.6 ± 0.1	3.2 ± 0.2	5.5	-	12.4
1	1.4 ± 0.1	4.5 ± 0.2	8.0 ± 0.5	9.0	2.1	8.3
2	26.3 ± 1.4	32.5 ± 2.0	20.7 ± 1.2	2.0	9.1	2.7
3	51.8 ± 3.3	74.0 ± 5.7	60.5 ± 4.7	2.6	22.9	7.9
4	56.9 ± 3.2	65.0 ± 3.9	5.7 ± 0.4	1.2	12.0	9.3
5	94.1 ± 8.2	57.6 ± 3.4	109.2 ± 6.9	1.8	28.4	6.5

Table 2. Biosorption of As by plants (mean ± SD), translocation factors, accumulation and enrichment coefficient, using soil medium (silty sand).

(mgAs L⁻¹)	Arsenic, mg kg⁻¹			TF	AF	EC	Biomass (g)
	Root	Stalk	leaves				
Test Solutions	*E. macrostachya*						
Control	4.3 ± 0.3	2.5 ± 0.1	-	0.6	-	-	66.0
1	12.1 ± 0.7	4.8 ± 0.2	-	0.4	1.9	0.5	58.8
2	11.4 ± 0.7	18.7 ± 1.0	-	1.6	7.6	1.1	33.0
3	16.4 ± 0.7	30.5 ± 2.0	-	1.9	12.3	1.1	95.7
4	40.4 ±1.7	32.1 ± 2.3	-	0.8	13.0	0.9	66.0
5	72.9 ± 3.9	71.9 ± 6.1	-	1.0	29.1	1.6	84.2
Test Solutions	*S. americanus*						
Control	6.7 ± 0.3	2.2 ± 0.1	-	0.3	-	-	86.3
1	3.7 ± 0.1	5.0 ± 0.3	-	1.3	2.3	0.6	158.6
2	29.1 ± 1.3	2.0 ± 0.1	-	0.1	0.9	0.1	110.2
3	48.1 ± 2.0	4.8 ± 0.3	-	0.1	2.2	0.2	155.8
4	24.9 ± 1.9	11.7 ± 0.7	-	0.5	5.4	0.3	149.1
5	14.1 ± 1.0	24.4 ± 1.4	-	1.7	11.2	0.5	191.3
Test Solutions	*B. salicifolia*						
Control	11.3 ± 0.7	28.8 ± 1.3	2.5 ± 0.1	0.2	-	-	17.6
1	18.5 ± 1.0	57.9 ± 3.02	3.4 ± 0.2	3.3	2.0	6.6	19.6
2	25.7 ± 1.3	118.3 ± 9.1	4.6 ± 0.2	4.8	3.9	6.7	27.0
3	329.6 ± 19.9	64.6 ± 3.1	3.3 ± 0.2	0.2	2.2	2.4	18.0
4	321.5 ± 12.0	140.8 ± 10.2	33.2 ± 1.9	0.5	5.6	4.0	15.2
5	40.5 ± 3.0	79.2 ± 4.0	3.7 ± 0.1	2.0	2.6	1.8	33.1

These physical changes were consistent with the high translocation factors (TF) obtained by the chemical analysis of the plants at the end of the experimentation (1.3, 1.7, 1.3 and 1) for As concentrations of 2, 3, 4 and 5 mg L^{-1} respectively. Indicating that, when the plant is under high As concentrations, the metaloid is translocated to the shoot, causing damage to the cell membrane. This can be attributed to the possible interaction of arsenic with sulfhydryl groups of proteins in the plant [16]. For As concentrations lower than 3. The root of the plant suffered no apparent damage, but its size increased proportionally to the increase in As concentration in water (Figure 1)

Figure 1. Root and stem size in E. macrostachya, after undergoing As concentrations of 0,016 mg L^{-1} and 5 mg L^{-1} for a period of 10 weeks.

Accumulation factors (AF) calculated for *E. macrostachya* in soil (Table 2) shown that at higher concentrations of arsenic in the irrigated water, the plant also accumulated more arsenic in root and stem. The higher values correspond to the higher As concentration of 5 mg L^{-1}. These values are approximately 7 times higher than those reported in previous studies of the plant when it was subjected to arsenic concentrations in irrigation water, between 3 and 9 mg L^{-1}, for a period of four months (Nuñez et al., 2007). However, translocation factors obtained in both the studies are a coincident, confirming that the plant is tolerant to arsenic concentrations lower than 2 mg L^{-1} whereas above this value, the damage is visible, ceasing to be tolerant when the As concentration increased to 3 mg L^{-1} in the irrigated water.

S. americanus in soil, irrigated with 3 mg L^{-1} of arsenic, was able to accumulate 48 mg/kg of arsenic in their roots and 4.8 mg/kg in their stems (Table 2). In previous studies (Flores et al., 2003) reported that for soils irrigated with concentrations of 9 mg L^{-1} of arsenic in water, the arsenic accumulation in the plant roots was approximately 6 times less than the results obtained in the present study (7.6 mg kg^{-1}). However, the amounts of arsenic in the stalk are a coincident (4.7 mg kg^{-1}). This behaviour is attributable to the fact that the plant decreases arsenic absorption at concentrations greater than 3 mg L^{-1} and it behaves as exception to arsenic, possibly to restrict the adverse effects on the vegetal structure (Castillo-Michel et al., 2009[17]).

Studies with plants associated with desert environments shows that other plants like *Prosopis sp. and Chilopsis linearis* accumulate As up to 445 mg kg^{-1} in their roots[18,15]) *S. americanus* accumulated As up to 616 mg kg^{-1} in hydroponic medium (Table 1). Due to this characteristic feature researchers are suggesting its potential use in phytoremediation of contaminated water and soil. *E. macrostachya* can also be considered in phytoestabilization techniques for sites with concentrations up to 2 mg L^{-1}. Considering that the characteristic of extracting metals from water is known as 'rhizofiltration', *E. macrostachya* and *S. americanus* could, therefore, also be considered as rhizofilterers of As, due to its capability of grow in flooded environments[19].

This research shows that, *B. Salicifolia*, has least tolerance for environments with high concentrations of arsenic. *E. macrostachya* and *S. americanus* are tolerant to high concentrations of arsenic in soil and water. The higher concentrations of As, the greater the As accumulated in the roots of plants. The maximum tolerated concentration of arsenic in hydroponic medium for *E. macrostachya* was 2 mg L^{-1}, and for soil (silty sand) it was 4 mg L^{-1}.

S. americanus showed the highest As accumulation capacity and greater tolerance for As concentrations up to 3 mg L^{-1}, showing no evidence of physical damage to the cell or tissue limitation in their reproduction and growth. Both species *E. macrostachya and S. americanus* behave as tolerating and excluding with a high potential for use in phytoremediation strategies.

ACKNOWLEDGEMENTS

REFERENCES

[1] Wickramasinghe, S. R., Han, B., Zimbron, J., Shen Z., Karim, M. N., *Desalination,* **2004,** *169*, 231-244.

[2] Caceres, D. D., Pino, P., Montesinos, N., Atalah, E., Amigo, H., and Loomis, D., *Environ. Res.,* **2005**, *98(2),* 151-159.

[3] Agusa. T., Kunito, T., Fujijara, J., Kubota, R., Minh. T. B., Trang. P. T. K., Iwata. H., Subramanian A., Viet. P. H., and Tanabe. S. *Environ. Pollut.,* **2006**, *139(1),* 95-106.

[4] Morton, W. E., Dunette, D.A. Health effect of environmental arsenic. In: Nriagu, J. O., Editor. *Arsenic in the environment, Part II: Human and ecosystem effects.* New York: Wiley and sons; **1994**, 17-34.

[5] Lasat, M. M., *J. Environ. Qual.* **2002**, *31*, 109-120.

[6] Mc Grath, S. P., Zhao, F. J., Lombi, E. *Adv. Agron.* **2002**, *75,* 1-56.

[7] USEPA (United States Environmental Protection Agency). *Arsenic treatment technologies for soil, waste and water.* Office of Solid Waste and Emergency Response. EPA 542-R-02-004. **2002.**

[8] Secretaria de Salud, Modificación a la Norma Oficial Mexicana NOM-127-SSA-1994, Salud ambiental. Agua para uso y consumo humano. Límites permisibles de calidad y

tratamientos a que debe someterse el agua para su potabilización. **2000**.

9 Flores-Tavizòn, E., Alarcón-Herrera, M. T., Gonzàlez-Elizondo, S., Olguín, E. J., Arsenic tolerating plants from mine sites and hot sprongs in the semi-arid región of Chihuahua, Mexico, *Acta Biotechnol.,* **2003** 113-119.

10 Nuñez Montoya, O. G., Alarcón Herrera, M.T., Melgoza Castillo, A., Rodríguez Almeida, F.A. y Royo-Márquez, M.H. Evaluation of three native species from Chihuahua desert for use in phytoremediation, *Terra Latino*., **2007** *25*(1) 35-41.

11 Fitz, W. J Y Wenzel, W. W. Arsenic transformations in the soil-rhizosphere-plant system: fundamentals and potential application to phytoremediation. *Biotechnol.,* **2002** *99,* 259-278.

12 Zu, Y.Q., LI, Y., Chen, H,Y., Qin, L., Schvartz, C. Hyperaccumulation of Pb, Zn and Cd in herbaceous grown on lead-zinc mining area in Yunnan, China. *Environ. Int.* **2005**, *31*, 755-762.

13 Gonzalez-Mendoza, D., Zapata-Perez, O. Mecanismos de tolerancia a elementos potencialmente tóxicos en plantas. Boletín de la Sociedad Botánica de México, Distrito Federal, México. **2008**, *82*, 53-61.

14 Shanker, A.K., Cevantes, C., Loza-Tavera, H., Avudainayagam, S. Chromium toxicity in plants. *Environ. Int*., **2005**, *31*, 739-753.

14 Haque N., Peralta-Videa, J. R., Jones, J. L., Gill, T. E., Gardea-Torresdey J. L. Screening the phytoremediation potential of desert broom (Baccharis sarothroides gray) growing on mine tailing in Arizona, USA. *Environ. Pollut*., **2008**,*153*, 362-368.

15 Haque N., Peralta-Videa, J. R., Jones, J. L., Gill, T. E., Gardea-Torresdey J. L. Screening the phytoremediation potential of desert broom (Baccharis sarothroides gray) growing on mine tailing in Arizona, USA. *Environ. Pollut*., **2008**,*153*, 362-368.

16 Wauchope, R.D. Uptake, translocation and phytotoxicity of arsenic in plants. In: Arsenic: Industrial, Biomedical, Environmental Perspectives (Lederer y Fensterheim (ed.)). Arsenic Symposium, Gaithersburg, Maryland. Van Nostrand Reinhold Company. New York, N.Y. **1983**, 348-374.

17 Castillo-Michel H. A., Zuverza-Mena N., Parsons J. G., Dokken K.M., Duarte-Gardea M., Peralta-Videa J. R., Gardea-Torresdey J.L. Accumulation, spatiation and coordination of arsenic in an inbred line and a wild type cultivar of the desert plant species Chilopsis linearis (desert willow), *Phytochem.*, **2009**, *70,* 540-545.

18 Haque N., Peralta-Videla, J. R., Duarte-Gardea M., Gardea-Torresdey J. L. Different effect of metals/metalloids on the growth and element uptake of mesquite plants obtained from plants grown at a Cooper mine tailing, *Biores.,***2009**,*100*, 6177-6182.

19 Mielke, M.S., Almeida, A.-A.F., Gomes, F.P., Aguilar, M.A.G., Mangabeira,P.A.O., 2003. Leaf gas exchange, chlorophyll fluorescence and growthresponses of Genipa americana seedlings to soil flooding. *Environ. Exp.Bot.,* **2003**, *50*, 221-231.

ANALYSIS OF *FICUS CARICA* L. – VOLATILE COMPONENTS AND MINERAL CONTENT

Emese Ficsor[a], Klára Szentmihályi[b], Éva Lemberkovics[a], Anna Blázovics[a], Andrea Balázs[a]

Ficus carica L. is a well-known Mediterranean plant, its fructus - the fig- is consumed widely, mostly in the southern region of Europe. It's a member of the Moraceae family, one of the earliest crops. It can be consumed raw, dried or even as jam as a part of the Mediterranean diet. One part of our research was to determine the volatile components of *Ficus carica* L. The composition of volatile components are important for the determination of fruit quality. We compared two extraction methods, examined by SPME-GC/MS. Two preparation methods were used: directly measured by SPME, and also samples made by steam distillation. Figs has an important role as phytonutrition. Mineral element content was determined by ICP. Fig is a good source of elements for Ca, Cr, Cu, Fe, K, Mg, Mn and Mo, since eating 5 dkg of dried fig covers more than 15% of the Recommended Dietry Allowances.

* Corresponding Authors
    E-Mail: fiemes@indamail.hu
[a] Semmelweis University, Department of Pharmacognosy, H-1086 Budapest, Üllői street 26, Hungary
[b] Institute of Materials and Environmental Chemistry Research Centre for Natural Sciences of the HAS, H-1025 Budapest, POBox 17, Hungary.

Introduction

As Hippocrates said: "Let food be thy medicine and medicine be thy food", phytonutritions role are becoming more important. Many researches are carried out to determine the active components of plants of traditional medicine and nutrition.

Ficus carica L. is part of the Moraceae family, it has been cultivated since ancient times. It requires wasp pollination of a particular species of wasp to produce seeds. *Ficus carica* L. is a widely known and consumed Mediterranean plant. Its fruit is without fat and cholesterol, it contains lots of vitamins, good source for dietary fiber. It's also a good source for mineral elements. In medicine, it is internally used to control digestion. As a part of the Mediterranean diet, it's little laxative effect is quite useful. Fresh *Ficus carica* L. fructus contains lots of pectin, which influences the human body to reduce the cholesterol amount. It contains a lot of antioxidants, a good source of polyphenols and flavonoids.[1]

One of the essential parameter of fruit quality is the aroma, which is determined by the volatile components. They can be derived from amino acids, fatty acids and carbohydrate compounds.[2] Volatile compounds present in the fresh and processed fruits affect the flavour and food quality which is formed by a complex mixture of chemical substances like aldehydes, alcohols, ketones, esters, terpenes and other compounds.[3] The variability of aroma components depend on climatological conditions, cultivar, maturity and technological factors, like harvest, post-harvest treatments, processing and storage conditions. [4,5]

Traditional methods used for determine volatile components are time consuming and require several steps. Methods using solid phase micro extraction (SPME) technique save preparation time, solvent and can improve the detection limits.[6] This type of extraction is a solventless extraction alternative and no modifications occur in the components due to the solvent or the temperature effect. SPME technique has been widely used for the analysis of volatile and semi-volatile components from environmental, biological and food samples.[7]

Mineral elements (macro-, meso- and trace-) play an important role in effecting the proper mechanism in the human body.[8] These components usually obtained from nutrition, but usually not enough is gained. The improper dietetic culture and the unhealthy food consumption play part in prelatent, latent or manifested metal deficiency. Nowadays lots of supplements are commercially sold, but hardly any of them contains the needed elements in the right natural form, therefore their absorption or bioavailability in the human body is not as it is expected.[9,10] Nutrition is the best for gaining these elements by natural form. Previous studies indicate that *Ficus carica* L. is a good source of minerals, vitamins and dietary fibre. [7,11]

The aims of our research was to examine the volatile components in extracts obtained by different extraction methods and determine the mineral element content of the *Ficus carica* L. fructus and folium as well as evaluate as a phytonutrient.

Experimental

Ficus carica L. samples

The *Ficus carica* L. folium and fructus from Hungarian origin was used. The fructus was obtained from the Hungarian trade in order to examine what would get into the human organ by randomly bought fruit, while the folium was collected from Budakeszi under Hungarian weather conditions. The Italian origin folium and cortex were collected in Latina (Italy). The fructus was lyophilised, the folium and cortex were both air-dried.

Microscopical preparations

The fructus and folium samples with Hungarian origin were examined. Due to the regulation of the eighth Pharmacopoea Hungarica, cross sections and powder preparations were made to determine the microscopic features.[12]

GC analytical procedures

The analysis was carried out with an Agilent 6890N/5973N GC-MSD (Santa Clara, CA, USA). Separations were performed using an Agilent HP-5MS capillary column (30 m × 250 μm × 0.25 μm). The GC oven temperature was programmed from 60 ºC (3 min isothermal) to 200 ºC at 8 ºC min^{-1} (2 min isothermal), 200-230 ºC at 10 ºC min^{-1} (5 min isothermal) and finally 230-250 ºC at 10 ºC min^{-1} (1 min isothermal). Helium was the carrier gas at 1.0 mL min^{-1} (37 cm s^{-1}) in constant flow mode.

The mass selective detector was equipped with a quadrupole mass analyzer and was operated in electron ionization mode at 70 eV. The MS was operated in full scan mode (41-500 amu at 3.2 scan s[-1]), and data were evaluated by MSD ChemStation D.02.00.275 software (Agilent).

Volatile extraction

Samples from the Hungarian folium and fructus were created by steam distillation described by the Pharmacopoeia Hungarica VIII.[12] These results were compared by samples measured directly by SPME.

Measurement of element concentrations

The element concentration (Al, B, Ba, Ca, Cd, Co, Cr, Cu, Fe, K, Mg, Mn, Mo, Na, Ni, P, Pb, S, Si, Sn, Sr, Ti, V, Zn) of the fig fruit and folium from Hungarian trade and Italian origin plant was determined with an ICP-OES (inductively coupled plasma optical emission spectrometer). Type of instrument: Spectro Genesis ICP-OES (Kleve, Germany). The samples were measured three times.

Results and Discussion

Microscopic examination

First the microscopic features of folium and fructus were determined. Several Ca-oxalate rosettas and covering trichomes on the folium were found by cross section, these are good identification signs in the powder preparations as well. In the folium cross section the porous and columned parenchyma can be easily observed next to the many trichomes. In the fructus powder preparations oil drops and oil beads were present with several covering trichomes and Ca-oxalate rosettas.

GC-analytical measurements

One part of our research was to determine the volatile components of *Ficus carica* L. For the examination of volatile components, SPME method connected to GC-MS (SPME-GC/MS) was used beside the traditionally applied

extraction methods (solvent extraction and steam distillation). For these experiments *Ficus carica* L. samples of Hungarian origin was applied. The results of samples made by steam distillation were compared with the results obtained from direct examination by SPME (no extraction methods were used).

Examining the *Ficus carica* L. fructus directly with SPME, only one volatile compound, 2,3-butane-diol, was found. In the other side, when used steam distillation first and measured by SPME-GC-MS, the sample contained many other components. These components were mainly hydrocarbons, like the tetramethyl-decane, trimethyl-undecane, octadecane and one terpene, which was carvacrol. ß-Caryophyllene, caryophyllene-oxid and apiol were also present. Carvacrol is a monoterpenoid phenol, it has a characteristic, purgent odor. It inhibits the the growth of several bacteria strains like *Escherichia coli* and *Bacillus cereus*.[13] It also activates PPAR and suppresses COX-2 inflammation.[14] ß- Caryophyllene is known for its antibacterial properties.[15] Sesquiterpenes, like ß-caryophyllene, are released in response to the attack by *Spodoptera exigua* larvae in cotton plantlets. This confirm the hypothesis that these components play part in the defence against insects.[16] β-Caryophyllene has been shown to selectively bind to the cannabinoid receptor type-2 (CB$_2$) and to exert significant cannabimimetic antiinflammatory effects in mice. It doesn't have psychomimetic effects because it doesn't bind to the centrally expressed cannabinoid receptor type-1.[17] In the fructus damascenone is present, which is derived from the degradation of carotenoids. It belongs to a family of chemicals known as rose ketones, and has an important role in creating the rose aroma. [18]

Examined the folium volatile compounds directly by SPME, the main components were 3,5-octadiene-2-on and trimethyl-methylene-vinilbicyclononane. Other components were like aldehyde (hexanal), hydrocarbons (undecane, dimethyl-undecane) and alcohol (ethyl-cyclohexanol). Hexanal is an alkyl-aldehyde, which is used by the flavor industry to produce fruity flavour. Undecane has affects on moths as a mild sex attractant, and also as an alert signal for ants.[19] Benzaldehyde is one of the simplest aromatic aldehyde, which is used by the industry because it has an almond-like odor. It is the primary component of bitter almond oil, and can be extracted from other natural sources as well. Limonene is also present in the folium, it is a cyclic terpene. Mainly the D isomer is present, which gives a natural citrus smell like orange. It can be found in many citrus fruits. [20]

The samples made from the folium by steam distillation and measured by SPME-GC-MS contained well known substances, like hydrocarbons (methyl-undecane, dimethyl-undecane and nonadecane), sesquiterpenes - which are present in the fructus as well- like ß- caryophyllene and caryophyllene-oxid. Ionones are a series of closely related chemical substances, mostly aroma compounds found in the many essential oils, like in rose oils. β-ionone contributes to the aroma of roses, it is present in a low concentration, and also used in parfumery.[18]

Examining the folium and fructus by different extraction methods the data show that great variety can be observed in the determined components.

Mineral elements

Mineral element content was determined by ICP method. The fig fruit and folium from Hungarian trade and also Italian origin *Ficus carica* L. folium and cortex was measured.

The Italian origin *Ficus carica* L. samples (folium and cortex) contain the following mineral elements in about average plant concentration[21,22]: Al, B, Ba, Ca, Cd, Co, Cu, Mg, Mo, Na, Ni, Sn, V (Table 1). The concentrations of P (<3000 µg g^{-1}), S (<1000 µg g^{-1}) and (<20 µg g^{-1}) in both samples was low. The amount of Fe (<100 µg g^{-1}), K (< 20 000 µg g^{-1}) and Mn (<10 µg g^{-1}) was also found to be low in the folium and in the cortex as well.

Table 1. Mineral concentration ± standard deviation (µg g^{-1}) of Italian origin *Ficus carica* L.

Elements	Folium	Cortex
Al	131.8±5.1	34.36±3.60
B	84.57±4.30	66.50±4.37
Ba	13.46±0.06	10.70±0.30
Ca	27531±137	18623±712
Cd	0.65±0.01	0.63±0.01
Co	0.41±0.01	0.39±0.01
Cr	2.46±0.31	1.44±0.40
Cu	4.84±0.21	4.21±0.00
Fe	153.22±5.14	28.12±4.60
K	24786±280	13902±879
Mg	3519±70	2202±285
Mn	22.69±0.61	5.06±0.82
Mo	0.87±0.01	0.49±0.10
Na	239.4±8.3	87.40±18.32
Ni	1.44±0.19	0.73±0.01
P	945.9±3.1	960.7±107.5
Pb	1.12±0.17	2.90±2.66
S	819.3±37.6	356.7±26.4
Si	183.6±31.6	169.4±6.3
Sn	0.91±0.22	1.49±0.49
Sr	142.4±8.2	70.44±4.71
Ti	4.70±0.38	0.66±0.33
V	0.82±0.01	0.38±0.01
Zn	14.37±0.28	6.33±0.68

In the Hungarian origin *Ficus carica L.* samples, mineral elements like Al, B, Ba, Cd, Co, Cu, Mg, Mo, Na, Pb, Sn, V and Ti are present in average concentration compared to other plants as it can be seen in Table 2. The amount of Ca and Fe in the Hungarian folium was higher than usually available in other plants.[21] Relatively low concentration was found in the Hungarian origin fructus for Ca (<10000 µg g^{-1}), Fe (<100 µg g^{-1}), K (< 20 000 µg g^{-1}), Mn (<10 µg g^{-1}), and S (<1000 µg g^{-1}), while the Cr concentration was high (>1 µg g^{-1}) compared to the average plant concentration determined by other authors. [21,22] In the Hungarian samples the amount of P (<3000 µg g^{-1}) and Zn (<20 µg g^{-1}) was also low.

Comparing the macro element content of folium samples the amount of Ca is almost the same in the Italian and Hungarian folium. The amount of Na in the folium of Italian origin was much higher than in the folium of Hungarian origin, but it was also the same in the cortex and in the fructus. Regarding the K content, the Italian folium contains higher concentration than the others, since it is almost the same in them. The amount of Mg in the two foliums was almost the same, but it was less in the fructus.

Table2. Mineral concentration ± standard deviation (µg g^{-1}) of Hungarian origin *Ficus carica* L.

Elements	Fructus	Folium
Al	24.24±14.72	105.5±1.98
B	50.44±11.28	130.1±5.29
Ba	6.60±1.09	7.97±0.09
Ca	6006±613	27611±152
Cd	0.61±0.01	0.64±0.00
Co	0.69±0.33	0.41±0.01
Cr	1.34±0.49	1.25±0.07
Cu	5.66±0.00	8.57±0.13
Fe	41.62±3.47	182.6±3.06
K	13892±415	16000±234
Mg	1381±186	3565±174
Mn	7.76±0.01	27.02±1.31
Mo	0.54±0.17	0.84±0.09
Na	88.49±10.83	136.6±7.9
Ni	1.74±0.07	1.70±0.03
P	1054±44	1285±31
Pb	<detection limit	0.99±0.27
S	536.1±7.5	1150±67
Si	157.4±40.4	106.9±16.3
Sn	1.24±0.51	0.72±0.21
Sr	20.12±2.89	64.37±4.20
Ti	1.03±0.66	3.43±0.24
V	0.38±0.02	0.58±0.00
Zn	9.80±0.39	14.27±0.80

The amount of Fe was highest in the Hungarian origin folium, followed by the Italian folium. The amount of Fe in the fructus is not high. The Zn content was same in the foliums, while it was a little less in the fructus. The amount of Mn in both foliums was almost the same, nevertheless in the fructus it was less compared to the foliums. In the Hungarian *Ficus carica* L., both in the fructus and in the folium, the concentration of Cu was higher compared to the samples of Italian origin. The concentration of Cr (>1 µg g^{-1}) in both Italian samples, of Ti (>2 µg g^{-1}) in the folium and of Pb (>2 µg g^{-1}) in the cortex was high. Comparing the Hungarian and Italian samples it can be seen that the amount of Ca, Cd, Co, Mg, Sn and Zn doesn't differ significantly. These mineral elements are probably specific feature for the species which does not depend on the geological and weather conditions.

Mineral element intake

Fig fruit contains low calorie. Depends on the species of *Ficus*, the weight of one fresh fructus can be around 10-20 dkg. In dry form fig contains 4-5 times more dry matter content, so more precious components can be found. In dried form the fructus contains more calorie, it is around 249 calories counted for 100 g.

Calculating the mineral element intake by fig fruit, it can be stated that fig is a good source of elements for Ca, Cr, Cu, Fe, K, Mg, Mn and Mo, since eating 5 dkg of dried fig covers more than 15% of the Recommended Dietry Allowances (RDA).[23]

The RDA of K for the human body is 2000 mg/70 kg body weight/day and the Dietary Reference Intake (DRI)[24] of Na is also 2000 mg/70 kg body weight/day. The fig eating (5 dkg, 2-3 pieces of dried fruit) covers 34.7% of K requirement (RDA), while 0.2% of Na intake (DRI). The optimal Na:K rate is about 1:4. Usually, this rate is shifted to

Na, because of the used methods in the food industry. In this case, the Na:K rate is greatly shifted to the K side. The RDA of Ca for an adult is 800 mg/70 kg body weight/day. Five dkg of fig contains 37.6% of RDA. The RDA of Mg for the human body is 6 mg kg^{-1} so for a 70 kg person it is 420 mg d^{-1}, 16.4% of which may be ensured by fig. In general the ratio of optimal intake between Ca and Mg is from 2:1 to 1:1, which is about 4:1 in the case if fig. RDA values of Mn are 2.4 mg for men and 1.6 mg for women, that's why calculating for an average 2 mg need, the fig fructus contains 19.4% of the RDA. The RDA value of Cu is 1 mg d^{-1} now, so the fig fructus covers 38.8% of the RDA. According to the calculations relevant element intake can be got for Cr (167.5% of RDA), Fe (15%) and Mo (54%) as well.

In the case of non essential elements, high amount of intake could obtaine for Al with 30.3% of the DRI (DRI: 4 mg d^{-1}), B with 262.7% of the DRI (DRI: 0.96 mg d^{-1}, Ba with 33% of the DRI (DRI: 1 mg d^{-1}), Cd with 17.9% of the DRI (DRI: 0.17)[25], Co with 119% of the DRI (DRI: 0.029 mg d^{-1})[26], Ni with 22.9% of the DRI (DRI: 0.38 mg d^{-1}), Sr with 20.1-100% of the DRI (DRI: 1-5 mg d^{-1}) and V with 105.5% of theDRI (DRI: 0.018 mg d^{-1}).

Conclusion

Fig is consumed widely, as a part of the Mediterranean diet knowing the inner components combination can be useful to determine its role as a phytonutrient. Nutrition is important to gain and preserve human health. Macro- and microelements take part in many enzyme reactions, influencing the normal function from the base.

In our research, we wanted to highlight the importance of knowing what components get into the human body by consuming phytonutrients like *Ficus carica* L.

Since the Ca, Cd, Co, Mg, Sn and Zn concentration doesn't differ significantly between the Hungarian and Italian folium samples it is supposed to be a specific feature for the species which does not depend on the geological and weather conditions.

Fig fruit is a good source of Ca, Cr, Cu, Fe, K, Mg, Mn and Mo, since eating some pieces of dried fig covers more than 15% of the RDA.

References

[1]Balázs, A., Ficsor, E., Győry, H., *Orvosi Hetilap*, **2011**, *152 (2)*, 72-75.

[2]Guedes de Pinho, P., Pereira, D. M., Gonçalves, R. F., Valentão, P., Fernandes, F., Taveira, M. Andrade, P. B., *Functional plant science and biotechnology*. Middlesex: Global Science Books, **2009**, 1-15.

[3]Riu-Aumatell, M., Castellari, M., López-Tamames, E., Galassi, S., Buxaderas, S., *Food Chem.*, **2004**, *87*, 627-637.

[4]Botondi, R., De Santis, D., Bellincontro, A., Vizovitis, K., Mencarelli, F., *J. Agric. Food Chem.*, **2003**, *51*, 1189-1200.

[5]Lin, J. M., Rouseff, R. L., Barros S., Naim, M., *J. Agric. Food Chem.*, **2002**, *50*, 813-819.

[6]Dong, C., Mei, Y., Chen, L., *J. Chromatogr.A*, **2006**, *1117*, 109-114.

[7]Oliveria, A. P., Silva, L. R., Andrade, P. B., Valentão, P., Silva, B. M., Pereira, J. A., Guedes de Pinho, P., *Food Chem.*, **2010**, *121*, 1289-1295.

[8]Anke M., *Elements and their Compounds in the Environment,* Vol.1. General Aspects, Merian, E., Anke, M., Ihnat, M. (eds.), **2002**, 343-367.

[9]Szentmihályi, K., Vinkler, P., Fodor, J., Balla, J., Lakatos, B. *Orv. Hetilap*, **2006**, *147 (42),* 2027-2030

[10]Szentmihályi, K., Vinkler, P., Fodor, J., Balla, J., Lakatos, B. *Orv. Hetilap*, **2009**, *150 (15)*, 681-687.

[11]Solomon, A., Golubowicz, S., Yablowicz, Z., Grossman, S., Bergman, M., Gottlieb, H., et al., *J. Agric. Food Chem.*, **2006**, *54*, 7717-7723.

[12]*Pharmacopoeia Hungarica* VIII. (Ph.Hg. VIII): Medicina Publisher, Budapest, **2004.**

[13]Du, W. X., Olsen, C. E., Avena-Bustillos, R. J., McHugh, T. H., Levin, C. E., Friedman, M., *J. Agric. Food Chem.*, **2008**, *56 (9),* 3082–8.

[14]Hotta, M., Nakata, R., Katsukawa, M., Hori, K., Takahashi, S., Inoue, H., *J. Lipid Res.,* **2010**, *51*, 132–9.

[15]Kim, Y. S., Park, S. J., Lee, E. J., Cerbo, R. M., Lee, S. M., Ryu, C. H. et al., *J. Food Sci.*, **2008**, *73*, 540-545.

[16]Loughrin, J. H., Manukian, A., Heath, R. R., Turlings, T. C. J., Tumlinson, J. H., *Proc. Natl. Acad. Nat. Acad. Sci. USA*, **1994**, *91*, 11836-11840.

[17]Gertsch J, Leonti M, Raduner S, et al., *Proceedings of the National Academy of Sciences of the United States of America*, **2008**, *105 (26)*, 9099–104.

[18]Sachihiko, I., Shigeo, K., Takeo, S., *Helvetica Chimica Acta* **1973**, *56 (5),* 1514–1516.

[19]Hölldobler B, Wilson E. O., *The Ants*. Harvard University Press, **1990**, p. 287.

[20] Fahlbusch, K. G., Hammerschmidt, F. J.,Panten, J., Pickenhagen, W., Schatkowski, D., Bauer, K., Garbe, D.; Surburg, H. *Flavors and Fragrances. Ullmann's Encyclopedia of Industrial Chemistry,* **2003**.

[21]Kabata-Pendias, A., Mukherjee, A. B., *Trace Elements from Soil to Human.* Springer Verlag, **2007**.

[22]Szentmihályi, K., Hajdú, M., Then, M., *Medicinal and Aromatic Plant Science and Biotechnology*, **2008**, *2*, 57-62.

[23]*Recommended Dietary Allowances* (RDA) 10th ed. National Academy Press, Washington D.C., **1989**.

[24]*Dietary Reference Intakes for vitamin A, vitamin K, arsenic, boron, chromium, copper, iodine, iron, manganese, molybdenum, nickel, silicon, vanadium, and zinc.* Food and Nutritional Board, Institute of Medicine. National Academic Press, Boston, **2002**, 772-773.

[25] *EFSA: Summary of option, Cadmium in food*, **2009**.

[26]EFSA, *EFSA J.,* **2009**, *7(12)*, 1383.

ECO-FRIENDLY INHIBITOR GLYCINE-Zn²⁺ SYSTEM CONTROLLING CORROSION OF CARBON STEEL IN WELL WATER

A. Sahaya Raja[a], S. Rajendran[b,c], R. Nagalakshmi[d], J. AngelinThangakani[e] and M. Pandiarajan [b]

The environmental friendly inhibitor system glycine-Zn²⁺, has been investigated by weight loss method. A synergistic effect exists between glycine and Zn²⁺ system. The formulation consisting of 250 ppm of glycine and 50 ppm of Zn²⁺ offers good inhibition efficiency of 82%. Polarization study reveals that this formulation functions as an anodic inhibitor. The FTIR spectra study leads to the conclusion that the Fe²⁺-Gly complex formed on anodic sites of the metal surface controlled the anodic reaction and Zn(OH)₂ formed on the cathodic sites of the metal surface controlling the cathodic reaction. The surface morphology and the roughness of the metal surface have been analyzed with atomic force microscopy. A suitable mechanism of corrosion inhibition is proposed based on the results obtained from weight loss study and surface analysis technique. The eco-friendly inhibitor glycine-Zn²⁺ system may find application in cooling water system.

Corresponding Authors*
　　E-mail: sptheepandgl@gmail.com
[a]　SBM College of Engineering and Technology, Thamaraipadi, Dindigul-624005, Tamil Nadu, India.
[b]　PG and Research Department of Chemistry, GTN Arts College, Dindigul-624005, Tamil Nadu, India, Email: srmjoany@sify.com
[c]　RVS School of Engineering and Technlology, India
[d]　Department of Chemistry, Arupadaiveedu Institute of Technology,Chennai, Email: nagalakshmirajan@gmail.com
[e]　CEOA Matriculation Higher Secondary School,A Kosakulam, Madurai, India

The principles and practices of corrosion inhibition in recent years have begun taking into account the health and safety considerations. The use of hazardous chemicals has been restricted to no contact with the environment. Hence, there is a search for non-toxic, eco-friendly corrosion inhibitors. The use of inhibitors is one of the most practical methods to protect metals from corrosion. Corrosion inhibitor is a chemical substance which when added to the corrosive environment at an optimum concentration, there is a decrease in the corrosion rate of metals (or) alloys significantly. Unfortunately, many common corrosion inhibitors are highly toxic and health-hazardable, such as chromates,[1] nitrite[2] and aromatic heterocyclic compounds[3] etc. Therefore, it is better to look for environmentally safe inhibitors.[4-6] Some researchers investigated the inhibition effect of environment friendly inhibitors like amino acids on metal corrosion.[6-13] This is due to fact that aminoacids are non-toxic, biodegradable, relatively cheap and completely soluble in aqueous media and produced with high purity at low cost.

The environmental friendly, glycine, is chosen as the corrosion inhibitor for this present work. The literature presents some studies involving amino acids having the ability to prevent the corrosion of iron,[14] steel,[15-17] aluminium,[18,19] nickel [20] and copper.[21-25] The electrochemical studies such as polarization and AC impedance spectra [26-30] and cyclic voltametry have been studied by using amino acids. The adsorption of amino acids on carbon steel in acidic environment has been investigated by Akiyama et al. [31]

The aim of the present study is

1. To evaluate the inhibition efficiency of glycine in controlling the corrosion of carbon steel in the absence and presence of Zn²⁺.

2. To analyze the protective film on carbon steel by FTIR spectrophotometry.

3. To study the mechanistic aspects by potentiodynamic polarization study.

4. To analyse the surface morphology by AFM

5. To propose a suitable mechanism for corrosion inhibition based on the results from the above study.

Experimental Procedure

Preparation of specimens

Carbon steel specimens (0.0267%S, 0.067%P, 0.4% Mn, 0.1%C and the rest iron) of the dimensions 1.0cm x 4.0cm x 0.2cm were polished to mirror finish and degreased with trichloroethylene and used for weight loss method and surface examination studies.

Weight loss method

Relevant data on the well water used in this study are given in Table 1. Carbon steel specimens, in triplicate were immersed in 100 ml of well water and various concentrations of glycine in the presence and absence of Zn²⁺ (as ZnSO₄.7H₂O) for a period of seven days. The corrosion products were cleaned with Clarke's solution.[32] The weight of the specimens before and after immersion was determined using Shimadzu balance AY62.

The corrosion inhibition efficiency was calculated with equation (1)

$$IE = 100 \left[1 - \frac{W_2}{W_1} \right] \ (\%) \tag{1}$$

where

W_1 is the corrosion rate in the absence of the inhibitor and

W_2 is the corrosion rate in the presence of inhibitor.

From the weight loss, the corrosion rate (*CR*) was calculated

$$CR = \frac{\Delta m}{S \ t_{imm}} \frac{0.365}{\rho} \tag{2}$$

where

CR is the corrosion rate, (mmpy)

Δm is the loss in weight (mg)

S is the surface area of the specimen (dm²)

t_{imm} is the period of immersion (day)

ρ is the density of the metal in g cm⁻³ (7.86)

Potentiodynamic polarization study

Potentiostatic polarization studies were carried out using a CHI electrochemical impedance analyzer, model 660 A. A three-electrode cell assembly was used. The working electrode was a rectangular specimen of carbon steel with one face of the electrode (1 cm² area) exposed and the rest shielded with red lacquer. A saturated calomel electrode (SCE) was used as the reference electrode and a rectangular platinum foil was used as the counter electrode. Polarization curves were recorded using iR compensation. The results, such as Tafel slopes, and I_{corr}, E_{corr} and *LPR* values were calculated. During the polarization study, the scan rate (*v/s*) was 0.01; hold time at *Ef*(s) was zero and quit time(s) was 2.

FTIR spectra

The structure of glycine is shown in Fig.1. The carbon steel specimens immersed in various test solutions for seven days were taken out and dried. The film formed on the metal surface was carefully removed and thoroughly mixed with KBr, so as to make it uniform throughout. The FTIR spectra were recorded in a Perkin-Elmer 1600 spectrophotometer.
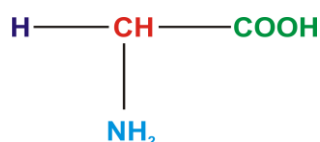
Figure 1. Structure of glycine

Atomic force microscopy

Atomic force microscope (AFM) is an exciting new technique that allows surface to be imaged at higher resolutions and accuracies than ever before.[33-35] The

microscope used for the present study was VECCO, Lab incorporation. Polished specimens prior to the initiation of all corrosion experiments were examined through an optical microscope to find out any surface defects such as pits or noticeable irregularities like cracks, etc., only those specimens, which had a smooth pit free surface, were subjected for AFM examination. The protective films formed on the carbon steel specimens after immersion in the inhibitor systems for different time durations were examined for a scanned area of 05 x 05 µm at a scan rate of 6.68 µm/second. the two dimensional and three-dimensional topography of surface film gave various roughness parameters of the film.

Results and Discussion

Weight loss method

The inhibition efficiency of glycine -Zn²⁺ system in controlling corrosion of carbon steel in well water (Table 1) has been evaluated by weight loss method.

Table 1. Physico –chemical parameters of well water.

Parameter	Well water
pH	8.0
Conductivity	3110 µmhos cm⁻¹
Total dissolved solids	2013 ppm
Chloride	665 ppm
Sulphate	14 ppm
Total hardness	1100 ppm

Analysis of results of the weight loss method

Inhibition efficiencies (IE%) of Gly-Zn²⁺ systems in controlling corrosion of carbon steel in well water (immersion period = 7 days) are given in Table 2 to 4. It is observed that Gly alone has poor inhibition efficiency. In the presence of various concentration of Zn²⁺ (25 and 50 ppm), the IE of Gly increases. A synergistic effect exists between Gly and Zn²⁺. For example, 50 ppm of Gly has only 28% IE; 50 ppm of Zn²⁺ has 20% IE. However, their combination has 82% IE. This suggests a synergistic effect existing between Gly and Zn²⁺. The corrosion rates of Gly-Zn²⁺ systems are shown in Fig.2.

Table 2. Corrosion rates (*CR*) of carbon steel immersed in well water in the presence and absence of inhibitor system at various concentrations and the inhibition efficiencies (*IE*) obtained by weight loss method.

Glycine, ppm	Zn²⁺ ppm	CR, mmpy	IE, %
0	0	0.0874	--
50	0	0.0629	28
100	0	0.0673	23
150	0	0.0787	10
200	0	0.0804	8
250	0	0.0865	1

Inhibitor system: glycine - Zn²⁺ (0 ppm), immersion period: 7 days, pH = 8.

Table 3. Corrosion rates (*CR*) of carbon steel immersed in well water in the presence and absence of inhibitor system at various concentrations and the inhibition efficiencies (*IE*) obtained by weight loss method.

Glycine, ppm	Zn^{2+}, ppm	CR, mmpy	IE, %
0	0	0.0874	--
0	25	0.0742	15
50	25	0.0603	31
100	25	0.0550	37
150	25	0.0524	40
200	25	0.0507	42
250	25	0.0472	46

Inhibitor system: glycine-Zn^{2+} (25 ppm), immersion period: 7 days, pH = 8

Table 4 : Corrosion rates (*CR*) of carbon steel immersed in well water in the presence and absence of inhibitor system at various concentrations and the inhibition efficiencies (*IE*) obtained by weight loss method.

Gly ppm	Zn^{2+} ppm	CR mmpy	IE %
0	0	0.0874	--
0	50	0.0699	20
50	50	0.0350	60
100	50	0.0280	68
150	50	0.0219	75
200	50	0.0192	78
250	50	0.0157	82

Inhibitor system: glycine - Zn^{2+} (50 ppm), Immersion period: 7 days, pH = 8

Synergism parameter (S_I) have been used to know the synergistic effect existing between two inhibitors.[36-41] Synergism parameter (S_I) can be calculated using the following relationship.

$$S_I = \frac{1 - \theta_{1+2}}{1 - \theta'_{1+2}} \qquad (3)$$

where

θ = surface coverage

$\theta_{1+2} = (\theta_1 + \theta_2) - (\theta_1 \theta_2)$

θ_1 = surface coverage by glycine

θ_2 = surface coverage by Zn^{2+}

θ'_{1+2} = surface coverage by both glycine and Zn^{2+}

and where

$$\theta = \frac{IE(\%)}{100}$$
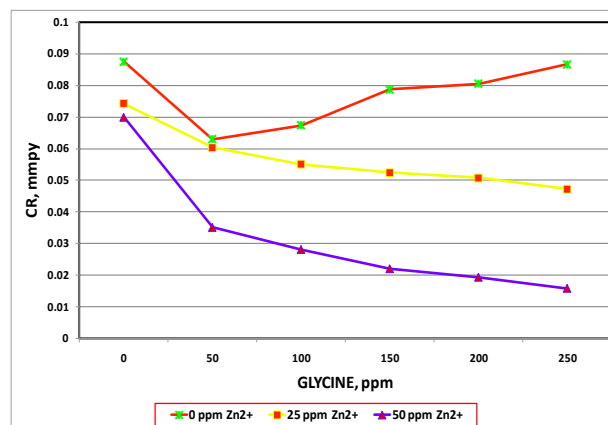
The synergism parameters of Glycine-Zn^{2+} system are given in Table 5. For different concentrations of inhibitors, S_I approaches 1 when no interaction between the inhibitor compounds exists. When $S_I > 1$, it points to synergistic effects. In the case of $S_I < 1$, it is an indication that the synergistic effect is not significant . From Tables 5 and 6, it is observed that value of synergism parameters (S_I) calculated from surface coverage were found to be one and above. This indicates that the synergistic effect exists between glycine and Zn^{2+} .[38,39,41] Thus, the enhancement of the inhibition efficiency caused by the addition of Zn^{2+} ions to glycine is due to the synergistic effect.

Figure 2. Corrosion rates (CR) of carbon steel immersed in various test solutions

Analysis of potentiodynamic polarization study (pH=8)

Polarization study has been used to confirm the formation of protective film formed on the metal surface during corrosion inhibition process.[42-47] If a protective film is formed on the metal surface, the linear polarization resistance value (LPR) increases and the corrosion current value (I_{corr}) decreases.

The potentiodynamic polarization curves of carbon steel immersed in well water in the absence and presence of inhibitors are shown in Fig.3. The corrosion parameters are given in Table 6. When carbon steel was immersed in well water the corrosion potential was -668 mV vs SCE. When glycine (250 ppm) and Zn^{2+} (50 ppm) were added to the above system the corrosion potential shifted to the noble side (-652 mV vs SCE). This indicates that a film is formed on the anodic sites of the metal surface. This film controls the anodic reaction of metal dissolution by forming Fe^{2+}-Gly complex on the anodic sites of the metal surface. The formation of protective film on the metal surface is further supported by the fact that the anodic Tafel slope (b_a) increases from 104 to 132mV.

Further, the LPR value increases from 5.630 x 10⁴ ohm cm² to 10.62 x 10⁵ ohm cm²; the corrosion current decreases from 5.775 x 10⁻⁷ A/cm² to 3.461 x 10⁻⁷ A/cm². Thus, polarization study confirms the formation of a protective film on the metal surface.

Table 5 : Inhibition efficiencies and synergism parameters for various concentrations of Gly-Zn²⁺ (50 ppm) systems, when carbon steel is immersed in well water

Glycine, ppm	Inhibition efficiency, IE (%)	Surface coverage, θ_1	Zn²⁺, ppm	Inhibition efficiency, IE (%)	Surface coverage, θ_2	Combined IE %, I'$_{1+2}$	Combined surface coverage, θ'_{1+2}	Synergism parameter, S_I
50	28	0.28	50	20	0.20	60	0.60	1.440
100	23	0.23	50	20	0.20	68	0.68	1.925
150	10	0.10	50	20	0.20	75	0.75	2.880
200	8	0.08	50	20	0.20	78	0.78	3.345
250	1	0.01	50	20	0.20	82	0.82	5.410

Immersion period: 7 days, pH = 8

Table 6. Corrosion parameters of carbon steel immersed in well water in the absence and presence of inhibitor system obtained from potentiodynamic polarization study

System	E$_{corr}$, mV vs SCE	b$_c$, mV/decade	b$_a$, V/decade	I$_{corr}$, Acm⁻²	LPR, ohm cm²
Well water	-668	268	104	5.775 x 10⁻⁷	5.630 x 10⁴
Well water+Gly(250ppm)+Zn²⁺(50ppm)	-652	235	132	3.461 x 10⁻⁷	10.62 x 10⁵
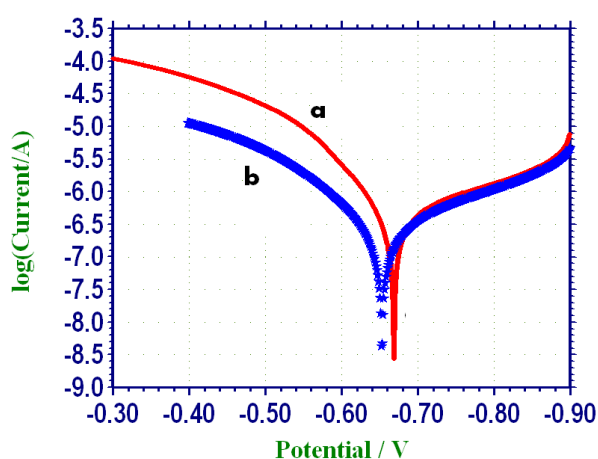
Figure 3. Polarization curves of mild steel immersed in various test solutions. a) well water (blank); b) well water + glycine (250 ppm) + Zn²⁺ (50 ppm)

Analysis of FTIR spectra

FTIR spectra have been used to analysis the protective film formed on the metal surface. [44,48-55] The FTIR spectrum (KBr) of pure glycine is shown in Fig.4(a). The C=O stretching frequency of carboxyl group appears at 1598 cm⁻¹. The CN stretching frequency appear at 1126 cm⁻¹. The NH stretching frequency of the amine group appears at 3105 cm⁻¹. [50-52]

The FTIR spectrum of the film formed on the metal surface after immersion in the solution containing well water, 250 ppm of glycine and 50 ppm Zn²⁺ is shown in Fig.4(b). The C=O stretching frequency has shifted from 1598 to 1609 cm⁻¹. The CN stretching frequency has shifted from 1126 to 1039 cm⁻¹. The NH stretching frequency has shifted from 3105 to 3209 cm⁻¹. This observation suggest that glycine has coordinated with Fe²⁺ through the oxygen atom of the carboxyl group and nitrogen atom of the amine group resulting in the formation of

Fe²⁺-glycine complex on the anodic sites of the metal surface. The peak at 1331 cm⁻¹ corresponds to Zn-O stretching. The peak at 3422 cm⁻¹ is due to OH⁻ stretching. This confirms that Zn(OH)₂ is formed on the cathodic sites of metal surface. [48,53-55] Thus the FTIR spectral study leads to the conclusion that the protective film consist of Fe²⁺-gly complex and Zn(OH)₂.
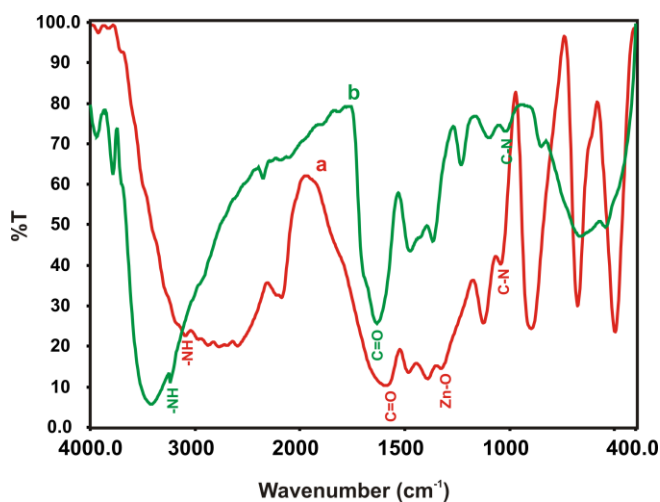
Figure 4. FTIR spectra of a) pure glycine; b) film formed on the metal surface after immersion in well water + Gly (250 ppm) + Zn²⁺ (50 ppm)

Atomic Force Microscopy Characterization

Atomic force microscopy is a powerful technique for gathering of roughness statistics from a variety of surfaces. [56] AFM is becoming an accepted method of roughness investigation. [57-63]

All atomic force microscopy images were obtained in a VECCO Lab incorporation AFM instrument operating in contact mode in air. The scan size of all the AFM images are 05 μm x 05 μm areas at a scan rate of 6.68 μm/second.

(a)

(b)

(c)
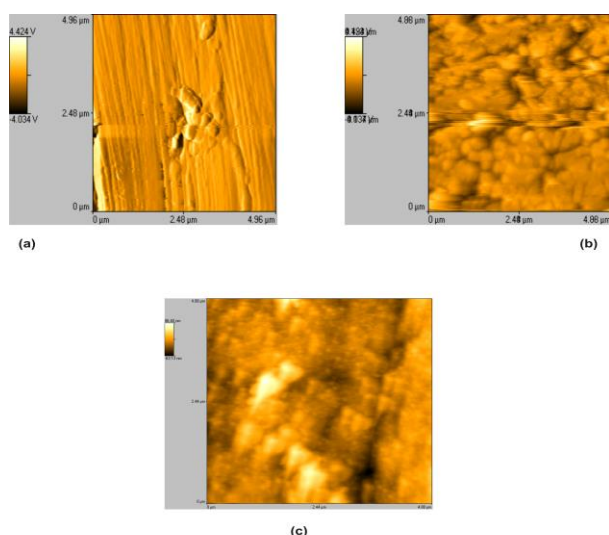
Figure 5. 2D AFM images of the surface of a) polished carbon steel (control); b) carbon steel immersed in well water (blank); c) carbon steel immersed in well water containing glycine (250 ppm) + Zn^{2+} (50 ppm)

The two dimensional (2D), three dimensional (3D) AFM morphologies and the AFM cross-sectional profile for polished carbon steel surface (reference sample), carbon steel surface immersed in well water (blank sample) and carbon steel surface immersed in well water containing the formulation of Gly 250 ppm and 50 ppm of Zn^{2+} are shown as Fig.5(a,d,g), (b,e,h), (e,f,i) respectively.

Root– mean-square roughness, average roughness and peak-to-valley value

AFM image analysis was performed to obtain the average roughness, R_a (the average deviation of all points roughness profile from a mean line over the evaluation length), root-mean-square roughness, R_q (the average of the measured height deviations taken within the evaluation length and measured from the mean line) and the maximum peak-to-valley (P-V) height values (largest single peak-to-valley height in five adjoining sampling heights).[62] R_q is much more sensitive than R_a to large and small height deviations from the mean .[63]

Table 7 is the summary of the average roughness (R_a), rms roughness (R_q) maximum peak-to-valley height (P-V) value for carbon steel surface immersed in different environments.

The value of R_{RMS}, R_a and P-V height for the polished carbon steel surface (reference sample) are 31 nm, 10 nm and 63 nm respectively, which shows a more homogeneous surface, with some places in which the height is lower than the average depth.[56] Fig.5(a,d,g) displays the uncorroded metal surface. The slight roughness observed on the polished carbon steel surface is due to atmospheric corrosion. The rms roughness, average roughness and P-V height values for the carbon steel surface immersed in well water are 68 nm, 18 nm and 131 nm respectively. These data suggest that carbon steel surface immersed in well water has a greater surface roughness than the polished metal surface. This shows that the unprotected carbon steel surface is rougher and is due to the corrosion of the carbon steel in

well water. Fig.5(b,e,h) displays the corroded metal surface with few pits.

The presence of 250 ppm of Gly and 50 ppm of Zn^{2+} in well water reduces the R_q by a factor of 32 nm from 68 nm and the average roughness is significantly reduced to 11 nm when compared with 18 nm of carbon steel surface immersed in well water. The maximum peak-to-valley height also was reduced to 60 nm from 131 nm. These parameters confirm that the surface appears smoother. The smoothness of the surface is due to the formation of a compact protective film of Fe^{2+}- Gly complex and Zn(OH)$_2$ on the metal surface thereby inhibiting the corrosion of carbon steel.

Also the above parameters observed are somewhat greater than the AFM data of polished metal surface which confirms the formation of the film on the metal surface, which is protective in nature.

Table 7. AFM data for carbon steel surface immersed in inhibited and uninhibited environments

Samples	Roughness, nm		Maximum peak-to-valley height (nm)
	RMS (R_q)	Average (R_a)	
Polished carbon steel (control)	31	10	63
Carbon steel immersed in well water	68	18	131
Carbon steel immersed in well water Gly (250 ppm) + Zn^{2+} (50 ppm)	32	11	60

(d)

(e)

(f)
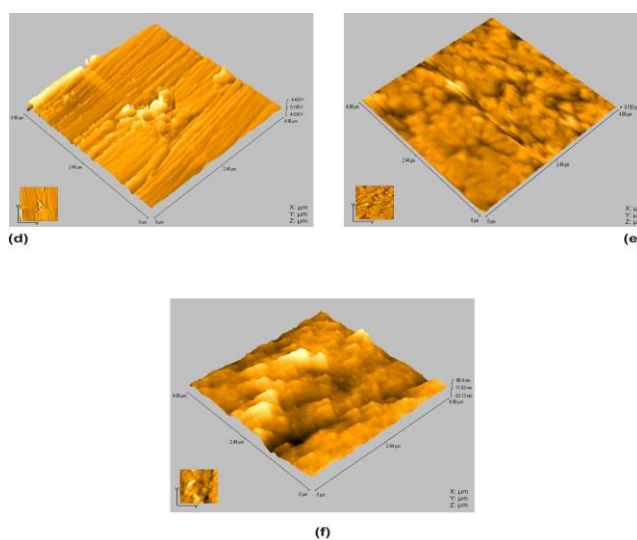
Figure 5. 3D AFM images of the surface of d) polished carbon steel (control); e) carbon steel immersed in well water (blank); f) carbon steel immersed in well water containing Glycine (250 ppm) + Zn^{2+} (50 ppm)
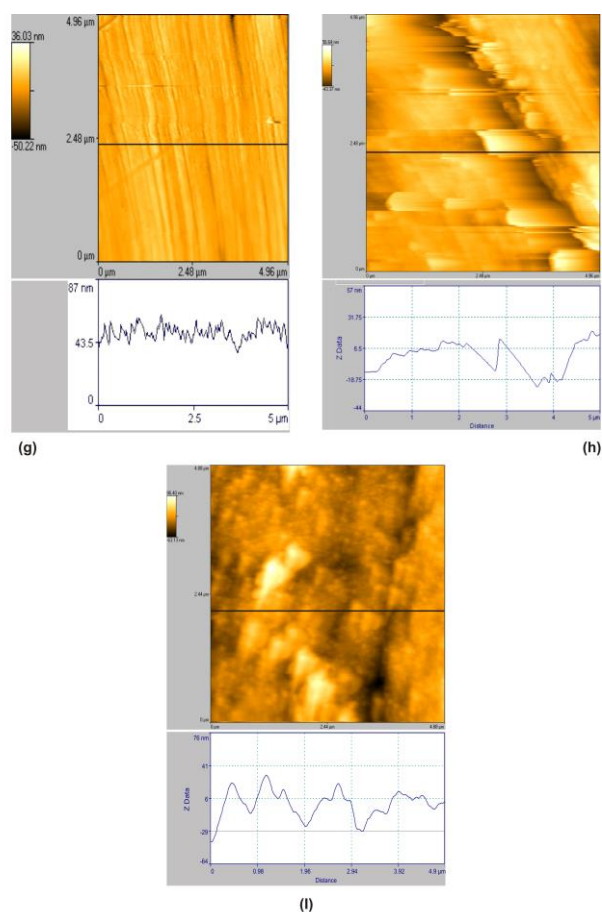
Figure 5. The cross sectional profile which are corresponding to as shown broken lines in AFM images of the surface of g) polished carbon steel (Control); h) carbon steel immersed in well water (blank); i) carbon steel immersed in well water containing Glycine 250 ppm + Zn^{2+} 50 ppm

Mechanism of Corrosion inhibition

The results of the weight-loss study show that the formulation consisting of 250 ppm Gly and 50 ppm of Zn^{2+} has 82% IE in controlling corrosion of carbon steel in well water. A synergistic effect exists between Zn^{2+} and Gly. Polarization study reveals that this formulation functions as anodic inhibitor. FTIR spectra reveal that the protective film consists of Fe^{2+}–Gly complex and Zn(OH)$_2$. (In order to explain these facts the following mechanism of corrosion inhibition is proposed.[64-70]

When the solution containing well water, 50 ppm Zn^{2+} and 250 ppm of Gly is prepared, there is formation of Zn^{2+}–Gly complex in solution.

When carbon steel is immersed in this solution, the Zn^{2+}-Gly complex diffuses from the bulk of the solution towards metal surface.

Zn^{2+}-Gly complex diffuses from the bulk solution to the surface of the metal and is converted into a Fe^{2+}-Gly complex, which is more stable than Zn^{2+}-Gly. [49]

On the metal surface Zn^{2+} - Gly complex is converted in to Fe^{2+} - Gly on the anodic sites. Zn^{2+} is released.

$$Zn^{2+} - Gly + Fe^{2+} \rightarrow Fe^{2+} - Gly + Zn^{2+}$$
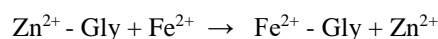
The released Zn^{2+} combines with OH$^-$ to form Zn(OH)$_2$ on the cathodic sites. [49]

$$Zn^{2+} + 2OH^- \rightarrow Zn(OH)_2 \downarrow$$
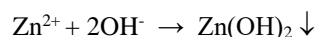
Thus the protective film consists of Fe^{2+}-Gly complex and Zn(OH)$_2$.[71,72] The AFM images confirm the formation of protective layer on the metal surface.

Acknowledgement

References

[1]Baral, A., Engelken, R. D., *Environ. Sci. Policy,* **2002**, *5*, 12.

[2]Gaidis, J. M., *Cement Concrete Comp.* **2004**, *26*, 181.

[3]Stupnisek-Lisac,E., Loncaric Bozic, A., Cafuk, I., *Corros,***1998***, 54,* 713

[4]El-Etre, A. Y., *Corros. Sci*, **2003,** *45*, 2485.

[5]El-Etre, A. Y., *Corros. Sci,***1998,** *40*, 1842.

[6]Ashassi-Sorkhabi, H.,,. Majidi, M. R., and Seyyedi, K., *Appl. Surf. Sci*, **2004**, *225*, 176.

[7]Ghasemi, Z., Tizpar, A., *Appl. Surf. Sci*. **2006**, *252* , 3667.

[8]Zhang, D. Q., Gao, L. X., Zhou, G. D., *J. Appl. Electrochem.* **2005,** *35*, 1081.

[9]Olivares, O., Likhanova, N. V., Gomez, B., Navarrete, J., Llanos-Serrano, M. E., Arce, E., Hallen, J. M., *Appl. Surf. Sci.,* **2006**, *252*, 2894.

[10]Badawy, W. A., Ismail, K. M., Fathi, A. M., *Electrochim. Acta*, **2006**, *51*, 4182.

[11]Ismail, K. M., *Electrochim. Acta*, **2007**, 52, 7811.

[12]Ashassi-Sorkhabi, H., Ghasemi, Z., Seifzadeh, D., *Appl. Surf. Sci.* **2005**, *249*, 408.

[13]Oguzie, E. E., Li, Y., Wang, F. H., *J. Colloid Interface Sci*, **2007**, *310*, 90.

[14]Onal, A. A., *Bull. Electrochem*, **1995**, *1*, 513.

[15]Gomma, G., *Bull. Electrochem*, **1998**, *12,* 456.

[16]Kalota, D., Silverman, D., *Corros. Sci*, **1994**, *50*, 138.

[17]Madkour, L., Ghoneion, M., *Bull. Electrochem.*, **1997,** *13*, 1.

[18]Morad, M., Hermas, A., Aal, M., *J. Chem. Technol. Biotechnol*, **2002**, *77*, 486.

[19]El-Shafei, A. A., Moussa, M. N. H., El-Far, A. A., *J. Appl. Electrochem.***, 1997***, 27*, 1075.

[20]Fouda,A., El-Semongy, M., *J. Indian Chem. Soc.,***1982**, *59*, 89.

[21]Aksut, A., Bilgic, S., *Corros. Sci,***1992**, *33*, 372.

[22]Gomma,G., Wahdan, H., *Mater, Chem. Phy.,***1994**, *39* ,142.

[23]Moretti,G., Guidi, F., *Corros.Sci,***2002**, *44*,1995.

[24]Rylkina, M., Chikanova, A., Trubacheva, L., Reshetinikov, S., *Protect. Metals,***1999**, *35*, 1987.

[25]Baba, H., Kodama, T., *Corros. Sci*, **1980**,41, 1995.

[26]Ita, B. I., *Bull. Electrochem.* **2005**, 21,319.

[27]Pech Canul, M. A., Bartolo-Perez, P., *Surf. Coat. Techn*, **2004**, *184*, 184.

[28]Pech Canul, M. A., Echeverria, M., *Corros. Engg. Sci. Techm.*, **2003**, *38,* 135.

[29]Rajappa, S. K.,. Venkatesha, T. V., *Turk. J. Chem.*, **2003,** 27, 189.

[30]Chi-Canul, L. P., *Corrosion*, **1999,** *55*, 948.

[31]Akiyama, A., Nobe, N., *J. Electrochem. Soc.*,**1970**, *117*, 999.

[32]Wranglen, G., "*An introduction to corrosion and protection of metals"*, Chapman & Hall, New York, **1985**.

[33]Holness, R. J., Williams, G., Worsley, D. A., and MacMurray, H. N., *J. Electrochem. Soc.,* **2005**, *152*, B73.

[34]Telegdi, J. Shaglouf, M. M., Shaban, A., Karman, F. H., Bertoti, I., Mohai, M., Kalman, E., *Electrochim. Acta,* **2001**, *46*, 3791.

[35]Arockia Selvi, J., Rajendran, S.,and Jeyasundari, J., *Zastit. Mater*, **2009**, *50(2)*, 91.

[36]Gomma,G. K., *Mater. Chem. Phys.*, **1998**, *55*, 241.

[37]Aramaki, K.,and Hackermann, N., *J. Electrochem. Soc.*, **1969**, *116*, 568.

[38]Quraishi, M. A., Rawat, J., and Ajmal, M., *Corrosion,* **1999**, *55*, 919

[39]Agnesia Kanimozhi S. and Rajendran, S., *Int. J. Electrochem. Soc.*, **2009**, *4,* 353.

[40]Gopi, D., Manimozhi, S., Govindaraju, K. M., Manisankar, P., and Rajeswari, S., *J. Appl. Electrochem*, **2007**, *37*, 439.

[41]Rajendran, S., Amal Raj, A. J., Joice, M. J., Anthony, N., Trivedi, D. C., Sundaravadivelu, M., *Corros. Rev*. **2004,** *22*, 233

[42]Morales Roque, J., Padiyan, T., Cruz, J., Garcia-Ochoa, E., *Corros. Sci*, **2008**, *50*, 614.

[43]Benali, O., Larabi, L., Traisnel, M., Gengembre, L., Harek, Y., *Appl. Sur. Sci.*, **2007**, *253*, 6130.

[44]Amar, H., Braisaz, T., Villemin, D., Moreau, B., *Mater. Chem. Phys. ,***2008,** *110*, 1.

[45]Arockia Selvi, J., Rajendran, S., Ganga Sri, V.,. John Amalraj, A., Narayanasamy, B., *Port. Electrochim. Acta*, **2009**, *27*(1), 1.

[46]Rajendran, S., Paulraj, J., Rengan, P., Jeyasundari, J., and Manivannan, M., *J. Dent. Oral Hyg.,* **2009**, *1*, 1

[47]Kalman, E., Felhosi, I., Karman, F. H., et al., *Corrosion and Environmental Degradation*, M. Schutze, Ed., *Weinheim :Wiky-VCH*, **2000**, *1*, 471.

[48]Kalaivani, R., Narayanasamy, B., Selvi, J. A., Amalraj, A. J., Jeyasundari J. and Rajendran, S., *Port. Electrochim. Acta*, **2009**, *27*, 177.

[49]Sathiyabama, J., Susai Rajendran, Arockia Selvi,J., and Jeyasundari,J., *The Open Corros. J.***2009**, 2,76.

[50]Silverstein, R. ., Bassler, G. C., Moril, T., "*Spectrometric Identification of Organic Compound"*, John Wiley and Sons, New York,**1981,** 95.

[51]Cross, A. D., "*Introduction to practical infrared spectroscopy",* Butterworths, Scientific Publication, London, **1990,** 73.

[52]Nakamoto, K., *Infrared and Raman spectra of inorganic coordination compound*, Wiley Interscience, New York, **1986**.

[53]Rajendran, S., Apparao, B. V., and Palaniswamy, N., *Bull. Electrochem.*, **1996**, *12*, 15.

[54]Sekine, I. and Hirakawa, V.,*Corrosion,* **1986,** *42*, 276.

[55]Rajendran, S., Apparao B. V., and Palaniswamy, *N., Proc.8ᵗʰ Europ. Symp. Corros. Inhibitors, Ferrara, Italy,* **1995**, 1, 465.

[56]Vera, R., Schrebler, R., Cury, P., Del Rio, R., and Romero, H., *J. Appl. Electrochem.*, **2007**, *37*, 519.

[57]Dumas, P., Butfffakhreddine, B., Am, C., Vatel, O., Ands, E., Galindo, R., and Salvan, F., *Europhys. Lett*. **1993**, *22*, 717.

[58]Bennett, J. M., Jahannir, J., Podlesny, J. C., Baiter, T. L., and Hobbs, D. T., *Appl. Opt.*,**1995**, *43*, 213.

[59]Duparre, A., Kaiser, N., Truckenbrodi, H., Berger, M., and Kohler, A., "*Microtopography investigations of optical surfaces and thin films by light scattering, optical profilometry, and atomic force microscopy, Int. Symp. on Optics"*, *Imaging and instrumentation, San Diego, CA, Proc. SPIE*. **1993**, (Publ. 1995), 181.

[60]Duparre, A., Kaiser, N., and Jakobs, S., *Morphology investigation by Atomic Force Microscopy of thin films and substances for excimer laser mirrors, Annual Symp. on Optical Materials for High Power Lasers.*, *Boulder, CO, proc. SPIE*, **1993**, **2114**, 394.

[61]Amra, C., Deumie. C., Torricini., D., Roche, P., Galindo, R., Dumas, P., and Salvan, F., *Int.Symp. on Optical Interference Coatings. 6-10 Jnne 1994. Grenoble, Proc. SPIE,***1994**. **2253**, 614.

[62]Thomas, T. R., *Longman, New York*, **1982**.

[63]Stout, K. J., Sullivan, P. J.,and McKeown, P. A., *Annals CRIP*, **1992**, *41*, 621.

[64]Gopi, D., Bhuvaneswaran, N., Rajeswari, S., *Bull. Electrochem.*, **2002**, *18*, 29.

[65]Gopi, D., Rajeswari, S., *J. Solid State Electrochem.*, **2002**, *6*, 194.

[66]Gopi, D., Rajeswari, S.,*Proc. International Conference on Advances in Surface Science and Engineering (INSURE), Chennai, India,* **2001**, 210.

[67]Gopi, D., Rajeswari, S., *Proc. NACE International Conf., Corrosion its Mitigation and Preventive Maintenance, Mumbai, India*, **2000**, *1*, 435.

[68] Gopi, D., Rajeswari, S., *Proc. Tenth National Congress on Corrosion Control, Conf., Madurai, India,* **2000,** 353.

[69]Veres, A., Reinhard, G., Kalman, E., *Brit. Corros. J.*, **1992**, *27*, 147.

[70]Kalman, E., *Corrosion Inhibitors, Published for EFC No.11, Institute of Materials London,* **1994**

[71]Ruba, H. F. G., Noreen, A. A., Sahayaraj, J. W., Amalraj, J. A., and Rajendran, S., *Indian. J. Chem. Technol.*, **2005**, *12*, 472.

[72]Selvarani, F. R., Santhamadharasi, S., Sahayaraj, J. W., Amalraj, A. J., and Rajendran, S., *Bull. Electrochem*, **2004**, *20*(12), 561.

NANO-SYNTHESIS OF PROMISING FAMILIES OF HT_C-SUPERCONDUCTORS TO SAVE ELECTRICAL LOSS IN THE ELECTRICAL POWER IN SAUDI ARABIA NET

(FREEZE DRY SYNTHESIS OF NANO-Zr-ADDED-2212-BPSCCO-SUPERCONDUCTOR)

Khaled M. Elsabawy[a,b]* and Waheed F. El-Hawary[a,c]

Saving energy loss through the conduction is the major objective of several advanced countries so superconductors are the essential material to achieve such these demands. The present investigations were concerned by synthesis of pure BPSCCO ($Bi_{0.5}Pb_{0.5}$)$_2$$Sr_2Ca_1Cu_2O_8$ and its variant zirconium containing composites with general formula : $Bi_{1+x}Zr_xPbSr_2Ca_1Cu_2O_z$, where x=0.1, 0.2 and 0.3 mole % respectively, were prepared via solution route (Freeze Drying Technique) to obtain nano-product. ZrO_2 has a limited effect on the main crystalline superconductive 2212-phase as x amount added increase as indicated in XRD measurements. SE-microscopy along with EDX proved that, solution route was the best in the degree of homogneties and exact molar ratios. ZrO_2 exhibits strong interactions on Raman spectral modes of 2212-phase . ZrO_2 has a slight effect on T_c's even with maximum addition x=0.3 mole. Finally the application of ZrO_2-nano-additives to the 2212-BPSCCO superconductors enhance the super-conduction mechanism and consequently save too much the amount of electricity loss on the main nets of electricity .

*Corresponding Authors
    *E-mail: ksabawy@yahoo.com and
    ksabawy@hotmail.com
[a]   Department of Chemistry, Faculty of Science, Taif
       University, 888- Taif, Kingdom of Saudi Arabia
[b]   Materials Unit , Chemistry Department ,Faculty of Science,
       Tanta University, 31725-Tanta –Egypt
[c]   Department of Chemistry, Faculty of Science, Cairo
       University, Egypt

Introduction

The cuprates offer a wide field of possibilities in terms of chemical composition, leading to required physical properties. Consequently, cationic substitutions and thermal treatments are commonly used as tools to modify the characteristics of a reference-compound.

Partial replacement of bismuth by lead in (Bi/Pb)$_2$$Sr_2CaCu_2O_{8+x}$ (Bi-2212) is known to induce important structural changes, as it suppresses the *c*-axis component of the modulation.[1,2] From the hole-doping point of view however, several reports suggest that Pb-incorporation does not affect the carrier concentration significantly.[3,4]

It was noticed from resistivity measurements[5-7] or diamagnetic shielding observations[8] that the interlayer coupling would be affected instead, resulting in a reduction of the material's anisotropy. On the other hand, oxygen non-stoichiometry in the Bi-based cuprates was not studied as extensively as it was for example in $YBa_2Cu_3O_z$ [9] and this is particularly true for the cation-substituted compounds. Nevertheless, it has been shown that oxygen excess in Bi-2212 varies in a small range but with a great effect on T_c [10-13] and is dependent on the cationic substitutions.[1416]

In the case of Bi-2212, the decrease of the oxygen content has been mentioned to explain the absence of a Pb-induced doping effect.[17,18] but only a few data are available in the literature. Superconducting properties of Bi-2212 depend on oxygen content.[19-23] The superconducting transition temperature T_c decreases for x≥8.18 and is dependent on annealing temperature and cooling rate.[24]

Oxygen vacancies have also been suggested as a major source of flux pinning in BSCCO.[25] The kinetics of oxygen motion and the formation and migration of oxygen defects in BSCCO have been studied by measurement of the oxygen–tracer diffusion parameters. These parameters provide not only input to the theoretical point–defect models, but can also be useful in developing fabrication techniques.

The pseudo-tetragonal 85 K -BSCCO superconductor of $Bi_2Sr_2CaCu_2O_x$, or 2:2:1:2 consists of one Ca atom symmetrically located between the following layers sequences Cu-O, Sr-O and Bi-O and each layer is parallel to the ab plane.[26] Most of studies reported on the 2223-phase are on Pb-doped compositions.[27-31] There are a few studies reported on the preparation of 2223 from Pb free compositions containing a large excess of Bi, Ca/or Cu, for example, the nominal compositions $BiSrCaCu_2O_x$,[32] $Bi_2Sr_2Ca_3Cu_4O_x$, $Bi_2Sr_2Ca_4Cu_5O_x$[33,34] were reported to lead a high volume fraction of the 2223 phase with variable amounts of impurity phases such as 2212,Ca_2CuO_3 and CuO.

A large number of precursor methods for preparation of 2223 were found to be superior to the conventional solid-state routes .It is known that, among the three superconducting phases of the Bi-Sr-Ca-Cu-O system, only 2201 is stable under high-oxygen pressures above 500°C both of 2212 and 2223-phases transform to a new non-superconducting orthorhombic perovskite with the same cation stoichiometry.[35-41]

Many previous workers[27-31] have investigated the doping effect of 3d-elements (M=Sc, Ti, V, Fe, Co, Ni and Zn) on the Cu-site of BPSCCO system and they reported that, the doping with 3d-elements affecting on stabilization of structural phase (2223) is responsible for HT$_c$-superconducting properties and there is a correlation between 2223-superconductive phase stability and the valency of 3d-metal cation dopant. Reaction kinetics and phase purity of the products were observed to be dependent upon the starting precursors during the formation of 2223, 2212 invariably forms as an intermediates have been incorporated to form 2223 plus some of impurity phases .The presence of transient liquid phase such as Ca_2PbO_4 is reported to be essential for diffusion of additional Ca and Cu ions into the 2212 framework.[42-45] A special method was used to introduce Pb which significantly influenced the phase development and superconducting properties of the 2223 product.[46]

Wu et al.[47] have used Raman techniques to identify variuos phases present in BPSCCO regime including alkaline earth cuprate, CuO, Bi-2212, Bi-2223 and Pb-containing phases specially $(Sr/Ca)_2PbO_4$.

Lu et al.[48] have determined the effect of MgO and Ag_2O oxides additives on the microstructure and superconducting properties of BPSCCO system and reported that , MgO addition did not affect the formation rate of 2212-phase which yields to 2223-phase, and could suppress the growth of Bi-free non-superconducting secondary phases furthermore, Shelke et al.[49] have investigated also the effect of HgO addition on the superconducting properties and microstructural properties of BPSCCO superconductor system deducing that, T$_c$'s-offsets for 2212-BPSCCO variated in between 60 and 72 K according to the amount of HgO added.

Orlova et al.[50] have determined the effect of ZrO_2 addition (1 wt.% to 5 wt.%) on the superconducting properties of sintered 123- Dy-Ba-Cu-O system and deduced that the best flux pinning in a magnetic field was achieved with maximum amount of addition ZrO_2 (5 wt %). The aim of the present work is to investigate the influence of high valency cations nano-Zr^{4+} inclusion additives on the hole-superconducting and physical properties PBSCCO regime aiming for stabilizing oxygen content by using high charge cation (Zr^{4+}) partially in place of lower one (Bi^{3+} /Pb^{2+}) site to avoid toxicity of heavy metal (lead) and enhancing the super-conduction mechanism to save energy loss during conduction .

EXPERIMENTS

Samples preparation

Solution route (Freeze dry Synthesis)

The pure $(Bi_{0.5}Pb_{0.5})_2Sr_2Ca_1Cu_2O_8$ and its variant zirconium containing composites with general formula : $Bi_{1+x}Zr_xPbSr_2CaCu_2O_z$, where x=0.1, 0.2 and 0.3 mole % respectively ,were prepared using freeze drying technique starting with estimated nitrate solutions (0.2M) for all cations except lead took as lead acetate followed by mixing the exact volumes in liquid nitrogen matrix then the resultant forwarded into freeze drying machine (slow program for sensitive samples ~ 90 h).

The obtained powders were ground and introduced to the same cycle of thermal treatment mentioned above.

Phase Identification

The X-ray diffraction (XRD) measurements were carried out at room temperature on the fine ground samples using Cu-K$_\alpha$ radiation source, Ni-filter and a computerized STOE diffractometer/Germany with two theta step scan technique .

Scannig Electron Microscopy (SEM) measurements were carried out using a small pieces of the prepared samples by using a computerized SEM camera with elemental analyzer unit (PHILIPS-XL 30 ESEM / USA) .

Superconducting measurements

The cryogenic AC-susceptibility of the prepared materials was undertaken as a function of temperature recorded in the cryogenic temperature zone down to 30 K using liquid helium refrigerator.

Raman Spectroscopy measurements

The measurements of Raman spectra were carried out on the finally ground powders with laser wavelength=632.8 nm (He-Ne laser) and laser power applied to the site of the sample = 0.4 mW with microscope objective = x20.

RESULTS AND DISCUSSION

Phase Identification:

Fig. 1a-d displays the X-ray powder diffractometry patterns of the pure $(Bi_{0.5}Pb_{0.5})_2Sr_2Ca_1Cu_2O_8$ and variant Zr-additive content composites: $BiZr_{0.1}PbSr_2CaCu_2O_z$, $BiZr_{0.2}PbSr_2CaCu_2O_z$, and $BiZr_{0.3}PbSr_2CaCu_2O_z$ prepared via freeze drying technique respectively. Analysis of the corresponding 2θ values and the interplanar spacings d(Å) were carried out ,and indicated that ,the X-ray crystalline structure mainly belongs to a single tetragonal phase 2212 in major besides Ca_2PbO_4 secondary phase in minor. The unit cell dimensions were calculated using the most intense X-ray reflection peaks (see Table 1) to be $a=b$=3.8141 Å and c=30.7732 Å for the pure 2212-BPSCCO phase which is in full agreement with those mentioned in literature.

Table 1. The calculated lattice parameters for the prepared samples

Material	a = b (Å)	c (Å)
$(Bi_{0.5}Pb_{0.5})_2Sr_2CaCu_2O_8$	3.8141	30.7832
$BiZr_{0.1}PbSr_2CaCu_2O_z$	3.8254	30.5720
$BiZr_{0.2}PbSr_2CaCu_2O_z$	3.8332	30.1827
$(BiZr_{0.3}PbSr_2CaCu_2O_z$	3.8264	30.1731

It is obvious that the additions of ZrO_2 has a negligible effect on the main crystalline structure 2212-phase by increasing Zr-content (x = 0.1→ 0.3 mole).

From Table 1 one can indicate that *c*-axis decreases as zirconium dopant concentration increase from 0.1 to 0.2 while no noticeable effect from 0.2 to 0.3. This is an indication for (Zr^{4+}) might substitute by some extent in the superconductive lattice and correlated with atomic radius of zirconium which is smaller than that of bismuth (Zr^{4+}=0.72 Å while Bi^{3+} is 1.17 Å) and alteration of Ca/Sr ratios which for c-axis is dependent.[2]
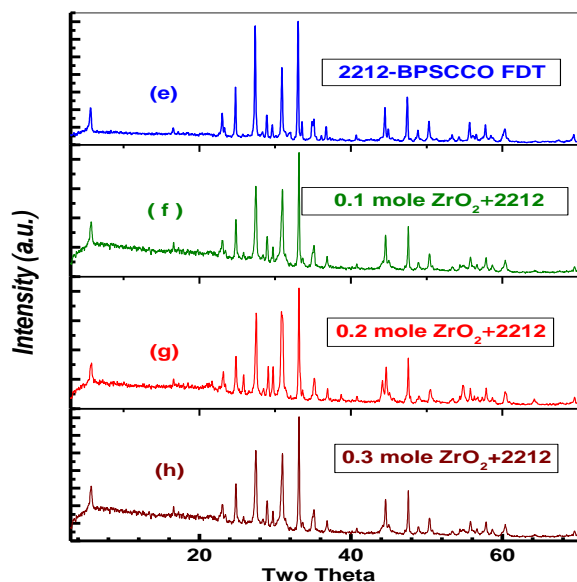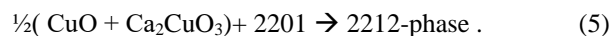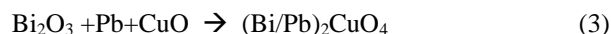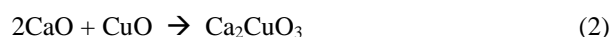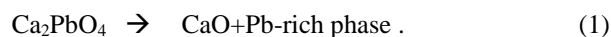

Figure 1.a-d. X-ray diffraction patterns for the pure and variant ZrO_2 2212-BPSCCO superconductors prepared by freeze drying technique. (e): x=0.0 mole; (f): x = 0.1 mole; (g): x=0.2 mole; (h): x=0.3 mole

Some authors such as Lu et al.[48] reported that the formation of 2212-phase comes from the step sequence reaction:

$$Ca_2PbO_4 \rightarrow CaO+Pb\text{-rich phase} . \qquad (1)$$

$$2CaO + CuO \rightarrow Ca_2CuO_3 \qquad (2)$$

$$Bi_2O_3 +Pb+CuO \rightarrow (Bi/Pb)_2CuO_4 \qquad (3)$$

$$(Bi/Pb)_2CuO_4+2SrO \rightarrow (Bi/Pb)_2Sr_2CuO_6 \text{ 2201-phase} \quad (4)$$

$$\tfrac{1}{2}(CuO + Ca_2CuO_3)+ 2201 \rightarrow 2212\text{-phase} . \qquad (5)$$

In this respect , one can expect that ZrO_2-additives to 2212 system produce some of Zr-based phases which is highly compatible with the superconductor phase specially the solubility of zirconium is enhanced via intermediate zirconate formation at the expense of the originally present Ca and Sr.[51]

Thus ,equilibrium between Bi-2201 and $Sr_{1-x}Ca_xZrO_3$ was achieved throughly the initial stage of synthesis :
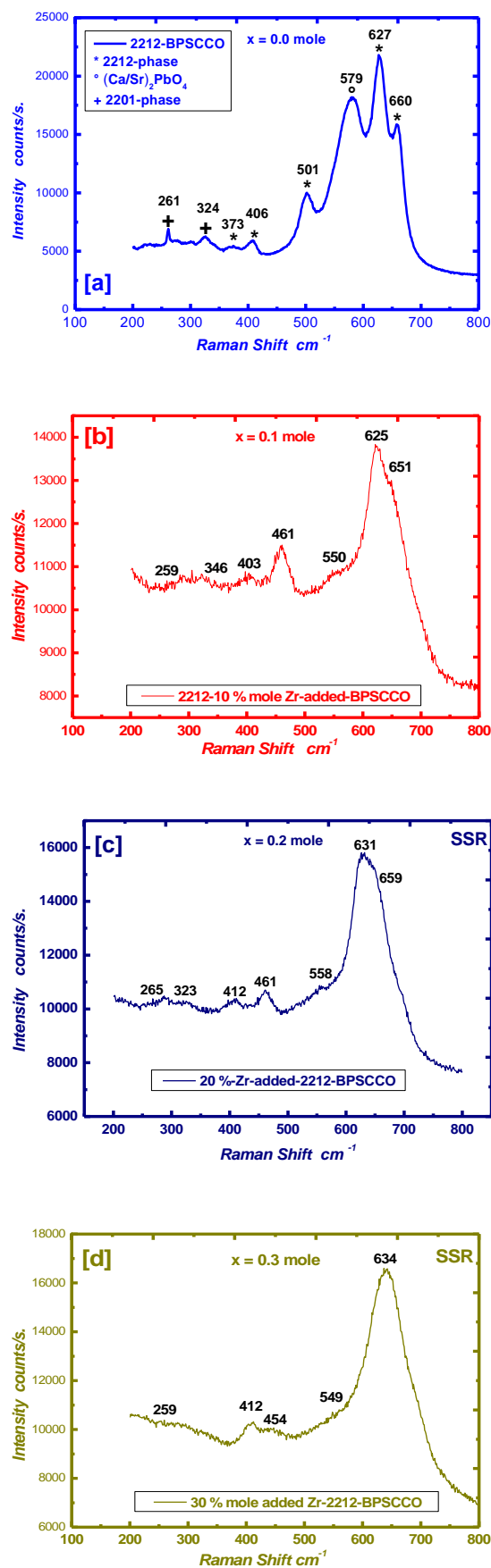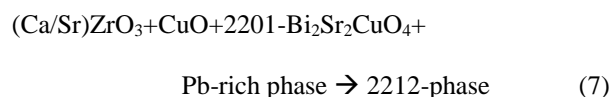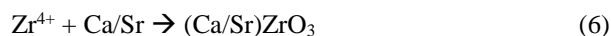
$$Zr^{4+} + Ca/Sr \rightarrow (Ca/Sr)ZrO_3 \qquad (6)$$

$$(Ca/Sr)ZrO_3+CuO+2201\text{-}Bi_2Sr_2CuO_4+$$

$$\text{Pb-rich phase} \rightarrow 2212\text{-phase} \qquad (7)$$

Figure 2.a-d. Raman Spectra for Zr-added-2212-BPSCCO; (a): *x*=0.0 mole; (b): *x*=0.1 mole; (c): *x*=0.2 mole; (d): *x*=0.3 mole

Thus, the amount of zirconate might be amorphous and consequently too difficult to be detected by X-ray means even for maximum Zr-addition x=0.3 mole. (see Fig.1d), these results are in partial agreement with Kazin et al.[51]

Liu et al.[52] support and reinforce our view in their studies on phase transformation and conversion for 2201->2212 deducing that the optimal annealing temperature to convert liquid phase of (Bi-Pb-Sr-Ca-Cu) mixture into 2212-phase is 795 °C and at annealing temperatures in the range (830-845 C°) 2223-phase decomposes to 2212 plus other phases and consequently 2212-becomes the major phase.

Raman Spectroscopy

Figs. 2a-d show the Raman spectra for pure and Zr(IV)-added 2212-BPSCCO system. From the modes frequencies which are listed and compared with some references see Table 2, one can indicate that 2212-BPSCCO phase is the domaining phase present in our polycrystalline BPSCCO beside small traces of strontium calcium plumbates and 2201-impurity phases .

It can be concluded from references[47,53,54] for the undoped 2212-phase the first order Raman mode frequencies are mainly located at the following ranges i.e., 290-330 ,460-470, and 620-640 cm^{-1} (the given ranges depend on samples compositions) and the most important modes frequencies are the A_g mode of O_{Bi} atoms vibration along the *c*-axis (290-330 cm^{-1}), the the A_g mode of O_{Sr} atoms vibration along the *c*-axis (460-470 cm^{-1}), and the the the A_g mode of O_{Bi} atoms vibration along the *a*-axis (620-640 cm^{-1}) which is induced by orthorhombic distortion. Furthermore, another shoulder peak (650-660 cm^{-1}) at the higher frequency side of the ~ 630 cm^{-1} line which is fully typical with our results. This shoulder is ascribed to A_g vibrational mode of extra oxygen atoms residing in the double layers.[53,54]

Table 2. Mode frequencies of Raman spectra recorded for Zr(IV) added-2212 BPSCCO in the present work in contrast with some references

References		2212			
[51]	[54]	*x* = 0	*x* = 0.1	*x* = 0.2	*x* = 0.3
282	285	261*	259*	265*	259*
296	295	324+	346+	323+	321+
313	355	373*	403*	412*	412*
391	400	406	461*	461*	454*
469	465	501*	-	-	-
-	497	579°	550°	558°	549°
631	630	627*	625*	631*	634*
659	660	660*	651*	659*	-

* 2212-phase, + 2201-phase,° (Sr/Ca)$_2$PbO$_4$

It is important to notify that the mode frequency lying at ~ 630 cm^{-1} is usually the most intense band for all three phases of BPSCCO superconductors (2201,2212 and 2223)when they are in a polycrystalline state[47] .

From Fig. 2a-d, Raman spectrograph for 2212-BPSCCO and its added Zr-2212 samples, the only violation from references of single crystal Raman spectrum is the band lies ~324 cm^{-1} which is ascribed to the 2201 phase as reported in[52] and the band appears ~ 500 cm^{-1} which also belongs to

our main phase 2212 as reported by Sapriel et al[55] who appears in their Raman spectrogram for 2212 single crystal band lies ~ 497 cm^{-1} which is fully supporting our results . The band appears ~ 560 ±10 cm^{-1} is indicated by existence of lead-rich phase (Sr/Ca)$_2$PbO$_4$ as reported in[47] that also confirmed in our XRD.
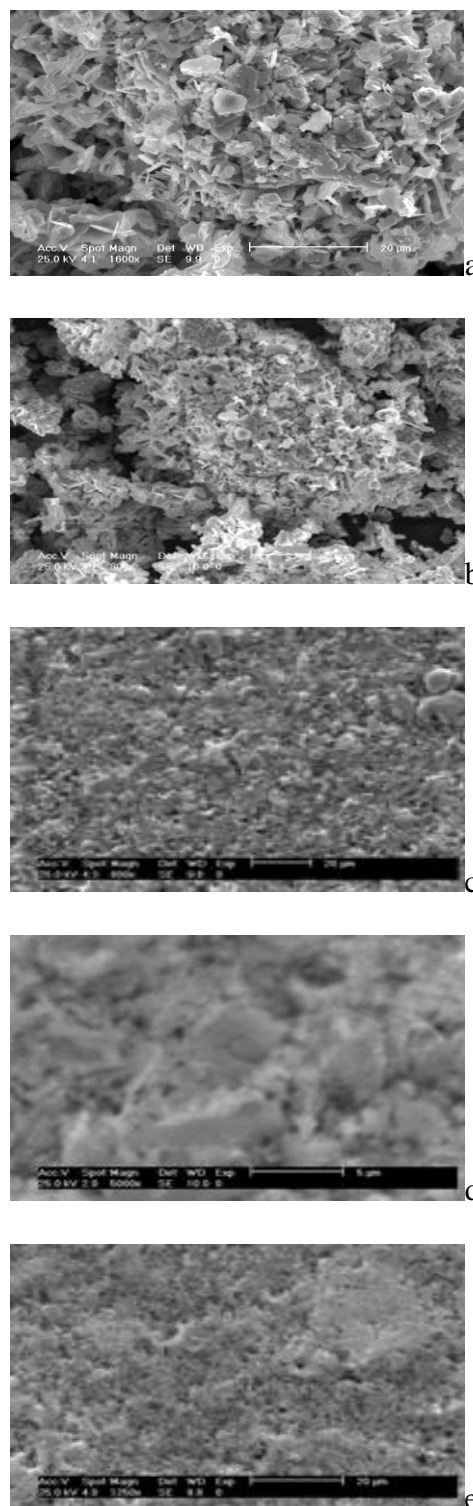

Figure 3.a-e. SE-micrographs for pure 2212-BPSCCO prepared by Freeze Drying Technique (FDT) and variant added-ZrO2 samples. [a]: Pure BiPb-2212 (FDT); [b]: 0.1 mole -ZrO$_2$-added BiPb-2212 (FDT); [c]: 0.2 mole -ZrO$_2$-added BiPb-2212 (FDT) [d] and [e] 0.3 mole -ZrO$_2$-added BiPb-2212 (FDT).

Table 3. EDX elemental data for pure -2212-BPSCCO (FDT).

2212-BiPb						
Element	Wt %	Average At %	K-Ratio	Z	A	F
O K	15.63	51.25	0.029	1.1894	0.1531	1.0004
CaK	5.14	6.32	0.0379	1.1433	0.6253	1.0021
CuK	18.11	12.48	0.1831	1.0236	0.9507	1.0323
PbL	18.71	5.65	0.1513	0.8181	1.0218	1.0178
BiL	19.24	5.98	0.1664	0.8155	1.0121	1.0211
SrK	21.21	12.51	0.1923	0.9674	0.9783	1

Table 4. EDX elemental data for 0.1 mole added-ZrO_2-2212-BPSCCO (FDT) .

Element	Average At %	K-Ratio	Z	A	F
O K	53.26	0.029	1.194	0.1531	1.0004
CaK	7.53	0.0379	1.1433	0.6253	1.0021
CuK	15.13	0.1831	1.0246	0.9507	1.0313
BiL	14.18	0.1664	0.8175	1.0131	1.0211
SrK	13.31	0.1923	0.9674	0.9783	1
ZrK	1.657	0.0253	0.9735	0.9832	1

Table 5. EDX elemental data for 0.2 mole added-ZrO_2-2212-BPSCCO (FDT) .

Element	Average At %	K-Ratio	Z	A	F
O K	53.56	0.029	1.194	0.1631	1.0004
CaK	7.63	0.0379	1.1433	0.6253	1.0021
CuK	15.18	0.1831	1.0246	0.9507	1.0313
BiL	14.28	0.1664	0.8175	1.0131	1.0211
SrK	13.31	0.1923	0.9674	0.9783	1
ZrK	3.157	0.0253	0.9735	0.9831	1

Table 6. EDX elemental data for 0.3 mole added-ZrO_2-2212-BPSCCO (FDT) .

Element	Average At %	K-Ratio	Z	A	F
O K	52.53	0.029	1.194	0.1531	1.0004
CaK	7.63	0.0379	1.1433	0.6233	1.0023
CuK	15.32	0.1831	1.0246	0.9507	1.0313
BiL	14.61	0.1664	0.8175	1.0131	1.0221
SrK	13.56	0.1923	0.9674	0.9783	1
ZrK	4.61	0.0253	0.9735	0.9824	1

From Fig.2a-d, it is clear that, as amount of Zr(IV)-added increases the bands lie ~ 579 corresponds to lead-rich phase plumbates) and the shoulder at 660 cm^{-1} (corresponds to the vibrational modes of extra oxygen atoms inside the bi-layer BPSCCO[53,54]) begin to be broad till complete broadening with maximum addition x=0.3 mole. In our opinion it might due to Zr(IV) added consumes some extent of Sr/Ca and extra oxygen to form zirconate impurity amorphous phase as described in eq.(6) .

SE-microscopy measurements

Fig.3a-d, show the *SE*-micrographs for pure and Zr-doped PBSCCO with x = 0.1 → 0.3 mole prepared by *Freeze Drying Technique*. The samples were measured as fine

ground powders ,the average particle size estimated to be in between 0.3 and 1.4 µm which is considered high to that estimated from solid state route.

The micrographs taken are more homogeneous than those for samples prapared via solid state route which reflect the priority to freeze drying technique than solid state route (SSR) .

Table 3-6, is the   EDX average data estimated from examinations of random spots inside the same sample for pure and Zr-added   polycrystalline doped –PBSCCO prepared by freez dry technique .

The analysis of EDX data obtained from Table 3 for pure 2212BPSCCO prepared by solid state route (SSR) give us the following , stoichoimetric molar ratios Bi/Pb : Sr : Ca : Cu : O = 1.63 : 1.66 : 1 : 1.89 : 7.7 while the EDX analysis for the same parent pure-2212 BPSCCO prepared by freez dry technique see Table (4)   Bi/Pb : Sr : Ca : Cu : O = 1.84 : 1.98 : 1 : 1.98 : 8.13 .   These results proved that, the differences in the molar ratios EDX estimated for the same sample is totally better in FDT that emphasized also in their magnetic behaviour and good evidence for the existence of 2212 superconductive phase with good approximate molar ratios .

Superconductivity measurements

Fig. 4a-d shows the AC-magnetic susceptibility curves (Meissner & Shielded lines) for pure and Zr-added samples with x=0.1–0.3 mole respectively prepared through solution route *Freeze Drying Technique* (FDT).

One can indicate that, 2212-undoped PBSCCO sample exhibits HT_c ~74.95 K corresponding to 2212-phase which is annealed in oxygen   and noticeable clearly in our XRD as major phase and this tc for 2212-phase is relatively better than that prepared by freez dry technique ΔT_c=0.65 K .This confirmed magnetically the existence of 2212 in highly homogeneous pure phase[56,57], while the samples with Zr-dopant *x*=0.1–0.3 mole exhibit slight surpress in their T_c's 70.7,69.34 and 68.3 K respectively, which reflects the promotion of the homogeneity degree in freeze drying (FDT) technique than that prepared by normal .   One can compare between the two techniques of preparation   SSR and FDT and conclude that, the differences in T_c's between the minimum T_c's samples with x=0.3 mole is ΔT_c = 2.75 K emphasize that, impurity phases such as zirconate inclusions or lead-rich plumbates dispersed regularly throughout the sample mixture with minimum ratios of formation achieving maximum degree of homogeneity as confirmed in SEM and EDX analyses .
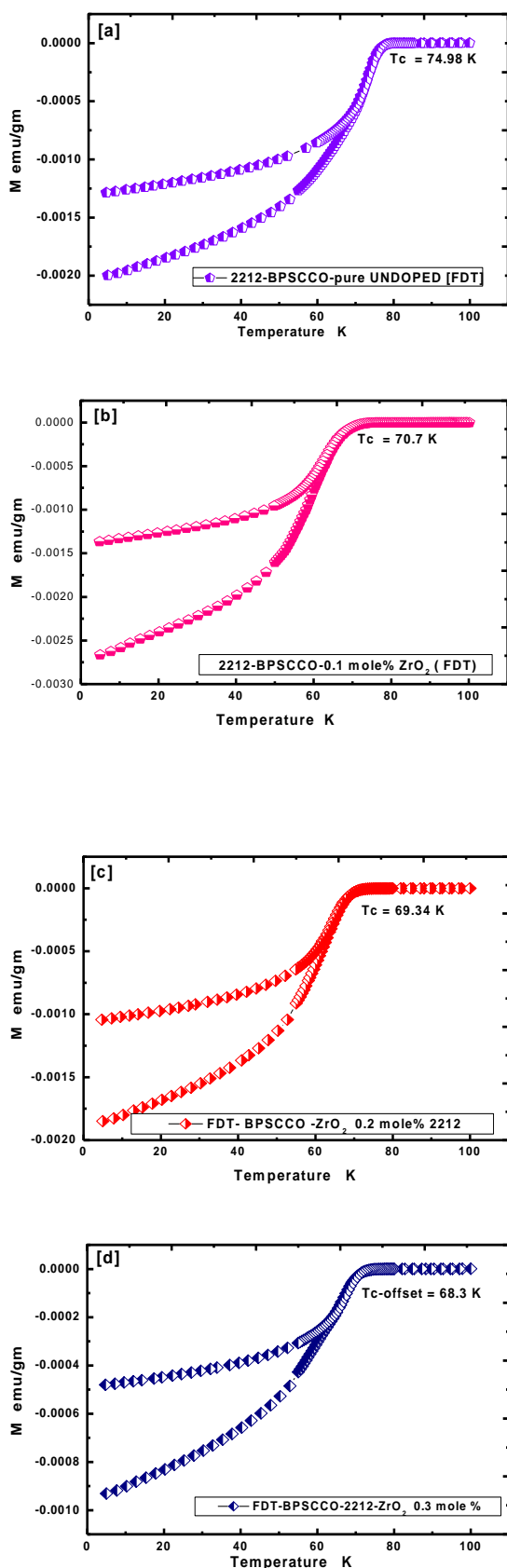
Fig.(4a-d): AC- Susceptibility curves for Zr-added 2212 (F DT).(a): x=0.0 mole, (b): x=0.1 mole, (c): x=0.2 mole and (d): x=0.3 mole

Conclusions

Conclusive remarks can be summarized as

1-Solution route (Freeze Drying Technique) yield to nano-product.

2-ZrO_2 has a limited effect on the main crystalline superconductive 2212-phase as Zr- amount added increases.

3-Only lead-rich-plumbates appears as secondary phase in minor.

4-SE-microscopy accompanied with EDX proved that, solution route was the best in the degree of homogeneities and exact molar ratios.

5-ZrO_2 exhibits strong interactions on Raman spectral modes of 2212-phase.

6-ZrO_2 has a slight effect on T_c's even with maximum addition x=0.3 mole.

7-Finally the application of ZrO_2-nano-additives to the 2212-BPSCCO superconductors enhance the super-conduction mechanism and consequently save too much the amount of electricity loss on the main nets of electricity .

Aknowlegements

References

[1]Chen C. H., Werder D. J., Espinosa G. P. and Cooper A. S., *Phys. Rev. B* , **1989**, *39*,4686**.**

[2]Schneck J., Pierre L., Tolédano J. C. and Daguet, C. ,*Phys. Rev. B* , **1989**, *39*, 9624.

[3]Maeda A., Hase M., Tsukada I., Noda, K., Takebayashi S. and Ushinokura K., *Phys. Rev. B,* **1990**, *41*, 6418.

[4]Weber M., Amato A., Gygax F. N., Schenk A., Maletta H., Duginov V. N., Grebinnik V.G., Lazarev A. B., Olshevsky V. G., Pomjakushin V. Y., Shilov S. N., Zhukov V. A., Kirillov, B. F., Pirogov A. V., Ponomarev A. N., Storchak V. G., Kapusta S. and Bock J., *Phys. Rev. B,* **1993**, *48*, 13022.

[5] Régi F. X., Schneck J., Savary H., Daguet C. and Huet F., *IEEE Trans. Appl. Supercond.*, **1993**, *3*, 1190.

[6]Ma J., Alméras P., Kelley R. J., Berger H., Margaritondo G., Cai X. Y., Feng Y.and Onellion M. ,*Phys. Rev. B*, **1995**, *51*, 9271.

[7]Winkeler L., Sadewasser S., Beschoten B., Frank H., Nouverté F.and Güntherodt G., *Physica C*, **1996**, *265*, 194.

[8]Manifacier L., Collin G. and Blanchard N., *Int. J. Modern Phys. B,* **1998**, *12*, 3306.

[9] Lindemer T. B., Hunley J. F., Gates J. E., Sutton A. L., Brynestad J. and Hubbard C., *J. Am. Ceram. Soc.*, **1989**, *72*, 1775.

[10]Allgeier C. and Schilling J. S., *Physica C*, **1990**, *168*, 499.

[11]O'Bryan H. M., Rhodes W. W. and Gallagher P.K. *Chem. Mater.,* **1990**, *2*, 421.

[12]Presland M. R., Tallon J. L., Buckley R. G. and Flower N. E., *Physica C*, **1991**, *176*, 95.

[13]Sieburger R., Müller P. and Schilling J. S., *Physica C*, **1991**, *181*, 335.

[14]Manthiram A. and Goodenough J. B., ,*Appl. Phys. Lett.* **1988**, *53*, 420.

[15]Groen W. A., Leeuw D. M. and Feiner L. F., *Physica C,* **1990**, *165*, 55.

[16]Mitzi D. B., Lombardo L. W., Kapitulnik A., Laderman S. S. and Jacowitz R. D. ,*Phys. Rev. B,* **1990**, *41*, 6564.

[17]Tallon J. L., Buckley R. G., Gilberd P. W. and Presland M. R., *Physica C*, **1989**, *158*, 247.

[18]Williams G. V. M., Pooke D. M., Pringle D. J., Trodahl H. J., Tallon J. L., , Crossley A. and Cohen L. F., *Phys. Rev. B,* **2001**, *63*, 589.

[19] Niu H., Fukushima N. and Ando K.; *Jap. J. Appl. Phys.*, **1988**, *27*, 1442.

[20]Morris D. E., Hultgren C. T., Markelz A. M., Wei J. Y. T., Asmar N. G. and Nickel J. H. ,*Phys. Rev. B* , **1989**, *39*, 6612.

[21]Zhao J. and Seehra M. S., *Physica C*, **1989**, *159*, 639.

[22]Presland M. R., Tallon J. L. ,Buckely R. G., Liu R. S. and Flower N., *Physica C*, **1990**, *176*, 95.

[23]Kao H. C. I., Chen W. L., Wei T. P., Lui J. C. and Wang C. M., *Physica C,* **1993**, *177*, 376.

[24]Tarascon J. M., McKinnon W. R., Barboux P., Hwang D. M., Bagley B. G., Greene L. H., Hull G. W., Lepage Y., Stoffel N. and Giround M., *Phys. Rev. B,* **1988**, *38*, 885.

[25]Chudnovsky E. M., *Phys. Rev. Lett.*, **1990**, *65*, 3060 .

[26]Hazen R. M., Prewitt C: T., Angel R. G., Ross N. L., Finger, L. W., Hadidiacos C.G., Veblen D. R., Hor P. H., Meng R. L. and Chu C. W., *Phys. Rev. Lett.*, **1988**, *60*, 1174.

[27]Sunshine S. A., Siegrist, T., Schneemeyer L. F., Murphy D.W., Cava R.J., Batlogg B., Van Dover R.B. , Nakahara S. , Farrow R. , Marsh P., Rupp L.W. and Peck W.P., *Phys. Rev. B*, **1988**, *38*, 898.

[28]Statt B. W., Wang Z., Lee M. G., Yakhmi J. V., De P.C., Major J. F. ,and Rutter J. W., *Physica C,* **1988**, *15*, 156 .

[29]Calestani G., Rezzoli C., Andreetti G. D., Buluggiu E., Giori D. C., Valenti A. and Ammoretti G. G., *Physica C*, **1988**, *158*, 217.

[30]Ueyama M., Hikata T., Kato T. and Sato K., *Jap. J. Appl. Phys.*, **1991**, *30*, 1384.

[31]Li Q., Brodersen K., Hjuler H. A. and Freltoft T., *Physica C,* **1993**, *217*, 360.

[32]Larbalesteir D. C., Cai X. Y., Feng Y., Edelman H., Umezawa A., Riley G. N. and Carter W. L., *Physica C,* **1994**, *221*, 299.

[33]Namgung C., Lachowski E. E., Irvine J. T. S. and West A. R., *Powder Diff.*, **1992**, *7*, 49.

[34]Shi D., Tang M., Boley M. S., Hash M., Vandervoort K., Claus H. and Lwin Y. N., *Phys. Rev. B*, **1989**, *40*, 2247.

[35]Sumiyama A., Yoshitomi T., Endo H., Tsuchiya J., Kijima W., Mizuno M., and Oguri Y. *Jap. J. Appl. Phys.*, **1988**, *27*, 542 .

[36]Sastry P. V., Yakhmi J. V. and Iyer R. M., *Physica C,* **1989**, *161*, 665.

[37]Dorris D. E., Prorok B. C.,Lanagan M. T., Sinha S. and Poepppel R. B. ,*Physica C,* 1993, *212*, 66.

[38]Pandey D., Mahesh R., Singh A. K., Tiiwari V. S.,and Singh S. K., *Solid State Commun.*, **1990**, *67,* 655.

[39]Zhengping X., Lian Z. ,and Chunlin J., *Supercond. Sci. Technol.*, **1992,** *5*, 240.

[40]Smith M. G. , Wills J. O., Poterson D. E., Binger J. F., Phillips D. S., Coulter J. Y., Salazar K. V. and Hults W. L., *Physica C,* **1994**, *231*, 409 .

[41]Cloots R., Bougrine H., Houssa M., Stassen S., Urzo L. D., Rulmont A. and Ausloos M., *Physica C*, **1994**, *231*, 259.

[42]Sastry P. V. S. ,and West A. R., *J. Mater. Chem.*, **1994**, *4*, 647.

[43]Wong-Ng W., Chiang C. K., Freiman S. W., Cook L. P. and Hiill M. D., *Am. Ceram. Soc. Bull.* **1992**, *71*, 1261.

[44]Huang Y. T., Wang W. N., Wu S. F., Shei C. Y., Hurang W. M., Lee W. H. and Wu P. T., *J. Am. Ceram. Soc.*, **1990**, *73*, 3507.

[45]Chen Y. L. and Stevens R., *J. Am. Ceram. Soc.*, **1992**, *75*, 1150.

[46]Dorris S. E., Prorok B. C.,. Lanagen M. T., Browning N. B., Hazen M. R., Parell J. A., Feng Y., Umezawa A. and Larbalester D. C., *Physica C,* **1993**, *223*, 163.

[47]Wu K. T., Fisher A. K. and Maroni V. A., *J. Mater. Res.*, **1997,** *12*, 1195.

[48]Lu X. Y., Nagata A., Sugawara K. and Kamada S., *Physica C,* **2000,** *335*, 51.

[49]Shelke V., Tewari H., Gaur N. and Singh R., *Physica C,* **1998**, *300*, 217.

[50]Orlova T. S., Laval J., Huong C. N. and Dubon A., *Supercond. Sci. Technol.,* **2001**, *14*, 59.

[51]Kazin P. E., Makarova M., Jansen M., Adelsberger T. and Tretyakov Y., *Supercond. Sci. Technol.*, **1997,** *10*, 616.

[52]Liu H. K., Zeng, R., Fu X. and Dou S. X. ,*Physica C,* **1999**, *325*, 70.

[53]Cardona M., Thomson C., Liu R., Von Schnering H. G. , Hartweg M., Yan Y. F. and Zhao Z. X., *Solid State Commun.*, **1988,** *66*, 1225.

[54]Farrow L. A., Greene L. H., Tarascon J. M., Morris P. A., Bonner W. A. and Hull G. W., *Phys. Rev. B* , **1988**, *38*, 752.

[55]Sapriel J., Pierre L., Morin D., Toledano J., Schneck J., Savary H., Chavignon J., Primot J., Daguet C. and Etrillard J., *Phys. Rev. B* , **1989**, *39*, 339.

[56]Zang L. D., Mu J. M., *Nanomaterial Science, Liaoning Science & Technology Press*, Shengyan, China, **1994**, 92.

[57]Bradea I., Popa S., Aldica G., Mihalache V. and Crisan A.*, J. Supercond.*, **2002**, *15*, 237.

REMOVAL OF Cr(III) BY ACTIVATED *ACACIA NILOTICA* LEAF POWDER

Magan Lal[a], Sumit[a], Shobha Sharma[a] and Vikal Gupta[a]*

Keywords: Cr(III), adsorption isotherm, desorption.

The present work describes the removal of Cr(III) by adsorption on activated *Acacia nilotica* leaf powder using batch process. This plant is locally available in arid and semi arid zone of Rajasthan (local name-Babul). Parameters like adsorbent mass, pH, shaking speed, particle size, contact time were studied at different initial Cr(III) concentrations. The adsorption process of Cr(III) was tested with Langmuir and freundlich models. Desorption studies were also performed.

Corresponding Authors*
    E-mail: vikal_chem@yahoo.co.in
[a]   Department of chemistry, Jai Narian Vyas University, Jodhpur-342001, Rajasthan, India.

Introduction

Population growth, couples with industrialization and urbanization, has resulted in an increasing demand for water thus leading to water crisis and serious consequences on the environment. The effluent stream released from the industries mainly comprises of hazardous chemicals and heavy metal ions like lead, mercury, copper, cadmium, chromium, nickel etc. These heavy metals are highly toxic even in trace amount. In India and all over the world, chromium (Cr) is dominant in most of the effluent streams as compared to other heavy metal ions. Chromium is one of the toxic substances which occur in aqueous system in both the trivalent form (Cr^{3+}) and the hexavalent form (Cr^{6+}). Chromium and its compounds are widely used in many industries such as metal finishing, dyes, pigments, inks, glass, ceramics and certain glues. It is also used in chromium tanning, textile, dyeing and wood preserving industries. The effluent from these industries contain trivalent chromium, (Cr^{3+}), at concentrations ranging from tens to hundreds of mgL^{-1}. Cr(III) is considered by the IARC (international agency for research on cancer) as a powerful carcinogenic agent that modifies the DNA transcription process causing important chromosomic aberrations[2]. On the other hand, the presence of Cr(III) in water causes significant environmental problems. The US environmental protection agency recommends that the levels of Cr(III) in drinking water should be less than 0.1 mg/L consequently, the removal of Cr(III) from industrial waste water becomes a research topic of great interest in the recent times.

Different alternatives for treating effluents as described in literature are electrochemical precipitation[3], membrane filtration[4] and ion exchange treatment[5], but these methods are expensive and not applicable in local conditions. Therefore, it is necessary to develop easily available inexpensive and equally effective alternatives for waste water treatment. In India *Acacia nilotica* is abundantly found in dry zones and easily available. Adsorption is proved to be a cost effective and versatile method for the removal of heavy metals. The uptake of metals by adsorbents has been attributed to the biochemical constituents namely, proteins, carbohydrates and lignin that

contain many functional groups including carboxyl, hydroxyl and amine moieties which are responsible for metal sorption[6].

In recent years, several studies have been reported on various low cost adsorbents such as sawdust[7], wool[8], sugar industry waste[9], wheat straw[10], tea factory waste[11], activated neem leaves[12], pine needles[13], activated tamarind seeds[14], sphagnum moss peat[15], soya cake[16], red mud[17] etc. However many of these natural adsorbents low adsorbing capacity and most of them have are not locally available.

The present work describes the role of *Acacia nilotica* leaf powder for the removal of Cr(III) from effluent streams. The effects of various parameters such as adsorbent mass, pH, shaking speed, particle size, contact time and initial metal ion concentration were investigated.

Materials and methods

Preparation of adsorbent

Acacia nilotica leaves were collected from the campus of Jai Narayan Vyas University, Jodhpur (Rajasthan) India. The Collected leaves were then washed with distilled water for several times to remove water soluble impurities and surface adhered particles. The washed materials were dried in a hot air oven at 110°C for 50 h. Dry *Acacia nilotica* leaves were crushed into small particles by using Jaw crusher and the resulting crumbs were sieved to different particle sizes: 100-175, 175-250, 250-325 and 325-400 μm. *Acacia nilotica* leaf powder of different particle size was activated separately by heat treatment and with concentrated Sulphuric acid. Finally, the products obtained were stored in glass bottle for further use.

Preparation of Cr(III) solutions

A stock solution of Cr(III) was prepared by dissolving 1.585 gm of 99.9% chromium chloride ($CrCl_3$) in one liter of solution. This solution was diluted as required to obtain the standard solution containing 50-350 mgL^{-1} of Cr(III). The solution pH was adjusted in the range of 1-10 by adding 0.5 N HCl or 0.5 N NaOH solutions as per the requirement and was measured by a pH meter.

Characterization of adsorbent

FTIR spectra of the adsorbent samples were recorded to characterize the main functional groups that might be involved in adsorption. As shown in Fig. 1 the spectra displayed a number of absorption peaks.
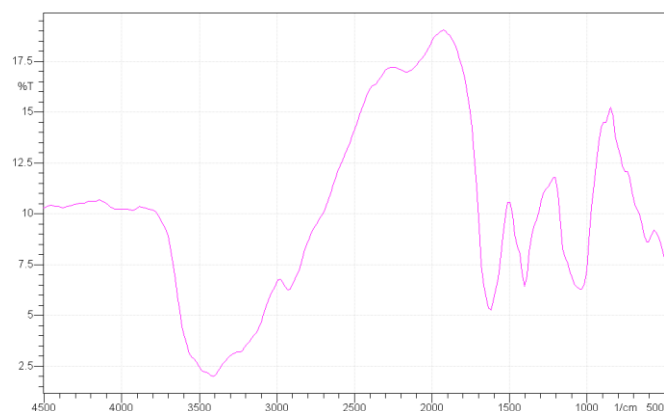

Figure 1. FT-IR spectra of activated *Acacia nilotica* leaf powder

The FT-IR spectroscopy analysis indicated bands at 3410 cm^{-1}, representing bonded –OH groups. The bands observed at 2940 cm^{-1}, could be assigned to the aliphatic –C-H group. The peak around at 1620 cm^{-1} corresponded to -C=O stretching. The peak around at 1404 cm^{-1} corresponded to CH$_3$ bending vibration. The peak at 1049 cm^{-1} was due to –C-OH stretching of carboxylic group. The peak at 617 cm^{-1} is due to -C-H bending vibration of more than four -(CH$_2$)- groups.

Batch adsorption experiments

Adsorption experiments were studied in batch mode at room temperature. Sorption studies were carried out in batch experiment as function of adsorbent mass, pH, shaking speed, particle size, contact time and initial metal ion concentration. Parameter was changed at a time and all other were maintained constant according to Table 1.

After completion of every set of experiments the residual was separated by filtration using whatman filter paper no. 42 and only 10 ml of each sample was stored for residual Cr(III) analysis. The concentration of residual Cr(III) after adsorption was directly measured by atomic adsorption spectrophotometer with an air acetylene flame.

Eq. (1) is used to determine the percentage adsorption of the metal (φ, in %) by adsorbent.

$$\varphi = \frac{C_O - C_e}{C_O} \times 100 \qquad (1)$$

where C_o is initial metal concentration, C_e is metal concentration after shaking.
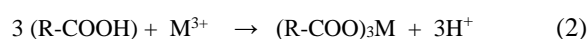
Adsorption mechanism

The ion exchange or hydrogen bonding may be the principal mechanism for the removal of heavy metal ions from industrial effluent by *Acacia nilotica* leaf powder. It has long been recognized that the heavy metal cations readily form complexes with O-,N-,S- or P- containing functional group in adsorbent.
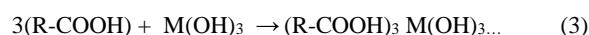
Adsorption process quite is dependent on pH of the aqueous solution. In most cases, the % of adsorption of metal ions is increased with an increase in pH up to a certain value and decreased with further increase of pH. Due to different properties of various heavy metal ions, the maximum adsorption takes place in a slightly different pH range for different metals.

In a specific pH range, for one specific heavy metal there may be a species present in solution, such as M(OH)$_3$. At lower pH, the positive charged metal ion species are adsorbed at the surface of the adsorbent by ion exchange mechanism. With increasing pH, metal ion species mainly neutral, may be adsorbed by hydrogen bonding mechanism. These mechanisms are shown in the following equation:

Ion exchange

$$3\ (R\text{-}COOH) + M^{3+} \quad \rightarrow \quad (R\text{-}COO)_3M\ +\ 3H^+ \qquad (2)$$

Hydrogen bonding

$$3(R\text{-}COOH) +\ M(OH)_3 \rightarrow (R\text{-}COOH)_3\ M(OH)_{3\dots} \qquad (3)$$

Results and discussion

Effect of adsorbent mass

The influence of biosorbent material dosage on % biosorption and uptake of Cr(III) is shown in Fig. 2. The percent removal of Cr(III) was increased up to 78% when the dosage of biosorbent material was increased from 4-15 gL^{-1}. After this maximum, there was no effect of mass of adsorbent on removal efficiency due to equilibrium formation.
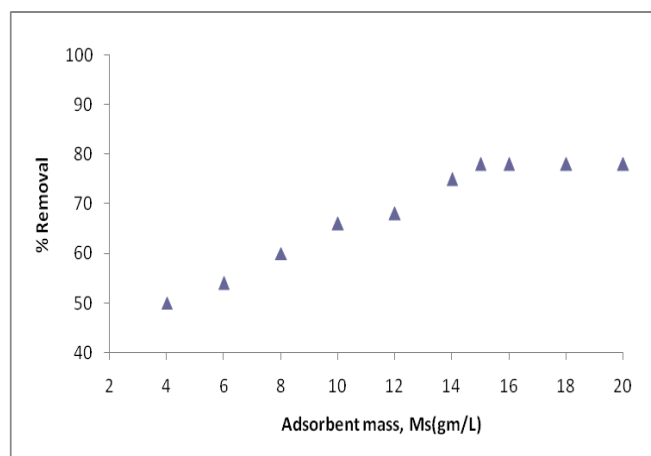
Effect of pH

The effect of the initial pH of solution on Cr(III) removal is shown in Fig. 3. Removal efficiency was found decreasing with an increase in the initial pH. The maximum removal efficiency of 81% was obtained when initial pH was maintained between 1 and 3. Hence, the low pH value of 2 results in higher percentage removal of Cr(III) using activated *Acacia Nilotica* leaf powder. The decrease in adsorption of Cr(III) by increasing the value of pH may be due to decrease in H$^+$ ion on the adsorbent surface that results in less strong electrostatic attraction.
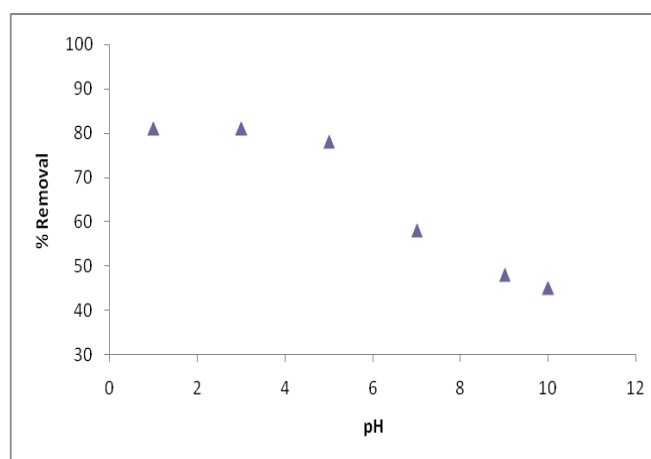
Effect of shaking speed

Shaking speed is an important parameter which affects the removal efficiency. Studied were conducted at different values of shaking speed from 50-250 rpm. The maximum removal efficiency was obtained when shaking speed was 200 rpm (Fig. 4). This is due to the fact when we increase shaking speed, the energy is librated and this energy is used in the formation of bond between adsorbent and metal ions.

However after 200 rpm (shaking speed) the removal efficiency decreases (2 to 10%) due to the fact that high shaking speed provides extra energy, which is used in
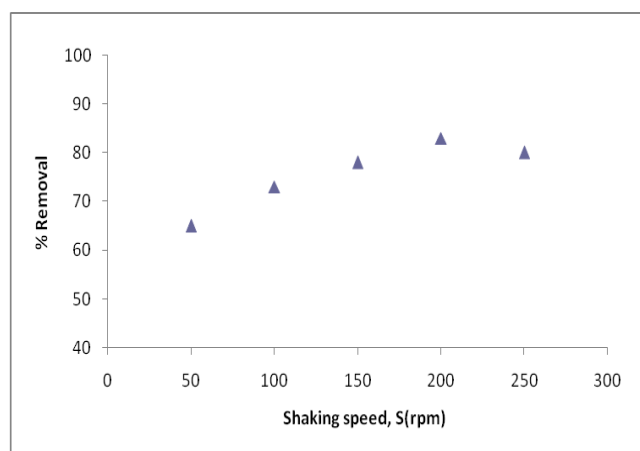

breaking the bond between adsorbent and metal ions.

Figure 2. Effect of Adsorbent mass on adsorption of Cr(III) by activated *Acacia Nilotica* leaf powder

Figure 3. Effect of pH on adsorption of Cr(III) by activated *Acacia Nilotica* leaf powder

Figure 4. Effect of shaking speed on adsorption of Cr(III) by activated *Acacia Nilotica* leaf powder

Effect of particle size

The fixed bed adsorption experiments were carried out using four different particle sizes (100-175, 175-250, 250-325 and 325-400 of the adsorbent) by using all other parameters keeping constant. The result shown in fig.5 shows that by decreasing the size of adsorbent, removal efficiency increases.

Effect of contact time

Fig.6 shows the percentage removal of Cr(III) as a function of time for the initial Cr(III) concentration 50 mgL^{-1} at pH value of 2. It is apparent from the figure that till a time of 60 min., the percentage removal from aqueous solution increases rapidly and reaches up to 86%. After that, the percentage removal of Cr(III) increases slowly till a time of 80 min and then subsequently becomes constant. A further increase in contact time has a negligible effect on the percentage removal of Cr(III). Therefore, the contact time 80 min. is considered for the adsorption of Cr(III) on activated *Acacia Nilotica* leaf powder for the entire batch studies.

Effect of initial metal ion concentration

The Cr(III) adsorption is significantly influenced by initial concentration of Cr(III) in aqueous solutions. The initial Cr(III) concentration was varied from 50-300 mgL^{-1} while maintaining the adsorbent amount 15 gL^{-1} at an initial pH value of 2. Fig.7 shows that the effect of initial Cr(III) concentration on the percentage removal of Cr(III). The percentage removal decreases from 88% to 60% with an increase in the initial Cr(III) concentration from 50 to 300 mgL^{-1} respectively. The decrease in the percentage removal of Cr(III) can be explained with the fact that all the adsorbents has a limited number of active sites, which would have become saturated above a certain Cr(III) concentration. It indicates that if the initial Cr(III) concentration increases, more and more Cr(III) ions compete for the same given active sites and thus the percentage removal decreases.

Adsorption Equilibrium Study

Adsorption isotherm are important to describe the adsorption mechanism for the interaction of Cr(III) on the adsorbent surface. A variety of isotherm equations have been in use, some of which have a strong theoretical base and some being of mere empirical nature. It is needed to examine the obtained experimental equilibrium data for Cr(III) removal using activated *Acacia Nilotica* leaf powder with different isotherm modals available in literature. In the present work Langmuir and Freundlich isotherm modals are tested with the experimentally obtained equilibrium data.

Langmuir isotherm

The Langmuir isotherm equation is given by the equation (4)

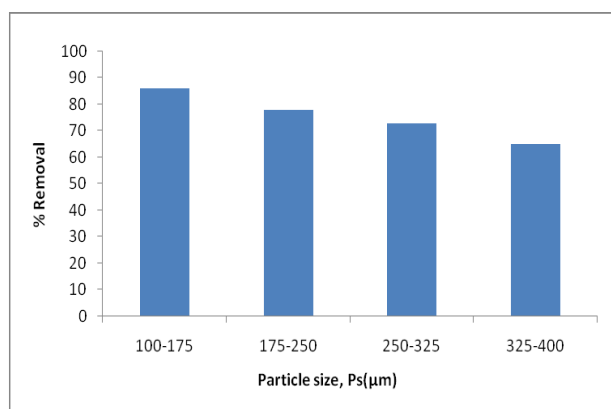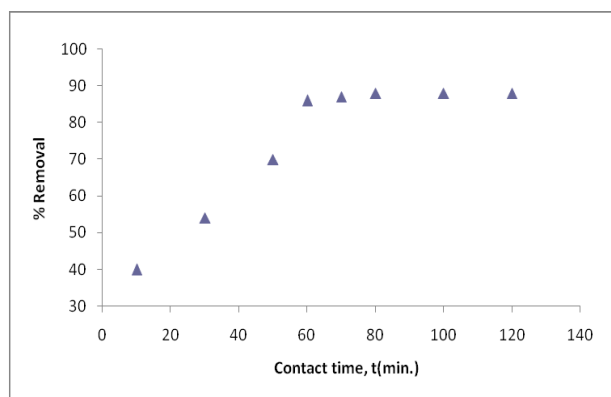$$q_e = \frac{q_{\max} b C_e}{1 + b C_e} \qquad (4)$$

Table 1. Experimental conditions

	M_s (g L^{-1})	pH	S (rpm)	P_s(μm)	t (min.)	C_0 (mg L^{-1})
Effect of adsorbent mass, M_s(g L^{-1})	4-20	4	150	100-175	60	50
Effect of pH	15	1-10	150	100-175	60	50
Effect of shaking speed, S (rpm)	15	2	50-250	100-175	60	50
Effect of particle size, P_s (μm)	15	2	200	100-175 to 325-400	60	50
Effect of contact time, t (min.)	15	2	200	100-175	10-120	50
Effect of metal concentration, C_0 (mg L^{-1})	15	2	200	100-175	80	50-350

where q_e is the solid phase adsorbate concentration in equation (mg g^{-1}), q_{max} is the maximum adsorption capacity corresponds to complete monolayer coverage on the surface (mg g^{-1}) and b is the Langmuir constant (mg L^{-1}). Equation (4) can be rearrange to the following linear form:

$$\frac{C_e}{q_e} = \frac{1}{q_{max}b} + \frac{C_e}{q_{max}} \qquad (5)$$

The plot of C_e/q_e versus C_e gives the straight line of intercept $1/q_{max}b$ and slope $1/q_{max}$ (Fig. 8). The Langmuir constants are represented in Table 2. The correlation coefficient showing that data correctly fit the Langmuir relation.

Table 2. Isotherms parameters for adsorption of Cr(III) on ACLP

Langmuir constants		
q_{max} (mg g^{-1})	B (mg^{-1} L)	R^2
10.15	0.065	0.997
Freundlich constants		
K_f	n	R^2
0.239	2.565	0.985

Freundlich isotherm

It is an empirical equation used to describe heterogeneous system given by following equation

$$q_e = K_f C_e^{1/n} \qquad (6)$$

where q_e is the amount of adsorbate adsorbed per unit mass of adsorbent (mg g^{-1}), C_e the equilibrium concentration of adsorbate (mg/L), K_f the freundlich constant related to the adsorption capacity and $1/n$ is the heterogeneity factor. A linear form of the freundlich equation is obtained by taking the logarithm of the equation (6).

$$\ln q_e = \ln K_f + \frac{1}{n} \ln C_e \qquad (7)$$

Figure 5. Effect of Particle Size on adsorption of Cr(III) by activated *Acacia Nilotica* leaf powder
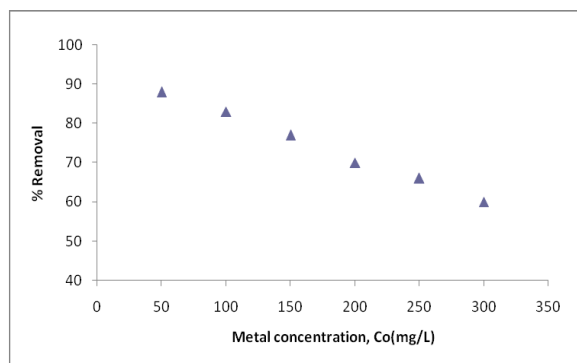
The plot of $\ln q_e$ versus $\ln C_e$ gives a straight line of intercept $\ln K_f$ and slope $1/n$ (fig 9). The Freundlich constant are represented in table 2.

Desorption studies

The desorption of Cr(III) from previously Cr(III) loaded *Acacia Nilotica* leaf powderusing distilled water was attempted but Cr(III) desorption was not observed. Hence experiments were conducted with acid and alkali solutions to desorb Cr(III) ions. The results indicated that the desorption of Cr(III) ions with acid was not achieved even when 0.1, 0.2 and 0.3 N HCl were used (not shown). However, there was little desorption with basic solutions. It was observed that desorption of Cr(III) was 25.3 % with 0.2 N NaOH. The results of desorption studies have revealed that either ion exchange or hydrogen bonding as the possible mechanism for Cr(III) binding on the *Acacia Nilotica* leaf powder.

Figure 6. Effect of contact time on adsorption of Cr(III) by activated *Acacia Nilotica* leaf powder

Conclusions

The present study shows that the *Acacia nilotica* leaf powder is an effective adsorbent for the removal of Cr(III) from aqueous solution. Ion exchange and hydrogen bonding are the principal mechanism for the removal of Cr(III) ions.

Experimental data indicate that the adsorption efficiency is dependent on operating variables such as adsorbent mass, pH, shaking speed, particle size, contact time and initial metal ion concentration. The adsorption data fit well with Langmuir and freundlich adsorption isotherm model.

Figure 7. Effect of Metal ion concentration on adsorption of Cr(III) by activated *Acacia Nilotica* leaf powder
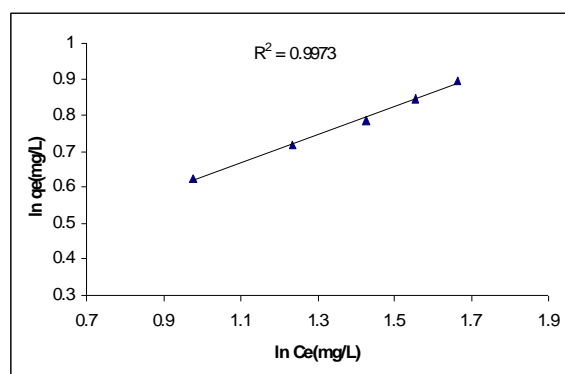
Figure 8. Langmuir isotherm for the adsorption of Cr(III) by *Acacia Nilotica* leaf powder
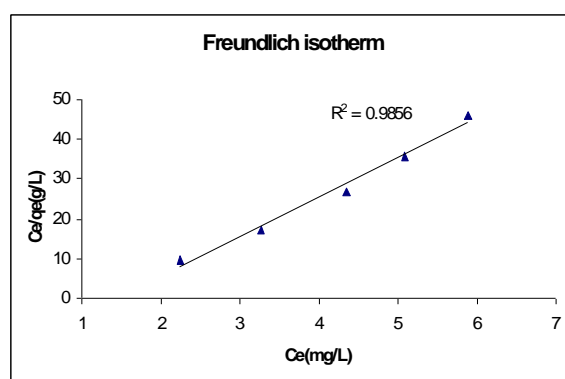
Figure 9. Freundlich isotherm for the adsorption of Cr(III) by *Acacia Nilotica* leaf powder

References

[1]Kumar, R., Bishnoi, N. R. and Bishnoi, G. K. *J. Chem. Eng.,* **2007,** *135,* 202.

[2]Sheng, P. X., Tan, L. H., Chen, J. P. and Ting, Y.P. *J. Disp. Sci. and Technol.,* **2004,** *25,* 681.

[3]Meunier, N., Drougi, P., Montance, C., Hausler, R., Mercier, G. and Blais, J. F. *J. Hazard. Mater.,* **2006,** *137,* 581.

[4]Pehlivan, E. and Altun, T. *J. Hazard. Mater.,* **2006,** *B-134,* 149.

[5]Uysal, M. and Irfan, A. *J. Hazard. Mater.,* **2007,** *149,* 482.

[6]Gupta, V., Sumit, Lal, M. and Bhati, M. *J. Indian Chem. Soc.,* **2012,** *89,* 1253.

[7]Argun, M. E., Dursun, S., Ozdemir, C. and Karatas, M. *J. Hazard. Mater.,* **2006,** *141*(1), 77.

[8]Dakiky, M., Khamis, M., Manassra, A., Mereb, M. *Adv. Environ. Res.,* **2002,** *6,* 533

[9]Gupta, V. K and Ali, I. *J. Colloid Inter. Sci.,* **2004,** *271,* 321.

[10]Li, C., Chen, H. and Li, Z. *Proc. Biochem.,* **2004,** *39,* 541.

[11]Malkoc, E. and Nuhoglu, Y. *Sep. Purif. Techno.l,* **2007,** *54,* 291.

[12]Ho, Y. S., Wase, D. A. J. and Forster, C. F. *Water Res.,* **1995,** *29*(5), 1327.

[13]Hadmohammadi, M. R., Salary, M. and Biparva, P. *J. Appl. Sci. Environ. San.,* **2011,** *6*(1), 1.

[14]Babu, B. V. and Gupta, S. *J. Environ. Eng. Sci.,* **2008b,** *7,* 553.

[15]Babu, B. V. and Gupta, S. *Adsorption,* **2008a,** *14,* 85.

[16]Daneshvar, N., Salari, D. and Aber, S. *J. Hazard Mater.,* **2002,** *B-94,* 49.

[17]Gupta, V. K. and Sharma, S. *Environ Sci. Technol.,* **2002,** *36,* 3612.